TECHNISCHE UNIVERSITÄT
MÜNCHEN

Fakultät für Chemie, Lehrstuhl Technische Elektrochemie

The influence of different parameters on the discharge capacity and cycling performance of an S/C-composite cathode

Anna-Marietta Eberle

Vollständiger Abdruck der von der Fakultät für Chemie der Technischen Universität München zur Erlangung des akademischen Grades eines

Doktors der Naturwissenschaften
(Dr. rer. nat.)

genehmigten Dissertation.

Vorsitzender: Prof. Dr. Lukas Hintermann

Prüfer der Dissertation:

1. Prof. Dr. Hubert A. Gasteiger
2. Prof. Dr. Thomas F. Fässler

Diese Dissertation wurde am 12.12.2016 bei der Technischen Universität München eingereicht und durch die Fakultät für Chemie am 30.03.2017 angenommen.

"If you can´t explain it simply, you don´t understand it well enough."

Albert Einstein

Eidesstattliche Erklärung

Ich erkläre an Eides statt, dass ich die bei der Fakultät der Chemie der TUM zur Promotionsprüfung vorgelegte Arbeit mit dem Titel:

"The influence of different parameters on the discharge capacity and cycling performance of an S/C-composite cathode"

am Lehrstuhl Technische Elecktrochemie unter der Anleitung und Betreuung durch Herrn Prof. Dr. Hubert A. Gasteiger ohne sonstige Hilfe erstellt und bei der Abfassung nur die gemäß § 6 Abs. 6 und 7 Satz 2 angegebenen Hilfsmittel benutzt habe.

(x) Ich habe keine Organisation eingeschaltet, die gegen Entgelt Betreuerinnen und Betreuer für die Anfertigung von Dissertationen sucht, oder die mir obliegenden Pflichten hinsichtlich der Prüfungsleistungen für mich ganz oder teilweise erledigt.

(x) Ich habe die Dissertation in dieser oder ähnlicher Form in keinem anderen Prüfungsverfahren als Prüfungsleistung vorgelegt.

( ) Die vollständige Dissertation wurde in .....veröffentlicht. Die promotionsführende Einrichtung.....hat der Vorveröffentlichung zugestimmt.

(x) Ich habe den angestrebten Doktorgrad noch nicht erworben und bin nicht in einem früheren Promotionsverfahren für den angestrebten Doktorgrad endgültig gescheitert.

( ) Ich habe bereits am.....bei der Fakultät für.....der Hochschule .....unter Vorlage einer Dissertation mit dem Thema .....die Zulassung zur Promotion beantragt mit dem Ergebnis: .....

Die öffentlich zugängliche Promotionsordnung der TUM ist mir bekannt, insbesondere habe ich die Bedeutung von § 28 (Nichtigkeit der Promotion) und § 29 (Entzug des Doktorgrades) zur Kenntnis genommen. Ich bin mir der Konsequenzen einer falschen Eidesstattlichen Erklärung bewusst. Mit der Aufnahme meiner personenbezogenen Daten in die Alumni-Datei bei der TUM bin ich

(x) einverstanden

( ) nicht einverstanden

München, den 28.11.2016

Unterschrift

Lithium Sulfur batteries are thought to be the next generation energy storage device, because of their high theoretical capacity and energy density. At the moment, their practical application is hindered by several issues, for example fast degradation, low Sulfur (S) utilization or the often too low S loadings to give high areal capacities. Here, a Sulfur/Carbon-composite (S/C-composite) is introduced, which can be synthesised by an easy bottom-up approach with a high S-content in the resulting powder. The existence and appearance of S on the carbon support was investigated by XRD and SEM/EDX and the S amount was measured by TGA. The influence of two different synthesis routes, cell storage before cycling, S loading on the cathode, different carbon supports, use of a polysulfide enriched electrolyte as well as novel electrolyte solvent and additive on the cycling behavior of the S/C-composite cathode were examined by galvanostatic cycling of test cells.

Lithium Schwefel Batterien sind aufgrund ihrer hohen theoretischen Kapazität und Energiedichte ausgewählt worden die nächste Generation der Energiespeichersysteme darzustellen. Momentan wird jedoch die praktische Anwendung durch mehrere Probleme erschwert, wie zum Beispiel die schnelle Degradation, geringe Schwefelnutzung oder ein zu geringer Schwefelanteil auf der Kathodenseite für hohe Flächenkapazitäten. Im folgenden wird ein Schwefel-Kohlenstoff Komposit vorgestellt, welches mittels einer einfache „bottom-up“ Synthese hergestellt werden kann und einen hohen Schwefelanteil im resultierend Pulver enthält. Der Nachweis von Schwefel und seine Erscheinungsform auf dem Kohlenstoffträgermaterial wurde mittels XRD und REM/EDX untersucht und der Schwefelanteil wurde mit TGA bestimmt. Der Einfluss zweier verschiedener Syntheserouten, der Lagerung der Testzellen vor dem Zyklisieren, der Schwefelbeladung auf der Kathode, verschiedener Kohlenstoffträger, der Verwendung eines mit Polysulfiden angereichterten Elektrolyten sowie die Verwendung eines neuen Elektrolytlösungsmittels und Additives auf das Zyklenverhalten wurde mittels galavnostatischem Zyklen der Testzellen untersucht.

Table of Contents

1. Introduction

Nowadays, portable devices like laptops, mobile phones and digital cameras are powered by Li-ion batteries. But this commercially available electrochemical system almost reached its ceiling performance for portable devices, and further enhancement are not possible.[1,2] Due to the increasing gasoline prices and the more strict environmental regulations for emission vehicles, the requirement to find an alternative "fuel" is getting more important than ever before. But to reach the goal of an on-board battery in an electrical automotive vehicle with a range of 500 km is not reachable with the current Li-ion technology.[3]

Generally, Li-ion batteries are based on an intercalation mechanism and are limited due to the capability of the active electrode material to take up Li-ions.[4] Furthermore, a lot of "dead weight" is part of the system in addition to the active materials Sulfur and Lithium . In typical Li-ion batteries, layered graphite is used as anode and Lithium cobalt oxide ($LiCoO_2$) or Lithium iron phosphate ($LiFePO_4$) are often used as cathode.

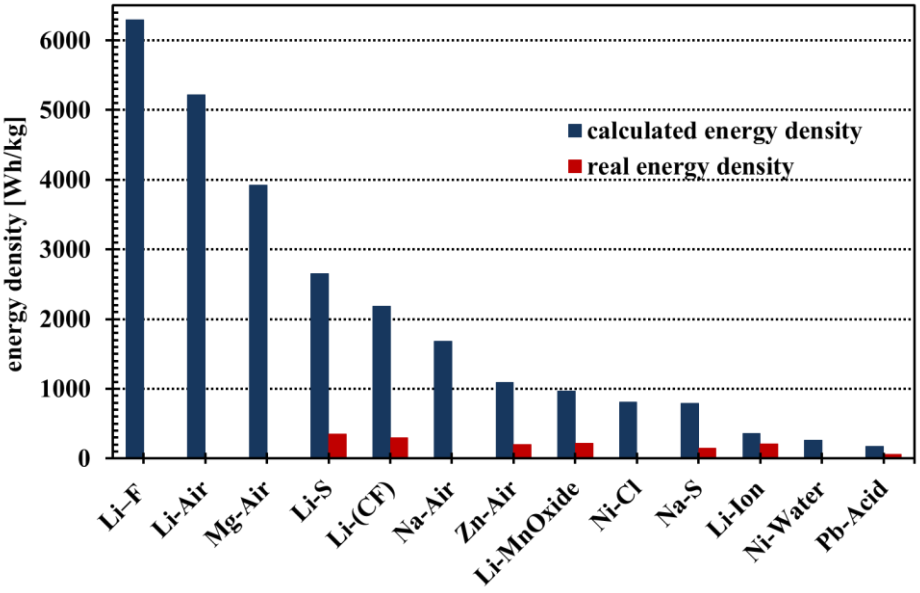

Figure 1: Comparison of the calculated energy density of different Li-ion battery active materials (blue) and the real energy densitiy of a battery stack (red). (The calculation of the values are based on the cathode and anode material. The values can be found in *Energy. Environ. Sci.* 4 (2011) 2614-2624, calculation based on the cathode and anode material Table 2 or S4)

Graphite can take up one Li-atom per six carbon atoms and a maximum specific capacity of 372 $mAh/g_{Graphite}$ can be reached, but typical cathode materials have much lower specific capacities, e.g. at 137 mAh/g for $LiCoO_2$ and 170 mAh/g for $LiFePO_4$.[5,6] Due to these characteristics, todays practical available energy densities of Li-ion batteries range between 150 Wh/kg to 200 Wh/Kg[6,7] which is much below the required value of 500 Wh/kg to

700 Wh/kg to reach the target of a driving range comparable to a gasoline vehicle.[3,5,8] To increase the specific capacity of active material as well as the energy density in a battery system, it is necessary to replace the traditional intercalation electrodes by materials which can store more Li-ions per atom of active material and which are lighter in weight.[9]

One of the most promising candidates in this field is the Li-S battery. Due to the combination of these two light active materials, Li-metal as anode and the elemental Sulfur (S) on the cathode side, a high specific energy battery can be established. In contrast to a commercial Li-ion material, S has the ability to bind two Li-ions per single atom[4,10] and can so provide an energy density of 2600 Wh/kg_{Sulfur}, which in theory is 3 to 5 times higher compared to the Li-ion batteries.[2,5,11,12,13] The big advantages of S compared to Li-ion intercalation materials are that it is cheaper and lighter in weight. Due to the low molecular mass of S (32 g/mol_{Sulfur}), a high theoretical discharge capacity of 1670 mAh/g_{Sulfur} can be reached, which is an order of magnitude higher than what can be achieved with conventional Li-ion materials.[4] However, to utilize the whole capacity of the S cathode a typically used graphite anode with only 372 mAh/$g_{Graphite}$ does not fit anymore and the bare Li-metal anode was re-established. A Li-metal anode can provide 3861 mAh/g_{Sulfur}, which is 10 times more compared to a graphite one, and also represents a nearly infinite Li^+ reservoir. Another aspect of the re-establishment of Li-metal is its light molecular weight (7 g/mol_{Li}), which is beneficial for the energy density of the battery.

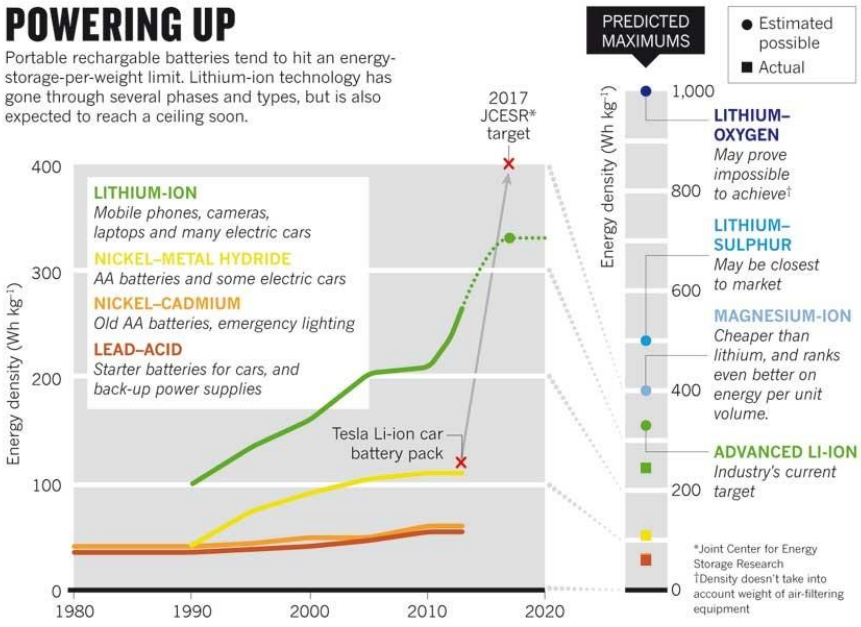

Figure 2: Evolution of the Li-ion technology and future trend. [14]
Reprinted with permission from *Nature* 507 (2014) 26-28. Copyright © 2014 Nature Publishing Group

With this battery system, it would be possible to reach the target of 500 Wh/kg, but the big hurdle for the Li-S battery technology is the transformation of a theoretical promising model into a real, safe and durable system.[15] In the last decade, a lot of research in understanding the mechanism of Li-S batteries[16,17,18,19] was done, and significant improvements in the cathode structure and durability could be noted.[13,20] For the safety issue, highly flammable organic electrolyte solvents were introduced and also gel-type or solid electrolytes were taken into account.[3,21,22,23] Investigations were also done on the Li-anode side and attempts to cover the Li-surface with a protective film to inhibit the shuttle phenomena as well as the dendrite formation were reported.[5,13]

The following work is focused on the improvement of the cathode structure and the discharge capacity as well as the cycling stability. For this, a composite material of S and carbon (S/C-composite) was developed, which is easy and cheap to produce and shows a good electrochemical behavior. The S/C-composite powder is made by a bottom-up approach and the analysis of the synthesised material shows that with this method nano-S could be precipitated homogenously on different carbon black supports and that a good contact between active material and the electrical conducting agent could be obtained. Because the synthesis of the material could be done in two ways and the analysis showed no significant difference between the S/C-composite powders, it will be checked on which route better electrochemical performance could be obtained. Because in Li-ion batteries a resting time after the cell assembly is a common procedure and also in electrical devices the battery has to stay in an open circuit voltage (OCV) state for some time, the influence on the electrochemical performance of an S/C-composite cell will be investigated. Furthermore, the electrochemical behavior of the S/C-composite cathodes with different S loadings in the cathode, different types of carbon black supports and electrolytes with different solvents and additives (e.g. polysulfides) will be tested for their effect on the battery performance that includes cycling stability and rate capability tests.

2. The Lithium-Sulfur Battery

The Li-S battery belongs to the post-Li battery systems that have the ability to undergo a reversible redox-reaction with Li and, due to this fact, they offer a very high theoretical specific capacity and energy density compared to common cathode materials (Figure 3). For the battery industry, S is a very interesting cathode material, because it is naturally abundant, relatively cheap and non-toxic.[8,24,25] Furthermore, at room temperature S is present in its stable S_8-ring configuration and it does not react with air or moisture, which makes the handling and storage of the raw material unproblematic.[4,26]

But for commercial application in the automotive industry, four key factors are not fulfilled, yet. First, the areal S loading of the cathode has to at least 2.5 mg_{Sulfur}/cm^2 to reach realistic capacities of 4 mAh/cm^2 to compete with a Li-ion battery.[28,29] Also, high gravimetric and volumetric capacities in the battery stack have to be realized to get a reasonable driving range for vehicles. Nowadays, Li-ion batteries with a practical energy density of 200 Wh/kg are able to perform up to 1 000 cycles. In an automotive application with an average driving range of 20 000 km/year, this corresponds to a lifetime of approximately 10 years. To be comparable with a Li-ion battery, the cycle life of the Li-S battery has to be prolonged to a minimum of 400 cycles[13] and to compete with a common combustion engine, which has an average driving life of 250 000 km (approx. 15-20 years), 10 000 cycles have to achieved. Last but not the least, the costs of the final product have to be comparable with the commonly usual battery systems and mass production should be possible.

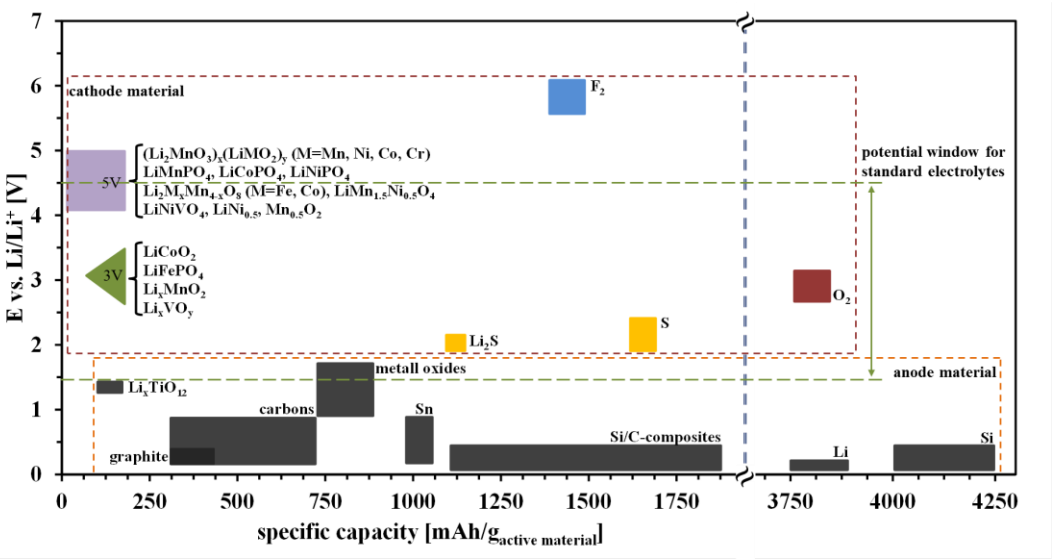

Figure 3: Overview of state-of-the-art battery materials compared to new possible electrode options. [27]
Reprinted with permission from *J. Mater. Chem.* 21 (2011) 9938-9954. Copyright © 2011 Royal Society of Chemistry.

2.1. The working principle

In general, the overall redox reaction in a Li-S battery during a discharge/charge cycle can be described as:

$$S_8 + 16\,Li \rightleftarrows 8\,Li_2S \qquad (2.1)$$

After the S-cathode and the Li-anode are combined in a cell configuration with a Li^+-ion conducting electrolyte, the Li-S battery is present in its charged state. Thus, the assembled cell when connected to an external load will be first discharged. During this process, Li^+-ions migrate from the Li-anode to the S-cathode and react with the solid S_8 to build up S intermediates called polysulfides, which can have different chain lengths (Li_2S_x, 1>x>8). In theory, the reaction from S to Li_2S via polysulfide species occurs in multiple steps.[8,30] But in reality, the potentials of the generated polysulfide species are so close that most often only two potential plateaus will be visible in the discharge curve (Figure 4).

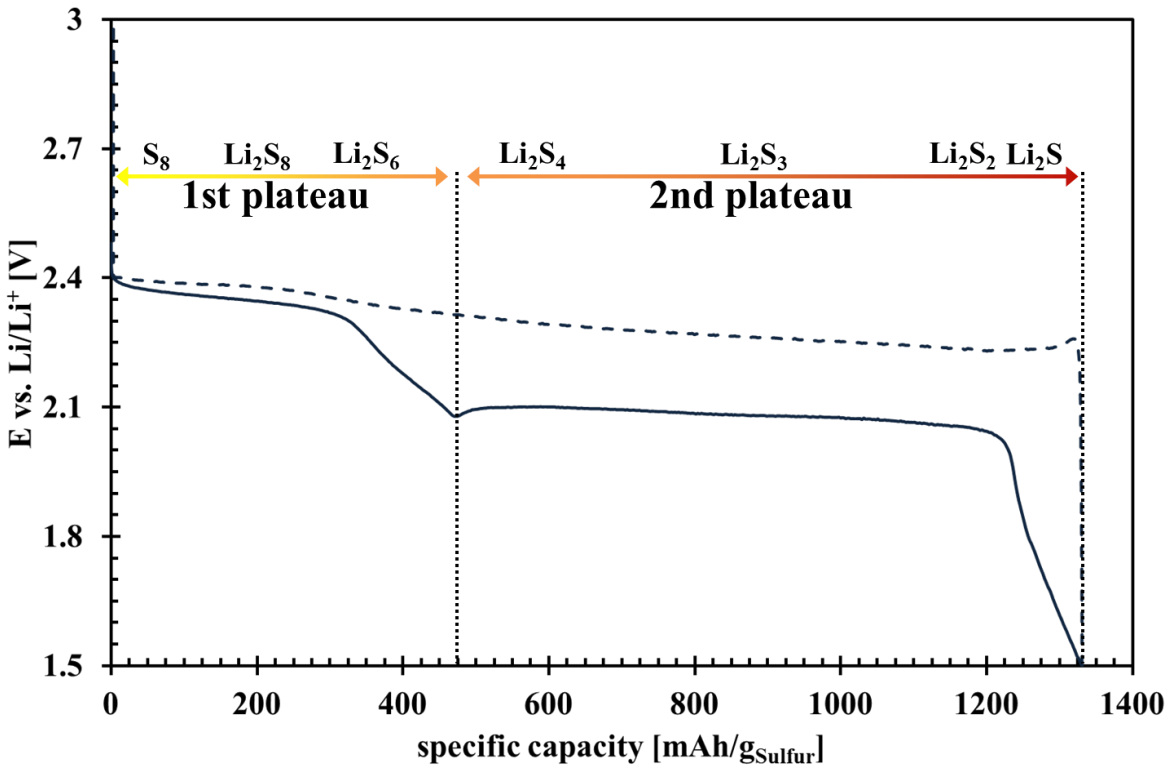

Figure 4: Scheme of a typical discharge and charge profile during a galvanostatic cycle of a Li-S battery

The first plateau appears in the common electrolyte solvents like 1,3-dioxolane (DOL), 1,2-dimethoxyethane (DME) or tetraethylene glycol dimethyl ether (TEGDME) at a potential of 2.4 $V_{Li/Li+}$ to 2.2 $V_{Li/Li+}$.[3,13,17,20] But the on-set potential of the first plateau is strongly dependent on the nature of the used electrolyte solvents, and for solvents with a high dielectric constant like dimethyl acetamide (DMAC) or dimethyl sulfoxide DMSO it can be

observed between 2.6 $V_{Li/Li+}$ to 2.7 $V_{Li/Li+}$.[17,18,31] The electrochemical reaction path of S to Li_2S, starts initially with the opening of the S_8-ring and the reduction to S_8^{2-}, followed by a further reduction to S_8^{4-}, which will immediately dissociate in $2S_4^{2-}$.

$$S_8 + 2e^- \rightleftarrows {S_8}^{2-} \tag{2.2}$$

$${S_8}^{2-} + 2e^- \rightleftarrows {S_8}^{4-} \rightleftarrows 2{S_4}^{2-} \tag{2.3}$$

In solvents with a high dielectric constant (DMSO, DMAC), S_8^{2-} has also the ability to undergo a disproportionation reaction to form $S_3^{\cdot-}$ radical.[18,31] Its formation can be clearly verified in solvents with a high dielectric constant by UV-Vis spectroscopy (absorption at 610 nm) or with bare eye (blue color)[25,32,33].

$${S_8}^{2-} \rightleftarrows {S_6}^{2-} + {}^1\!/_4\, S_8 \tag{2.4}$$

$${S_6}^{2-} \rightleftarrows 2{S_3}^{\cdot-} \tag{2.5}$$

In the second plateau, which is located at a potential between 2.1 $V_{Li/Li+}$ and 1.9 $V_{Li/Li+}$[7,18,20], various chain-growth and disproportionation reactions based on S_4^{2-} will take place (Figure 4). At the end of one disproportionation cycle S_8^{2-} and S_1^{2-} will be created. S_1^{2-} is not soluble anymore and gets precipitated as Li_2S on the S/C-cathode, while S_8^{2-} can again be reduced to S_4^{2-} and a new disproportionation cycle will start. When all reducible species are transferred into insoluble Li_2S and the precipitate insulates the cathode surface, a sharp potential drop will be observed and the discharge step ends.

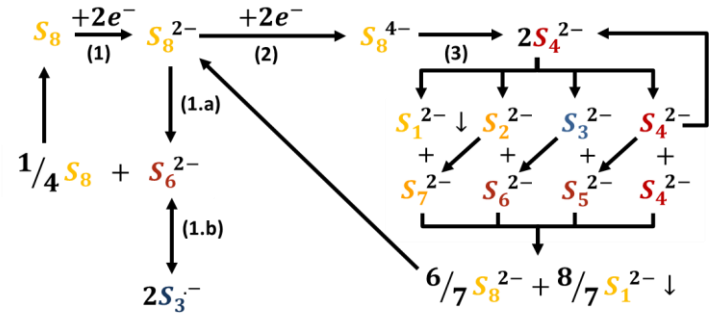

Figure 5: Suggested reduction and disproportionation mechanism during the discharge of a Li-S battery.[18]
Reprinted with permission from *J. Phys. Chem. C* 118 (2014) 5733-5741. Copyright© 2014 American Chemical Society

Compared to the discharge profile, in the charge step only one long plateau can be observed and the slope shows a slow increase in potential. When the current switches from negative to positive and the charge step gets started, a small overpotential is mostly needed to start the

oxidation of precipitated discharge product Li_2S.[34] The height of the potential peak depends on the used electrolyte solvent. In solvent with a high dielectric constant like DMSO or DMAC, the overpotential is small or not visible, but in solutions with a low dielectric constant, e.g. DOL:DME or TEGDME, it is comparably high. After the initial activation of the precipitated material, the potential drops to approximately 2.0 $V_{Li/Li+}$ and then gradually increases again to 2.4 $V_{Li/Li+}$. During the charge step, Li_2S will be transformed back to S, which will be deposited on the S/C-cathode. At the end of the charge step, ideally no oxidizable species are left and the potential starts to increase rapidly, which can be observed by a vertical slope in the charge curve.[35]

2.2. The Lithium anode

To tap the full potential of an S-cathode and create a balanced full cell system with a low weight, the common Li-ion anodes like graphite are not compatible anymore, because of their 4.5 to 10 times smaller specific capacity. The need of an anode with a sufficiently high specific capacity led to the re-launch of bare Li-metal as possible candidate. In terms of specific capacity (3860 $mAh/g_{Lithium}$) and weight it is a perfect match for the S-cathode (Figure 3).

The drawback, however, of batteries with metallic Li anodes are the poor safety aspects. Li is known for its high reactivity, especially with water (reaction 2.6). So, Li has to be handled and stored at least under dryroom conditions or even better in an inert atmosphere.

$$Li + H_2O \rightarrow LiOH \downarrow + {}^{1}/_{2}\, H_2 \uparrow \qquad (2.6)$$

In a Li-S battery cell further undesired behaviors of the Li-metal anode can be observed. First of all, the deposition of Li^+-ions on the Li-surface during charge is often not homogenous and results in the formation of so called Li dendrites.[36,37] Due to the stress imposed on the solid electrolyte interface (detailed description in Chapter 2.3; SEI) during the deposition of Li^+-ions on the anode, the SEI film can crack and the raw surface has access to the electrolyte. At these locations, Li^+-ions will be precipitated preferably, because of the higher electronic and ionic conductivity, which eases the reduction to metallic Li. In the course of time, more and more Li fibers will grow out of the surface and cover the anode. At that stage, the Li^+-ions will get predominately reduced at the kinks or tips of the Li fibers (Figure 6 [a]). When the plated Li gets oxidized to Li^+-ions, first the deposited metal at the kinks and tips will react and then at the base. The fiber can be cut from the Li-surface and dead Li will be generated (Figure 6 [b]). When the fibers do not lose the connection to the Li-anode, they can grow

through the separator towards the S-cathode and induce a short circuit, which can result in a thermal runaway of the battery cell.[38,39]

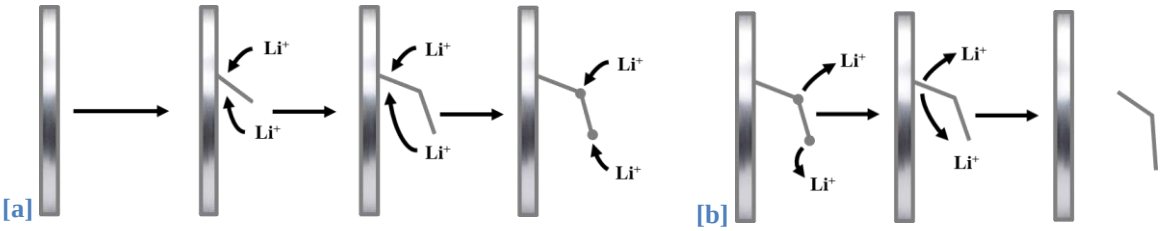

Figure 6: A possible mechanism of [a] dendrite growth during Li^+-deposition and [b] decoupling during Li^+-dissolution.[36]

Due to the small surface area of the Li-anode, high C-rates (high currents) cannot be realized without high capacity losses in a Li-S battery. When high currents are applied, Li is not able to provide enough energy carriers under this condition and the cell capacity breaks down immediately. This is a big issue for the application in vehicles, where high power, i.e. high currents, are required.

2.2.1. Alternative anode material

Despite the high specific capacity of pure Lithium as anode, the disadvantages like dendrite growth, which leads to safety issues in a battery cell, and the bad electron density distribution at high currents, hinder the technical application of this material at the moment. But, there are approaches to substitute the Li anode through different anode materials. One option could be graphite, but the potential of this anode is comparable with the Li anode potential and the issues with dendrite growth, especially at high C-rates, and Lithium plating on the anode structure during cycling are present.[40,41] Also, the small specific capacity (372 $mAh/g_{Graphite}$) makes Graphite uncomely as candidate.

If one wants to use the full capacity of the Sulfur cathode, the anode material has to have a high theoretical specific capacity, like Silicon (Si) and Tin (Sn). These two candidates come into consideration to fulfill these requirements (Figure 3). With a molar weight of 118.7 g/mol Sn is relatively heavy, but it has the ability to take up $4.4e^-$ per single atom and so the theoretical specific capacity lies at 993 mAh/g_{Tin}.[20,21,42] Electrochemically, Si can take up $3.75e^-$ per single atom, which results in an exceptionally large theoretical specific capacity of 3577 $mAh/g_{Silicon}$ and with 28.1 g/mol it is even lighter than Sn. [43,44] Both metals have a good electron conductivity and usually they are used in different nanostructures (nano powders, nanotubes, etc.), so high currents can be realized during cycling of a battery cell.[21,28,45] The

reported trials in the literature showed that it is possible to either combine the pre-lithiated metal anodes with a S-cathode or to combine a Li-free metal anode with a Li_2S cathode. But the new anodes suffer from volume changes during cycling, which destroys the electrode structure, leading to a loss of discharge capacity over time, and to a low cycle life of the battery.[21,42,43,44,46]

2.3. Challenges in Lithium-Sulfur Batteries

The use of Li and S in a battery is also associated with big challenges, which are influencing the cycling stability and hinder the commercial success of the system, despite its high theoretical capacity and energy density.[13,15,20,47]

2.3.1. Insulating Sulfur

First of all, a big hurdle is the non-conductive nature of S and its lithiated discharge product Li_2S. S has a very low electric conductivity of $5x10^{-30}$ S/cm (25°C)[13,24] and Li_2S is with a conductivity of 10^{-14} S/cm[47] and a band gap of 3.865 eV[48] at the edge between semi-conductor and insulator. To overcome these issues, an electron conducting support for the S is needed, which are in general carbon blacks. If the carbon support has additionally a high surface area this will be also advantageous, because the S can be finely distributed and a good electronic connection can be obtained.[13] But the addition of a support will lower the specific energy density of the battery stack, because of the additional weight of the inactive material. Unfortunately, S and Li_2S are not only bad electronic conductors; the ionic conduction is poor as well. To overcome this issue, electrolyte solutions with high ionic conductivity are required. Furthermore, the particle size of the S plays an important role and the particles should be small and homogenously distributed on the surface of the carbon black to get a good electronic connection between the support and the active material.[20,49]

2.3.2. Loss of active material

In almost all S/C-electrode systems described in the literature, the biggest loss of discharge capacity is observed between the first and the second cycle. The decrease in capacity can be attributed to the loss of active material, which is caused by two main reasons.

The deficit can be attributed to the morphology change of the S/C-cathode between the discharge and charge step and irreversible side reactions between polysulfide species and the Li-anode during the SEI formation. In the first discharge of a fresh Li-S cell, the solid S will be transferred into dissolved polysulfide species. Due to this process, void space in the carbon

framework is generated, which leads to a fragile host structure, especially in S/C-cathodes with a high S loading. The remaining carbon skeleton is not able to withstand the pressure inside the Li-S cell and a partial collapse of the carbon black structure is the consequence. The collapse leads to a loss of active surface area, which is not available anymore in further cycles.[50] Furthermore, parts of the S can be embedded and are rendered electrochemically inactive. In the first charge of an S/C-battery, the electrolyte reacts with the Li on the anode surface, which leads to a passivation layer formation. This layer is also called solid electrolyte interface (SEI) and protects the anode as well as the electrolyte from further damage. Ideally only the electrolyte and the Li-anode are involved in this process, but during the charge step polysulfide species will take part in the SEI-formation (Figure 9) and get incooperated in the SEI. Especially in S/C-cathodes with a low S loading, this phenomenon will be a major reason for the active material loss and the so induced discharge capacity loss.

At the end of each discharge cycle Li_2S gets precipitated on the carbon black surface, preferably at locations with a high current density. This leads to areas with thick Li_2S films or big Li_2S particles. In the following charge step, the active material at the surface of the carbon support will be oxidized first and can induce a loss of electrical contact between the upper layers of the film or the remaining part of the Li_2S particles[51,52,53,54]. If that happens, the active material is getting inactive and a decrease in discharge capacity in the next cycle is the consequence. The remaining Li_2S residues also have a passivation effect on the S/C-cathode and increase the cell resistance, which results in a higher polarization.[55] In subsequent cycles, this phenomenon can also be observed, but to a lesser degree. [50,51,56,57]

In subsequent cycles, the degradation of the Li-S battery has several causes, in which both electrodes, the S/C-cathode as well as the Li-anode, are involved. The damage on the S/C-cathode will be caused by the different densities of S and Li_2S (2.07 g_{Sulfur}/cm^3 vs. 1.66 g_{Li2S}/cm^3). Between the discharged and charged state the volume changes about 145%[I] and due to the expansion of the product the stiff carbon black structure will break and gets pulverized.[58,59] Beside this, further electrically isolated S islands can be created in the carbon matrix or new Li_2S films on the S/C-cathode can be formed, in which the S is not accessible anymore.[20,54] At the discharge step, Li^+-ions get dissolved from the anode surface and have to diffuse through the SEI layer. During this process, the SEI layer can crack at some spots

[I] 1 g of S_8 equals 0.18 g of Li_2S. With $\rho = \frac{m}{V}$ the volume of the two species could be calculated and results in $V_{S_8} = 0.48\ cm^3$ and $V_{Li_2S} = 0.11\ cm^3$. It is assumed that in the charged state only S_8 is present and will be totally converted to Li_2S during the discharge step. V_{S_8} is set as 100%, which results in a volume change of 80% between S_8 and Li_2S.

and the bare Li-surface is again exposed to the electrolyte. In the following re-charge of the cell, a new film has to be built at these locations and leads to a further consumption of polysulfides, electrolyte and Li.[54,59,60,61] As mentioned above, the Li-plating during the charge is not homogenous and will preferably take place at spots with a high local current density and so dendrites will be formed over time. When Li gets plated on them, also a new SEI layer has to be formed and active material will be irreversibly consumed. The sum of these issues leads to a constant degradation and limits the cycle life of the Li-S battery dramatically.

2.3.3. Polysulfide shuttle

As described above, S builds up intermediate species in between discharged and charged state. In common electrolytes like DOL:DME or TEGDME, they are highly soluble and can reach concentrations up to 10M.[25,33,36,62] The dissolution of S starts immediately when the electrolyte get in contact with the S/C-cathode and will react with the Li^+-ions from the electrolyte to polysulfide species. The intermediate species can diffuse to the anode side where they get reduced and cause an internal short cut, because the electrons, which are involved in this reaction, do not flow through the exterior circuit. The phenomenon can be observed at OCV or during the charge step while the Li-S battery is cycled and is also known as polysulfide shuttle.[36,50,52,63,64,65,66,67]

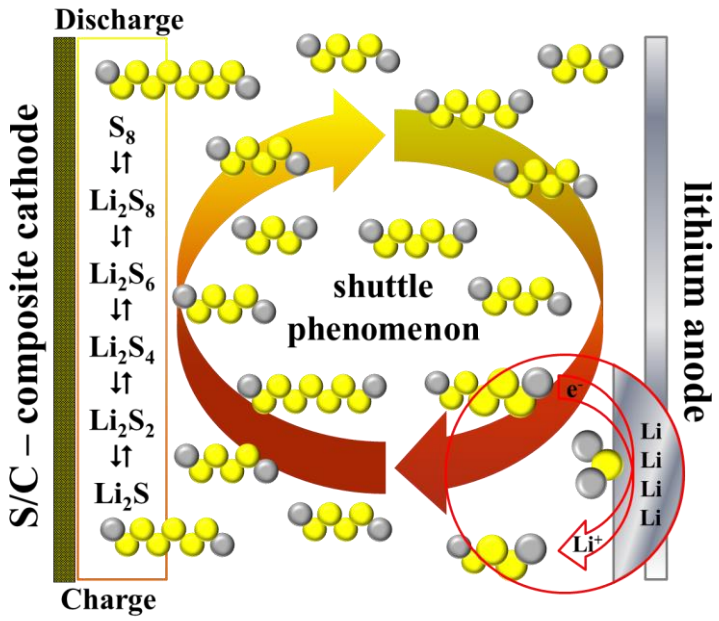

Figure 7: Schematic of a Li-S battery during the discharge and charge state and the polysulfide shuttle phenomenon, as described in past literature.[4,68,69]

Figure 7 shows a scheme of the polysulfide shuttle inside a Li-S battery. The dissolved polysulfides are not fixed at the cathode side of the cell and can diffuse to the Li-anode. Because of the direction of the electron flow during the charge step, they get reduced on the Li-surface from long-chain polysulfides to short-chain polysulfides. The shorter polysulfides can diffuse back to the S/C-cathode where they get oxidized again. This can lead to a circular flow of the polysulfides, in which they alternately get reduced and oxidized.

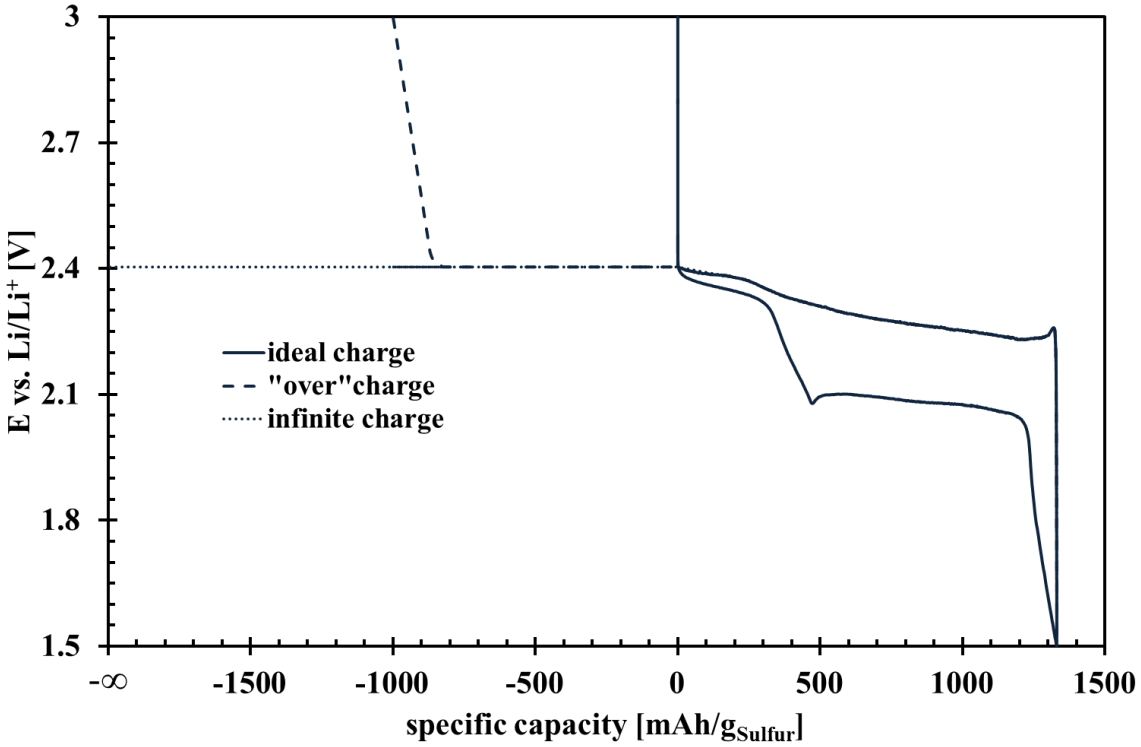

Figure 8: Exemplary cycling profile of a Li-S battery with an ideal charge (solid line), an "over"charge (dashed line) and an infinite charge (dotted line)

When the shuttle current is on the order of the current for the galvanostatic charge, the charge capacity is higher as the discharge capacity and in the worst case the battery will be infinitely charged (Figure 8).[69,70] The polysulfide shuttle reaction does not consume active material and protects the Li-S battery against overcharge[36], but the coloumbic efficiency will be lowered and the circuit essentially contributes to the self-discharge of a Li-S battery.[67,68,71]

$$(x-1)Li_2S_x + 2Li^+ + 2\,e^- \rightarrow xLi_2S_{x-1} \qquad (2.7)$$

When the shortened polysulfides do not diffuse back to the S/C-cathode, they will get further reduced and create solid precipitates on the Li-surface. If insoluble S-species are deposited, an irreversible loss of active material will be caused.[20,67] This leads to passivation of the anode, which inhibits the growth of dendrites but also increases the polarization of the electrode.[34,36,55]

$$Li_2S_x + 2Li^+ + 2e^- \rightarrow Li_2S_{x-1} + Li_2S \downarrow \quad (2.8)$$

$$Li_2S_x + 2Li^+ + 2e^- \rightarrow Li_2S_{x-2} + Li_2S_2 \downarrow \quad (2.9)$$

To reduce or even inhibit the currently described shuttle mechanism, different additives can be added to the electrolyte solution. Depending on their chemical nature, they can help to improve the stability of the SEI on the Li-surface (e.g.. P_2S_5, LiBOB or toluene) or oxidize the precipitate Li_2S on the Li-surface (e.g., LiBr).

Commonly, the most used additive salt is Lithium nitrate ($LiNO_3$) to suppress the shuttle phenomenon and increase the cycle life as well as the coloumbic efficiency of the Li-S battery.[59,147] When $LiNO_3$ gets in contact with the surface of the Li-anode, it gets reduced to Lithium nitric oxides (Li_xNO_y) or oxidizes polysulfide species to form different Lithium sulfate types (Li_xSO_y). The products of both reactions are not soluble in the electrolyte solution and will precipitate on the Li-surface. On the bare anode surface, also the other components of the electrolyte like the solvents, conductive salt or the polysulfides will react to solid residues. But only after the combination with the deposited products from $LiNO_3$, a stable and effective SEI will be built on the Li-surface, which minimizes the reaction of polysulfides on the anode and enhances the overall performance of the Li-S battery.[72]

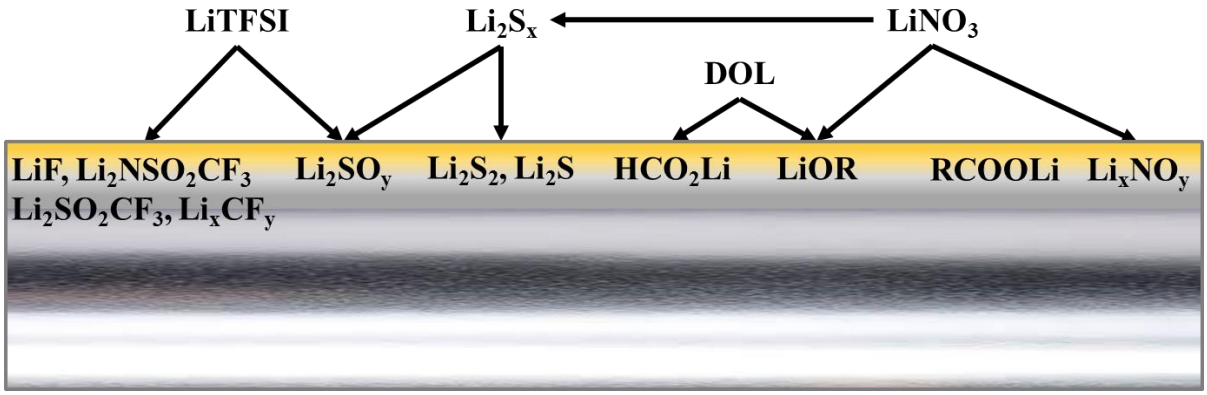

Figure 9: Schematic of various products formed in an electrolyte mixture of DOL, LiTFSI, $LiNO_3$ and polysulfides after contact with the bare Li-anode surface.[59]
Reprinted with permission from Electrochem. Soc. 156 (2009) A694-A702. Copyright© by The Electrochemical Society.

2.4. Concepts of S/C-cathodes

Because of the low conductivity S has to be generally combined with a conductive support. A look in the literature shows different possibilities to interconnect the two materials, and in the past ball milling of the S/C-cathode materials or grinding them together manually before coating on a current collector were the common way to produce an S/C-cathode.[31,58,56,73,74,75]

But the cycling performance of these electrodes was bad, because of the weak connection between the carbon black support and the active material as well as the big particle size of the commercial S (µm range).[20,24] Nowadays, the main strategies to adhere the active material to the conductive host, which deliver promising results, are: homogenous distribution in a high surface matrix and establishing a chemical or physical barrier to hinder the diffusion of the polysulfide.[20,47,67,76] Therefore, different types of nanostructured carbon black particles with high surface area, nanofibres, nanotubes, nanowires, graphene or graphene oxides were used, but also aerogels, sponges and inorganic materials like TiO_2 or metal organic frameworks were investigated as possible carrier material.[20,36] To incorporate the S in the carbon structure the most common methods are melt-infusion[77,78,79], deposition from the vapor phase[80,81,82] or precipitation from the liquid phase.[83,84] The combination of the highly structured carbon matrix and the fine distribution of the S, lead to thin S-films or small S-particles and a good electronic connection between the two materials.[51,85,86] A high pore volume in the carbon black has also a beneficial effect on the cell performance. It has the ability to cushion the volume change between S and Li_2S, and high S loadings in the composite can be achieved.[87,88,89] These approaches lead to good discharge capacities in the beginning, but nevertheless the active material loss is still quite high, due to the shuttle mechanism. To minimize the loss of S and to increase the cycle stability, different innovation were made to trap the active material on the cathode side. The simplest option is to optimize the pore size distribution in high surface carbon blacks. A good ratio between meso and micro pores has a beneficial effect on the cycling stability and lowers the active material loss, because the small pores have the ability to chemisorb S and polysulfides, while the bigger pores offer electrolyte and Li^+-Ions for the electrochemical reaction.[88,90,91,92,93,94] But the chemisorption of the active material cannot be compared to a molecular bond, and in the long term the decrease in discharge capacity due to the active material loss is still prominent. To enhance the absorption ability of the substrate, nitrogen doping of the carbon black surface can be done to influence the electronic structure of the surrounding oxygen atoms and increase their potential to bind polysulfide species. With this method, higher discharge capacities and a better coloumbic efficiency could be obtained.[67,88,95] The incooperation of a physical barrier is another possible method to improve the cycling performance of a S/C-cathode. This can be realized by coating the primary S/C-cathode structure with a conductive polymer film consisting of e.g., poly(3,4-ethylene dioxythiophene) plus poly(styrene sulfonate) or graphene.[47,97,148] The active material can also be encapsulated in a core shell structure.[81,98,99] For the hollow spheres, in general conductive polymers like

polythiophene[99], Poly(3,4-ethylenedioxythiophene)[98] or polyaniline[81] were used as material for the shell. Inside of these "micro-reactors" the polysulfides are trapped and an agglomeration of S can be inhibited, which leads to a good electronic contact.[20] But this structure has one big drawback: the hollow spheres are completely filled with S and in long term experiments they are not able to buffer the volume change between the two basic materials sufficiently, which results in a burst of the outer shell. To deal with this issue, only the inner surface of the shell was coated with S [81] or a yolk-shell strategy was pursued.[100,101] For the yolk-shell approach also polymers like polyaniline[101] can be used as basis for the outer skin, but inorganic materials like titanium oxide (TiO_2) can be taken into account, too.[4] Due to the free space of the hollow sphere, the active material can expand without damaging the shell and good cycling performances with a low capacity decrease are reported.[4,97] A similar effect can be achieved in frameworks assembled from nanotubes/nanorods units or in carbon sponges synthesised via a graphene precursor. These structures can buffer the volume change excellently, high S loadings can be realized and great cycling performances could be achieved.[51,102,103,104] Additionally, the electronic conductivity and the mechanical stability[105,106,107] of the S/C-cathode will be improved by nanotubes, nanorods or nanofibres and so an electrode without binder or additional current collector like aluminum can be built, which minimize the "dead" weight and increases the energy density of the S/C-cathode.[83,108,109]

There are a lot more strategies and possibilities to create S/C-cathodes with highly structured carbon supports, which help to increase the cycling performance of an S/C-battery, enhance the mechanical stability of the S/C-cathode or decrease the diffusion of polysulfide to the anode side by adsorption or impermeable embedding of the S in the host structure. For example, electro-active polymers can be used as support, not only as physical barrier in form of a coating on a conventional S/C-cathode. Furthermore, inorganic Magnéli phases[110,111] have a high polysulfide adsorption ability and allow a homogenous deposition of Li_2S, also, metal organic frameworks[112,113] can be considered, because of their stable structure and high internal surface area. One´s attention is also turned on graphene, which offers a high surface area[114] and graphene oxide, which has the capability to trap polysulfides successfully[115] and in combination with other materials or as modification of the basic material, great cycling results could be obtained.[116,117,118119]

The above mentioned support materials with their different structures and various strategies, how they were synthesised, can be mixed up and lead to a nearly infinite range of possible

host structures in which S could be embedded. But the clear focus in designing a new S/C-cathode structure do not lie anymore exclusively on high cycle numbers, also the amount of S in the S/C-composite should be higher than 50wt% to increase the energy density of the S/C-battery and a mechanically stable support structure with the ability to impede the polysulfide shuttle to minimize the capacity loss over cycle time have attracted major attention.[20,24]

3. Experimental

3.1. S/C-composite synthesis

The cathode material was synthesised via a bottom up approach investigated by Himendra Jha[II]. The goal of the synthesis is making an S/C-composite, in which the carbon acts as support for the active material (S) and the S coats the carbon black particles or settle on them as small crystals with a homogenous distribution (Figure 10).

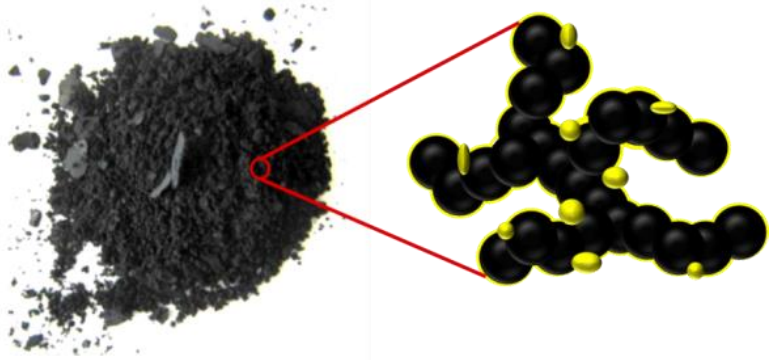

Figure 10: S/C-composite powder with estimated structure on nano-scale

3.1.1. Standard synthesis route

To realize the aim of the invention, the S was precipitated from a precursor solution (Figure 11). Therefore, a 1 molar (M) sodium thiosulfate ($Na_2S_2O_3$) water-based solution was chosen. For a targeted amount of around 2 g of S/C-composite and Sulfur-to-carbon-ratio of 66 wt%S to 34 wt%C, 120 mL of the 1 M $Na_2S_2O_3$ solution was provided in a big glass beaker and placed under an ultrasonic horn in a fume hood and 1.6 g of a carbon support (TANAKA KIKINZOKU International K.K., Table 7) was added. The mixture was then sonicated for 30 min in a pulsed mode (1sec on, 0.5sec off) to disperse the carbon particles in the $Na_2S_2O_3$-solution. The pulse mode was chosen to break up bigger agglomerates and distribute the carbon particles homogenously in the solution. Furthermore, it avoids excessive heat generation during the sonication process. To precipitate the S on the carbon, support a proton source is needed. Therefore, different acids are possible candidates (Table 3), but the choice which one is suitable depends on the resulting salts and their solubility in water, because the byproducts of the syntheses have to be removed at the end. Here, we decided to use nitric acid (HNO_3), because the resulting sodium nitrate salt ($NaNO_3$) has a very high solubility compared to the other salts (almost 2.5 times higher than sodium chloride (NaCl)) and for this reason it can be completely removed in the washing step.

[II] Current address: Atotech Deutschland GmbH, 10553 Berlin, Germany

To maintain the distribution of the carbon and to get homogenous S precipitation, the suspension was sonicated during the addition of 250 mL of 1 M HNO_3-solution. The acid was poured in slowly to avoid a high local S concentration, which can lead to an inhomogeneous S distribution and big particles. As soon as the acid gets in contact with the $Na_2S_2O_3$-solution, the following reaction takes place:

$$Na_2S_2O_3 + 2HNO_3 \rightarrow SO_2 \uparrow + H_2O + S \downarrow + 2NaNO_3 \qquad (3.1)$$

During the synthesis, also Sulfur dioxide (SO_2) is generated, which is a toxic gas. For that reason, the synthesis was conducted in a fume hood to ensure safe working conditions. To be sure that the components are well mixed and the S is homogenously distributed on the carbon support, the sonication was applied for further 20 min. After the second sonication, the mixture was filled in a Schott bottle with a capacity of 1 L and set aside until the so created S/C-composite settled down, which takes in general approximately 15 min. Subsequently, the solution on top can be simply poured out.

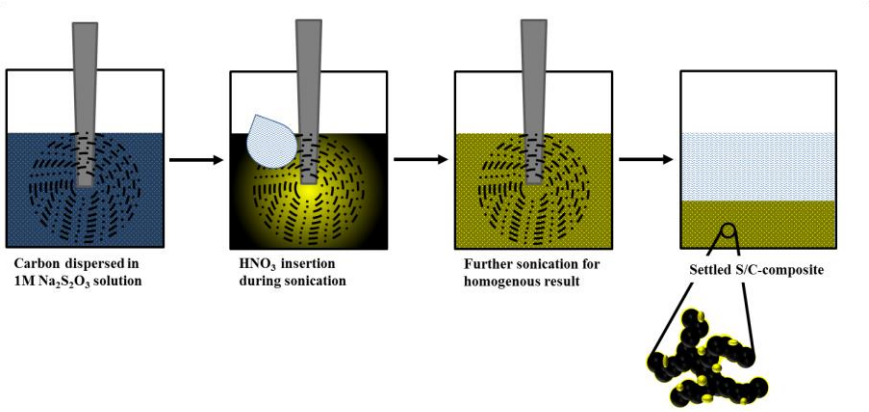

Figure 11: Standard synthesis route for the S/C-composite.

To quantitatively remove the remaining salt, the settled S/C-composite was washed three times with an excess of ultrapure water (Millipore, EPod, 15MΩ@25°C) in excess. Therefore, a stirrer was used to suspend the S/C-composite in the fresh water. After a short rest, the S/C-composite settles down again and the salt contaminated water can be decanted in between each washing step. Because of the high solubility of the resulting $NaNO_3$ salt, three times of washing is sufficient and no residual of the salt can be found in the final dry S/C-composite. After the washing step, the S/C-composite was first filtered through a filter disc with a separation range from 8 µm to 12 µm (Munktell 389, ø110 mm, Munktell & Filtrak GmbH) and dried at room temperature for 24 h to remove the main amount of water. Afterwards, the pre-dried S/C-composite was transferred in a mortar to grind it into a fine powder, which was

dried again at 45°C for 72 h in a Büchi oven to remove the remaining water in the S/C-composite. The manufactured S/C-composites were stored in a Schott glass flask in a drying cabinet to avoid soaking up of water from the air.

Table 1: Possible acids for S/C-composite synthesis and the resulting salts with their solubility in water

Acid	Resulting salt	Solubility
		[g/100mL$_{H2O}$]*
HCl	NaCl	35.9
$H_2C_2O_4$	$Na_2C_2O_4$	3.7 (at 20°C)
H_2SO_4	Na_2SO_4	17.0
HNO_3	$NaNO_3$	92.1

***(at 25°C)**

3.1.2. Alternative synthesis route

The above described synthesis is the standard synthesis route for our S/C-composite, but it can also be prepared on an alternative second synthesis route (Figure 12). Therefore, 250 mL of 1 M $Na_2S_2O_3$ water-based solution was provided without any carbon support and was placed below the sonication horn in the fume hood. In the first step the S was precipitated from the $Na_2S_2O_3$-solution with the nitric acid during sonication. This results in a colloidal S solution. In the second step, the carbon support was added and the mixture was sonicated for additional 30 min, to get the targeted homogenous distribution of S on the host surface. Further processing of the resulting S/C-composite, follows as described in the standard synthesis route.

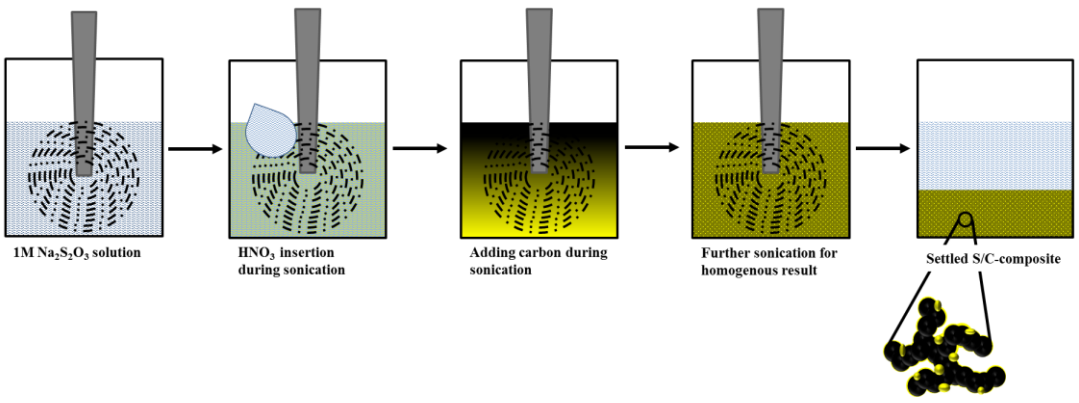

Figure 12: Alternative synthesis route for S/C-composite

The whole synthesis is patented and can be reread in the patent publication DE 10 2013 005 082 A1.

3.2. Composite characterization

In theory, it was expected that the synthesis would deliver a homogenous distribution of the precipitated S-particles on the carbon host, similar to a film without bigger agglomerates or isolated S-islands. To prove that the synthesis was successful and resulted in the expected morphology as well as the targeted amount of S, three different analysis methods were chosen to investigate these issues.

3.2.1. X-ray diffraction analysis

First, the S/C-composite was subjected to X-ray diffraction (XRD) analysis, to determine if the S had a crystalline or amorphous structure. The XRD-patterns were recorded with a STOE Stadi P diffractometer equipped with a linear position sensitive detector (Dectris Mythen 1K, STOE Darmstadt). For the sample preparation a piece of scotch tape was cut from a roll and a small amount of S/C-composite was placed on one half of the adhesive side. Then, the other side of the tape was placed above to trap the powder inside. Afterwards, the tape was cut in a suitable size, which fitted in the sample holder and was fixed with three screws. The so prepared S/C-composite sample was taken in the diffratometer sample holder. The XRD-patterns were measured over a range of 10° to 60° 2θ. The exposure time of each range was 15 min and repeated for 3 times, which adds up to an acquisition time of 45 min for each pattern.

Figure 13: X-ray diffractometer from STOE

During the measurements, the sample was rotated to get an average signal over the whole sample. The final pattern was analyzed with WinXPow (Version 3.0.2.1, 2011, STOE & Cie GmbH), by which the measured pattern was verified to correspond to Sulfur using the literature database ICDD.

3.2.2. Scanning electron microscopy and energy dispersive mapping

The XRD-pattern delivered information about the structure of the S in the S/C-composite powder, but not about the distribution and the shape of the S on the carbon support. Therefore, a scanning electron microscope (SEM) combined with an energy dispersive mapping (EDX) feature was used, to get the information about this issue. With the SEM, the formation of big S-particles or isolated S-islands during the synthesis process can be excluded and from the EDX analysis, the distribution and homogeneity of S and carbon in the S/C-composite can be determined. The pictures were carried out by a JEOL, JSM 5900 LV or a JEOL, JCM-6000 NeoScope™. The sample was prepared at ambient conditions and fixed on the sample holder with a carbon or copper tape. After the preparation, the sample holder was inserted in the vacuum chamber and evacuated subsequently. The measurements were carried out with a beam power of 5kV to minimize the local heating of the S/C-composite and to avoid the evaporation of the S during the analysis time.[III]

3.2.3. Thermo gravimetric analysis

Last but not least, the weight ratio of Sulfur-to-carbon in the S/C-composite was determined by thermo gravimetric analysis (TGA, Mettler Toledo, STAR®-System). For the measurement of the ratio of the components, 8 to 10 mg of the S/C-composite powder was taken. With the assistance of a micro balance (XP6, Mettler Toledo) the samples were weighed in a crucible. Afterwards, the crucible was placed in the furnace of the TGA and the measurement was started. The sample was first heated up to 400°C at a heating rate of 20 K/min under a constant Ar gas flow of 50 mL/min to remove the gaseous S, which starts to evaporate at 320°C to 400°C, depending on the used carbon support. At 400°C, the temperature was held for 10 min to make sure, that the entire S is evaporated. Then the purging gas was changed to oxygen with a gas flow of 5 mL/min and the temperature was held for additional 10 min, to be sure that the Ar is completely removed from the furnace. Afterwards, the sample was further heated up to 1100°C, with the same heating rate of 20 K/min and kept at this temperature for 10 min, to make sure that the carbon support was fully burned. The heating procedure used here was divided in two parts, because of two reasons. In the first step, Ar was used to avoid side reactions of S, which has a high reactivity with oxygen to Sulfur oxide species (SO_x). Afterwards, the purging gas was changed to oxygen, to burn the carbon to carbon dioxide

[III] SEM and EDX measurements were done by Dr. M. Hanzlik from the "Fachgebiet Elektronenmikroskopie"

(CO_2) at around 550°C, because the evaporation temperature of carbon is much higher and the device has temperature limitations.

In this study, only the first S/C-composites were examined with all three methods. Since, no changes between the synthesised batches could be determined, for further S/C-composites it was assumed, that the morphology of the powder does not change and the Sulfur-to-Carbon ratio was determined only by TGA, to calculate the exact amount of S in each S/C-composite cathode.

Figure 14: Thermo gravemetric analysis device from Mettler Toledo

3.2.4. Nitrogen absorption analysis

The four carbon blacks which were used as support for the S in the S/C-composite, offer different values for the surface area and pore size. To get the exact numbers for each sample, it was examined by nitrogen physisorption at 77 K (-196.15°C) on a Quantachrome Autosorb–iQ instrument. In the first step, the carbon had to be pretreated to make sure, that the pores and the surface are water free. This step is done very carefully, because residual water can block pores and distort the received values. Therefore, the samples to be measured were filled in a glass tube and dried for 12 h at 350°C under dynamic vacuum. Afterwards, the adsorption and desorption isotherms in a relative pressure range of $10^{-5} \leq (p/p_0) \leq 0.995$ were measured. For Vulcan XC72, Ketjen Black and Black Pearls, the BET surface area was calculated from the adsorption curve with the best fit between $0.01 \leq (p/p_0) \leq 0.25$, and the desorption curve delivers the information about the surface area of the micropores, their size and volume, which was calculated by the t-method of Lippens and deBoer with the best fit between $0.15 \leq (p/p_0) \leq 0.40$. To get the values for the external surface area of these carbons, the areas of the micropores (pore size ≥ 10 nm), which were calculated from the t-plot, were subtracted from the BET surface areas. Because of the absence of mirco- or mesoporosity in the Super C65 carbon, dense spheres can be assumed and the specific surface area can be estimated with the following equation:

$$surface\ area_{\ external} = \frac{6}{(\rho \cdot d)} \tag{3.2}$$

where ρ is the bulk density ($\approx 2\,\frac{g_{Carbon}}{cm^3}$) and d is the particle diameter.

3.3. Preparation of the S/C-composite cathodes

To investigate the electrochemical performance of the before described S/C-composite, the synthesised powder has to be brought in a measurable form – an electrode. Therefore, the powder was mixed with a binder and a solvent to prepare an ink, which can be coated on an aluminum current collector. After drying the resulting film, electrodes of desired shapes and sizes can be punched out.

3.3.1. S/C-composite ink preparation

For the cathodes 85 wt% of S/C-composite powder and 15 wt% of binder was used. As binder polyvinylidene fluoride (PVDF, Kynar HSV900) was chosen, because of its good thermal and chemical stability as well as its easy handling. To disperse the S/C-composite powder and prepare a paste with the PVDF binder, N-methyl-pyrrolidone (NMP, Sigma-Aldrich, 99.5%) was used as solvent. Despite its toxicity and high boiling point, NMP has the lowest vapor pressure of the few possible solvents, in which the PVDF binder can be dissolved. In solution, the long polymer chains of the binder wrap up the S/C-composite particles and connect them amongst themselves and with the current collector foil. The amount of NMP strongly depends on the surface area of the used carbon type in the S/C-composite and the preparation method of the cathode. It can range between 4 mL/g_{solid} and 8 mL/g_{solid} for Method 1 and 2 mL/g_{solid} and 5 mL/g_{solid} for Method 2.

To get a homogenous ink of suitable viscosity, in which the PVDF is dissolved and the S/C-composite is well dispersed, two methods were tested:

Method 1- stirring on heating plate

In the beginning, we used a stirring method to prepare the inks for the electrode coating. Therefore, the dry ingredients were placed in glass bottle with a stirrer and were dry mixed at 1000 rpm for approximately 2 min to distribute the dry compounds homogenously. A good mixing is reached, when the black S/C-composite and the white PVDF form a greyish powder. Then, the NMP was added and the suspension was stirred for at least 2 h at 50°C. After 2 h of stirring time, the glass bottle with the ink was opened to check the texture of the

slurry by eye. If the ink is getting thick and viscous, it can be further processed. When the slurry is still too liquid, the stirring time was extended till the right viscosity is reached.

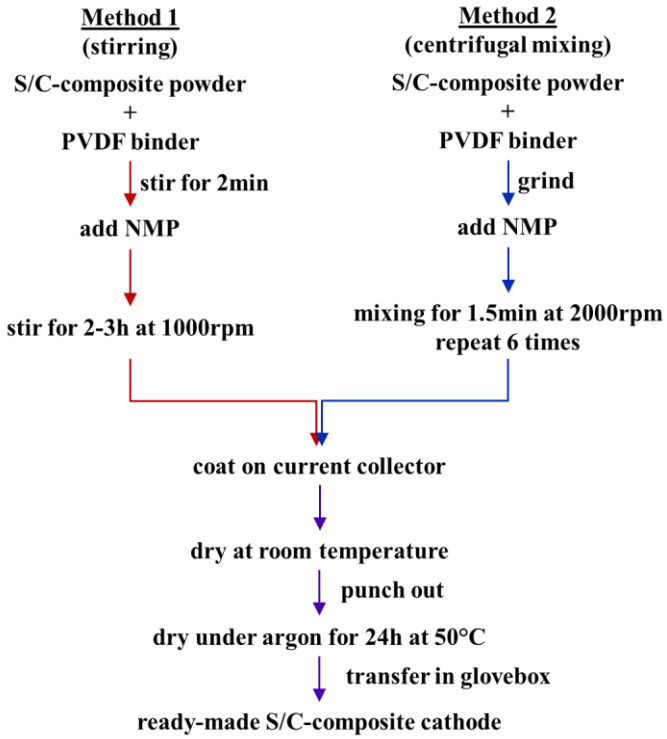

Figure 15: Preparation of S/C-composite cathodes with method 1 and 2

Method 2 – centrifugal mixing

To cut down the mixing time of the ink and the amount of NMP, which results in better ink with good homogeneity and viscosity, a centrifugal mixer was engaged. In the first step, the S/C-composite and the PVDF binder were dry mixed with a mortar and placed in a plastic container, in which the NMP was added immediately. The container was closed carefully and additionally sealed with a parafilm. Then, it was placed in the planetary centrifugal vacuum mixer (Thinky Mixer ARV-310, Thinky) and the specified mixing program for the S/C-composite ink was started: the slurry was mixed for 90 sec with a rotation speed of 2000 rpm at ambient pressure; then, the system stops the rotation softly and a manual rest of 10 sec was applied, to keep the temperature of the ink in a reasonable range, to avoid a loss of active material and a change in the S/C-composite structure, because of the low vapor pressure of S. This procedure was repeated for 6 times. After the last mixing cycle, the ink was removed and checked by eye, if the slurry thickened and no big particles are visible. If the texture has the right appearance, the ink was further processed. If the appearance was not as expected, the plastic container was closed again and the mixing was repeated, till the ink was smooth and viscous.

3.3.2. Coating process of an S/C-composite ink

After successfully converting the dry ingredients into a thick paste, the ink was coated onto a 15 µm thick aluminum foil (MTI) using an automatic coater (RK Print, Germany) and Mayer rods or gap bars with different wet film thickness sizes. Before the ink can be spread on the aluminum foil, it was cut from a big roll (350 m x 28 cm) into a rectangle, which fits on a glass plate with the measurements of 15 cm in width and 35 cm in length. Then, the aluminum foil was fixed with a stripe of adhesive tape on one side. Now, it was first cleaned with ultrapure water (Millipore, EPod, 15MΩcm@25°C) to remove dust from the surface on the aluminum foil and in a second step with isopropanol or ethanol to remove oil residues. To roughen the surface and in this way to improve the adhesion of the coating on the aluminum foil, it was etched with 0.1 M potassium hydroxide (KOH) solution and afterwards again washed with ultrapure water to remove possible residues of salt from the KOH solution. The cleaned aluminum foil was then also fixed at the bottom with a strip of adhesive tape, so that the foil lies flat and without wrinkles, on the glass plate, and the glass plate was placed in the designed recess of the automatic coater.

Depending on what kind of S loading should be achieved in the dried cathode film, the size of the Mayer rod or gap bar was chosen. For example, a 100 µm Mayer rod was taken to obtain an S loading between 0.8 mg_{Sulfur}/cm^2 and 1.4 mg_{Sulfur}/cm^2 (depending strongly on the carbon support and drying temperature). The size of the Mayer rod or gap bar defines the wet film thickness of the slurry on the aluminum foil. During the drying process, the thickness of the cathode film decreases due to the evaporation of the solvent. The feed motion of the Mayer rod or gap bar during the coating process was set to “2” on the scale of the coater, which equals 3 m/min, for every coating. There was no additional weight added on the rod or bar to avoid damage of the fragile aluminum foil. After the Mayer rod or gap bar was placed on the glass plate and fixed to the provided clamps on both sides, the ink was applied on the aluminum foil directly in front of the Mayer rod or gap bar with the assistance of a spatula. Then, the feed motion was applied and the Mayer rod or gap bar ink spread the ink on the aluminum foil, resulting in a thin cathode film. The so created wet coating was dried at room temperature for 24 h in a fume hood. After the first drying step, 10mm Ø electrodes were punched out manually with a normal punch or a costum made punch tool from the company Hohsen, and further dried for 48 h at 50°C in a Schlenk flask under a slight Argon (Ar) flow to remove the evaporated solvents and keep ambient air outside.

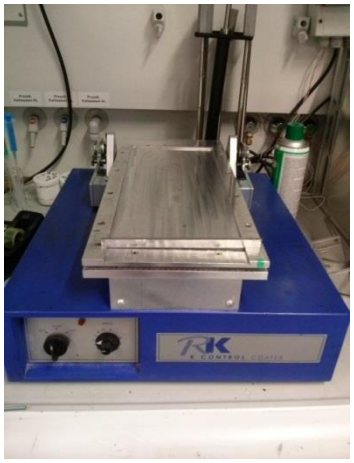

Figure 16: Modified automatic coater (K-control-coater-system K202, Erichson)

The well dried electrodes were transferred into an Ar-filled glove box (MBraun, Germany, <0.1 ppm O_2 and H_2O) without further contact to ambient air. The weight and thickness of the aluminum current collector was determined for every coating by weighing 10 blank 10mm Ø electrodes, which were taken from the uncoated part of the aluminum foil (the foil size was always oversized to avoid a spillover of the ink). The values from the single aluminum disks were averaged and subtracted from the measured S/C-composite cathodes to get the S loading on the used electrodes. The S loading and thickness of the electrode film was determined for every single S/C-composite cathode. The weight of the S/C-composite cathodes and the aluminum disks were measured with a semi micro balance (Cubis MSA, Satorius) with an error ratio of ±0.00001 g and the thicknesses were determined with a thickness measuring device with an error of ±3 µm (Mitutoyo, Serie 547).

Figure 17: Ar-filled glovebox with semi-microbalance for weighing electrodes and for manufacturing battery test cells

3.4. Electrolyte solutions

3.4.1. Preparation of electrolytes

Besides the electrical connection between the two electrodes, in every kind of battery an ion conducting agent is necessary, to make a current flow possible. While the electrons flow in the extended circuit between the electrodes, the ions inside the battery migrate in the opposite direction to balance the charge distribution in the system. Because of the high ion conductivity of liquid electrolyte solutions and their simple handling, they are preferably used in battery cells.[3,120] But there are also other possibilities for battery applications, like solid electrolytes with Li^+-ion conductivity between 10^{-5} to 10^{-3}S/cm (e.g. GARNET-phases, LTAP, Argyrodites) or gel type electrolytes (e.g. PEO, PAN).[22,23,121,122,123,124,125]

Before an electrolyte can be prepared, all ingredients have to be properly dried. The Li-anode in the test cell reacts with H_2O to form LiOH and H_2, which leads to passivation of the anode surface and consumption of active Lithium as well as to the generation of hydrogen inside the cell. Furthermore, the polysulfides which appear during the discharge or charge process and also the discharge product Li_2S are both highly H_2O sensitive. To avoid these undesired side reactions, the amount of H_2O was reduced to the lowest possible value.

Therefore, the components were ordered from chemical companies in the driest and cleanest version they offer. After receiving the chemicals, the solvents were transferred in an Ar-filled glovebox. Most of the solvents were received pre-dried, packed under an inert gas (mostly nitrogen) and sealed with a septum. So, they were first opened in an Ar-filled glovebox to avoid contact with ambient air, from which the solvents would immediately adsorb H_2O. After, the transfer and opening, they were further dried for at least 24 h over molecular sieves (Sylobead MS 564 C, 3 Å, Grace Division) to drop the H_2O amount below 20 ppm. The H_2O-content of the solvent after the drying period of 24 h was verified by Karl-Fischer titration (Table 2). If the limiting value exceeds 20 ppm, some additional molecular sieves were added and the drying procedure was extended for 24h. After the extended drying time, the H_2O-content was verified again. Conducting salts were opened after receiving and filled in a snap-on lid glass. Then, the glass was placed in a Büchi oven and dried at 120°C under dynamic vacuum for at least two days. After the Büchi oven was cooled down to room temperature, the sample chamber was closed by a tap to maintain the vacuum and transferred immediately to an Ar-filled glove box to avoid renewed water absorption.

Table 2: Electrolyte solvents, their purity and water content after drying over molecular sieves

Name	Acronym	Purity [%]	Water content [ppm]
1,3-DiOxoLane	DOL	99.8	5
1,2-DiMethoxyEthane	DME	99.5	10
1,4-DiOXane	DiOX	99.8	8

Table 3: Used conductive salts, their purity and molecular weight

Name	Acronym	Purity [%]	Molacular weight [mol/g]
Bis(TriFluoromethane)SulfonImide Lithium salt	LiTFSI	99.95	287.09
Lithium Nitrate	$LiNO_3$	99.99	68.95
TetraButhylAmmonium bis(TriFluoremethylSulfonyl) Imide	TBATFSI	≥99.0	522.61

Table 4: Electrolyte composition used in Li-S test cells

Solvent	Conducting salt	Additive	
DME	1M LiTFSI	-	0.5M $LiNO_3$
	0.5M LiTFSI	0.5M TBATFSI	0.5M $LiNO_3$
DOL:DME (1:1, v:v)	1M LiTFSI	-	0.5M $LiNO_3$
	0.5M LiTFSI	0.5M TBATFSI	0.5M $LiNO_3$
DiOX:DME (1:1, v:v)	1M LiTFSI	-	0.1M $LiNO_3$
	0.5M LiTFSI	0.5M TBATFSI	0.1M $LiNO_3$

All electrolyte solutions were mixed in brown volumetric flasks, to ensure that the electrolyte would not be decomposed by light over time. Before the flasks were used for electrolyte storage, they were rinsed with ultrapure water to remove possible dust residues from the packaging or manufacturing if they were new, or, if they were reused, cleaned by boiling in an isopropanol/water mixture and afterwards in ultrapure water, followed by rinsing with ultrapure water to remove the final residuals. After the cleaning step, the flasks were dried in a Binder oven at 70°C and ambient pressure for at least 12h. The solvent volumes required for preparing different electrolyte solutions were measured with an Eppendorf pipette and filled in a brown flask, equipped with a magnetic stir bar and placed on a magnetic stirrer. The amount of conducting salt was weighed on a semi-micro balance from Satorius (Cubis MSA, error ratio ±0.00001 g, Satorius, the balance is placed on a weighing stone, which is decoupled from the glovebox, to reduce vibrations and ensure precise weighing results). Afterwards, the chosen salt was added slowly to the electrolyte solvent, while it was stirred. The electrolyte solution was stirred until the salt was dissolved and to guaranty a homogenous distribution of the ions, it was additionally stirred for further 30 min. The H_2O-content of the

ready prepared electrolytes was not measured, because of the reactivity of some solvents or salts with the Karl-Fischer titrator solution, which leads to unreliable results. But, because of the carefully dried electrolyte components, the H_2O-content of the finished electrolyte solution should not increase significantly and one can assume that the electrolyte is dry enough to not influence the cycling results.

The specifications of the solvents and salts as well as the different electrolyte compositions, which were used during this study, are listed in the Table 2 to Table 4.

3.4.2. Preparation of a polysulfide enriched electrolyte

To prevent the loss of S on the S/C-composite cathode, a polysulfide enriched solution was synthesised and used as electrolyte in Li-S test cells. The method, which was used here, to saturate the solvent with polysulfide species, was developed by Oliver Groeger from VW in the context of the LiSSi-project (BMBF). The whole synthesis was done in an Ar-filled glovebox, because the polysulfides are highly moisture sensitive. Also, absorption of water should be prevented, because the electrolyte will have contact with the Li-anode in the battery test cell and Li reacts with water, as well.

In the first step, 1 g of pure S-powder (Sigma) was weighed. To contact the S electrically, the powder was wrapped in a stainless steel mesh (Spörl KG) to build some kind of electrode. The little S-“pocket” was hang onto a stainless steel wire, which is connected the S-cathode to the multi-potentiostat (Biologic, VMP-3). This part of the set-up of synthesis was done at ambient air, because for building the S-“pocket” one needs sure instinct, because the part of steel mesh in which the S powder had to be incooperated is very small. Furthermore, various tools are needed to wrap the mesh around the S powder properly and to connect it with the steel wire. After the S-“pocket” was assembled, it had to be dried. Together with the remaining set-up parts (snap-on lid glass, second steel wire, syringe with needle), the S-“pocket” was placed in a Binder oven for 24 h at 70°C, before everything could be transferred into an Ar-filled glovebox.

Figure 18: Picture of polysulfide synthesis set-up and S-“pocket”

After the warm components, had cooled down, the cell set-up was assembled as follows: for the anode side a rectangular piece of Li was cut out of a Li-foil (0.45 mm thickness, Rockwood Lithium). To connect the Li-anode with the potentiostat, the second steel wire was placed in the middle of the short side and the rectangular Li was folded around the wire. Because of the softness of the Li-metal, it sticks together very easily and with a little bit of pressure from the flat side of a tweezers, the Li pieces merged and fixed the steel wire in between. The wires were then pushed through the snap-on lid and the lid was snapped onto the glass. To close the cell properly and to avoid dissolution of the lid via solvent vapor in the electrolyte, an inert plastic foil was placed between the lid and the glass. Now, the electrodes were adjusted at the lowest position of the glass without touching the bottom. To control the temperature, the set-up was placed on a heating plate and a thermometer was implemented. Both electrodes were connected with crocodile clips with a multi-potentiostat (Figure 18). As setting, a constant current program was chosen and the current was set to 450 µA.

To insert the electrolyte into the closed cell, a needle was pushed through the lid and the foil. Then, 8 mL of DOL:DME + 1 M LiTFSI electrolyte was injected with a syringe via the needle and the current was applied by starting the program. Afterwards the needle was removed and because of the flexible material of the lid and the very small diameter of the needle, no further sealing of the hole was required and electrolyte evaporation was negligible. The used electrolyte was prepared following the description in Chapter 3.4.1.

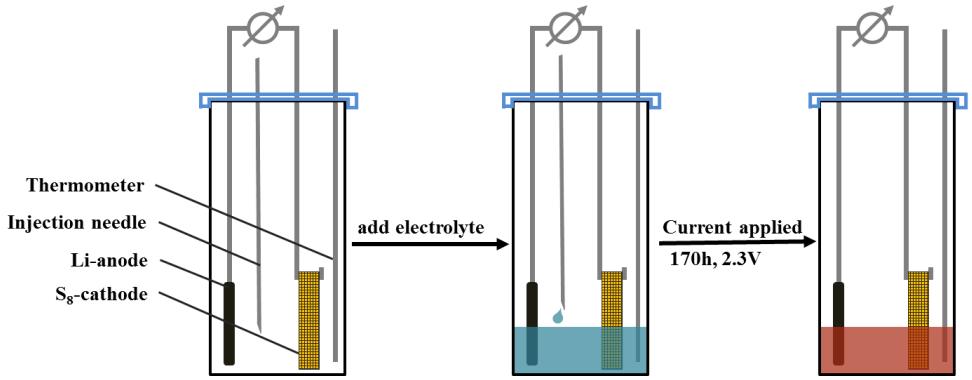

Figure 19: Scheme of synthesis route for the production of polysulfide enriched electrolyte

The voltage profile of the cell was recorded during the polysulfide enrichment of the electrolyte and checked every now and then to make sure that the synthesis was not stopped unintentionally by the instrument (Figure 20). At the beginning, the cell showed the expected OCV for a Li-S system of 2.38 $V_{Li/Li+}$, which dropped to 2.35 $V_{Li/Li+}$ when the current was applied and then gradually dropped to 2.31 $V_{Li/Li+}$ over a period of 100 h. Then, the potential jumped from 2.31 $V_{Li/Li+}$ to 2.28 $V_{Li/Li+}$ and the voltage signal started to get a little bit noisy, but did not decrease further.

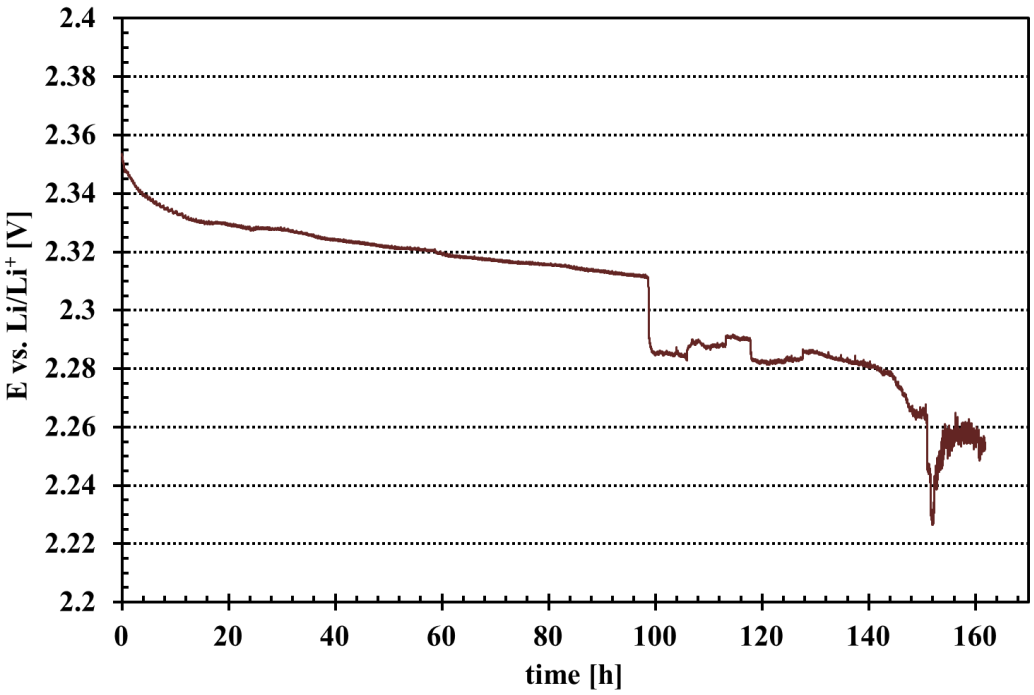

Figure 20: Potential vs. time curve of the polysulfide synthesis at a current of 450µA (1g S in 8mL DOL:DME + 1M LiTFSI)

At approximately 150 h, the potential dropped again to 2.23 $V_{Li/Li+}$ and went back to 2.25 $V_{Li/Li+}$ with an increased noise signal and remained there till the end of the synthesis at 170 h is reached. The noise voltage signal after the potential drop is probably related to the

saturation of the electrolyte with polysulfides, because the ionic conductivity and the viscosity of the solution changes. After the synthesis was done, the electrodes were removed and the polysulfide enriched electrolyte was filled in a brown volumetric flask. Before it was used in a test cell, 0.5 M $LiNO_3$ was added as additive.

3.4.3. Calculation of the Sulfur amount in the polysulfide enriched electrolyte

To get an indication how much S was dissolved as polysulfide in the electrolyte, the amount was calculated in two different ways. The first way to calculate the S amount was adopted from VW. From the synthesis, the exact reaction time t and applied current I are known and so the charge (C) can be calculated:

$$Q = I \cdot t \tag{3.3}$$

$$Q = 450\ \mu A\ \cdot 170\ h = 275.4\ C \tag{3.4}$$

For the further calculation of concentration of S it was assumed that only one polysulfide species exists at a time. As know from the literature, at 2.3 $V_{Li/Li+}$ the system is located at the first discharge plateau and the three polysulfide species Li_2S_8, Li_2S_6 and Li_2S_4 are the main products, which are present in the solution. In the first assumption, it was proposed that only Li_2S_8 ($M_{Li_2S_8} = 270.41\,\frac{g}{mol}$) would be present and the reaction could be described as follows:

$$8\,S + 2\,Li^+ + 2e^- \rightarrow Li_2S_8 \tag{3.5}$$

With $F \cdot e^- = \frac{Q}{n}$, where F is the Faraday constant ($9.648 \cdot 10^4\,\frac{C}{mol}$) and $e^-$is the number of electrons, and $c = \frac{n}{V}$, where c is the concentration of the dissolved species and V the volume of the solution, the concentration of Sulfur (i.e., on a S_1 basis) can be calculated:

$$c = \frac{Q}{e^- \cdot F \cdot V} \tag{3.6}$$

$$c = 1.427 \cdot 10^{-3}\ {mol_{Li_2S_8}}/{8\ mL} = 0.18\ {mol_{Li_2S_8}}/{L} \tag{3.7}$$

$$\boldsymbol{c = 1.44\ {mol_{Sulfur}}/{L}} \tag{3.8}$$

In a second assumption, only Li_2S_4 ($M_{Li_2S_4} = 142.15\,\frac{g}{mol}$) was assumed to be formed, whereby the reaction can be described as follows:

$$8\,S + 4\,Li^+ + 4e^- \rightarrow 2\,Li_2S_4 \tag{3.9}$$

For the calculation of the concentration of Sulfur (i.e., on a S_1 basis), also equation (3.6) was used and this results in:

$$c = 7.136 \cdot 10^{-4}\,{}^{mol_{Li_2S_4}}/_{8\,mL} = 0.089\,{}^{mol_{Li_2S_4}}/_{\mathrm{L}} \tag{3.10}$$

$$\boldsymbol{c = 0.714\,{}^{mol_{Sulfur}}/_{L}} \tag{3.11}$$

With this method, the resulting concentration of Sulfur (i.e., on a S_1 basis) in the electrolyte solution was estimated to lie between 0.7 $\frac{mol_{Sulfur}}{L}$ and 1.4 $\frac{mol_{Sulfur}}{L}$. The weak point of the calculation is that the real composition of polysulfides in the solution is not clear except that it will range between a composition of Li_2S_4 and Li_2S_8 based on the literature (Figure 4). Here, the two extreme conditions were chosen, where only Li_2S_8 or Li_2S_4 were expected as product of the reaction between S and Li, because in this way one get the upper and lower limit of the S concentration, which is dissolved as polysulfide species.

To provide a more defined result, the concentration of S was calculated in a second way. Therefore, the removed S-"pocket" was taken out of the Ar-filled glovebox and rinsed with a little bit of isopropanol and water to clean it from electrolyte solvent, conducting salt and polysulfide residues. Then, the S-"pocket" was placed in a Binder oven and dried at 70°C at ambient air for several days. After the drying process, the "pocket" was carefully opened and the remaining S was removed and weighed. With the initial and the final S amount, one can calculate the total amount of S, which was consumed in the electrolyte solution.

$$m_{dissolved} = m_{initial} - m_{final} \tag{3.12}$$

$$m_{dissolved} = 0.18g \tag{3.13}$$

With $c = \frac{n}{V}$, where c is the concentration of S, n is the quantity of material and V the volume of the solution, and $n = \frac{m}{M}$, where m is the mass of the dissolved S and M the molar weight of S ($32\,\frac{g}{mol}$) the S concentration in the electrolyte can be calculated.

$$c = \frac{m}{V \cdot M} \tag{3.14}$$

$$c = 0.70\ ^{mol_{Sulfur}}/_{L} \tag{3.15}$$

This result accorded very well with the calculation in which Li_2S_4 was assumed as reaction product and so this value was taken for further analysis of the cycling results in Chapter 4.2.5.

3.5. Cell description

For electrochemical tests, T-fittings from Swagelok were used as cell bodies and modified for our purposes. The T-fitting consists of stainless steel 316L with an inner diameter of 12.7 mm on the long side, which represent the main part of the cell. Here, the battery components were carried by two different stainless steel rods (Figure 21). The anode side consists of two parts: a stainless steel rod and a high density polypropylene (HDPE) cap. For the HDPE-cap two modifications are available. One type has a little slot, whilst the other one is completely closed. The HDPE-cap is used to insulate the battery components from the remaining cell and acts as reservoir for excess electrolyte. The rod has a step at one end, on which the HDPE-cap can be attached. The cathode side consists of three parts: a stainless steel rod with a small step at one end, a spring and a small stamp also with a small step. The spring has a spring constant of 3.71 N/mm and was compressed by 3.5 mm during the cell assembly procedure, which results in an overall pressure of 1 – 2 bar. The spring ensures a proper pressure in the cell and so guaranties a good contact between the single battery components. On top of the cell body is a third opening for the possibility to add a third electrode, i.e., a reference electrode. Compared to the other two openings, the diameter is reduced through a step at the half height, to avoid screwing in the rod too far. The rods were all fixed with hex nuts and two different sealing ferrules. The sealing has two functions in the cell. First, it isolates the rod from the body to avoid a short cut and second, it also seals the cell from the atmosphere, so no ambient air can penetrate into the cell and in this way, destroy the battery compounds, which are highly sensitive for O_2 and H_2O.

For cleaning, the cell compartments were placed in a beaker on a hot plate and first were heated up to 80°C in ethanol or isopropanol to remove all organic solvents and afterwards in ultrapure water to remove salt residues and other water soluble contaminations. Then the cell parts were rinsed with ultrapure water again and were subsequently dried in an oven at 70°C for at least 12 h at ambient pressure. For assembling of test cells, the cell parts were transferred into an Ar-filled glovebox (MBraun, UniLab ≥ 0.1ppm for O_2 and H_2O, Germany)

to avoid contamination with O_2 or H_2O, because some components or intermediates are highly reactive in contact with ambient air.

3.5.1. Cell set-up

The Li-S test cell set-up was started with the preparation of the anode side (Figure 21 [a]). As anode, a 10 mm Ø Li electrode was used. Therefore, a piece of Li-foil (0.45 mm thickness, Rockwood Lithium) was placed on a plastic underlay and was cut out with a punch. The Li disk was placed on the anode side rod, whilst pressing the part with the smaller diameter of the rod on the Li. The anode should be centered on the rod to ensure a good cycling performance of the cell. This was proved by eye, before the cell was further assembled. If the Li electrode was not centered, it was carefully removed with tweezers and the procedure was repeated. Once the Li was successfully placed on the rod, a HDPE-cap was placed on the step and inserted in the cell body (Figure 21 [b]). Then, the rod was fixed with a hex nut, containing sealing inside, and screwed with a wrench on the thread at one of the long sides of the T-cell body. In the next step, three pieces of a three layered separator, which is composed of two layers of polypropylene sandwiching polyethylene in the middle (C480, 25 µm thickness, Celgard®), with a diameter of 11 mm were placed on the Li, to isolate the anode from the cathode electrically and half of the electrolyte volume was added.

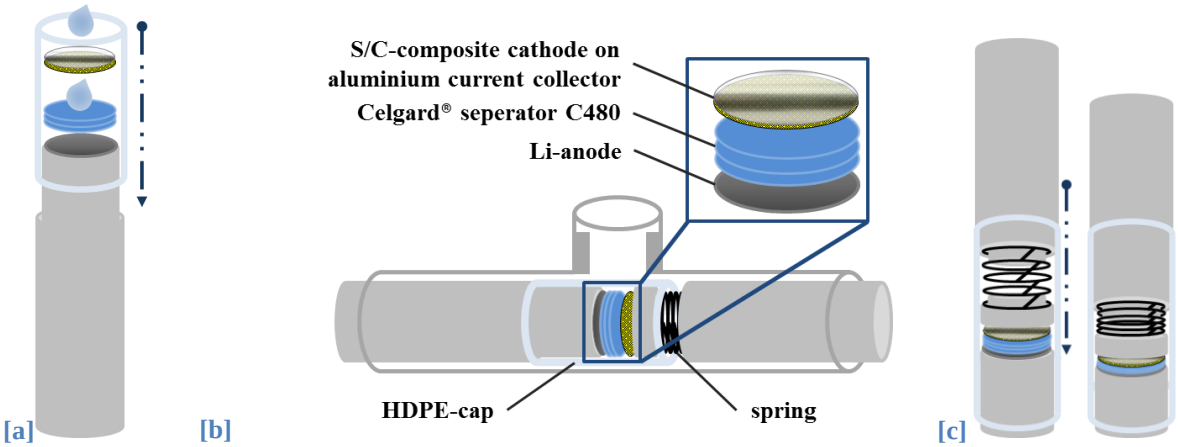

Figure 21: Schematic of a half cell assembly with S/C-composite cathode and Li-anode. [a] Schematic description of the assembly of the anode side with HDPE-cap (gray lines) and the active cell components. [b] Scheme of the completely assembled battery test cell (enlargement: battery components and their layering). [c] Schematic representation of the spring compression via the cathode side

On top, the S/C-cathode was placed with the active material side faced to the separator and the Alumina faced to the opening. After adding the other half of the electrolyte, which leads to a total amount of 30 µL (38.2 µL/cm^2), the cell was placed in a special holder (Figure 22) and was closed with the cathode rod, which is divided in three parts. Therefore, the first part,

a short stainless stamp with a step, was placed on the backside of the cathode and a spring was inserted. Then, the upper part of the rod was placed on the spring and fixed slightly with a hex nut (Figure 21 [c]).

The holder with the cell was placed in a costum made tool, which was designed to compress the spring about a defined height of 3 mm with a millimeter screw. Afterwards, the rod was fixed with a punched plate and the nut was closed with a wrench as tight as possible (Figure 22). During this process, the rod is drawn further in the cell body and the spring is additionally compressed for 0.5 mm. In the last step, the opening on top of the test cell was closed properly with a sealing cap and in assistance of a wrench.

Figure 22: Costum made tool for battery test cell assembly and finished test cell connected to the battery cycler (MACCOR)

3.6. Electrochemical test procedure

The test cells were measured under the same standard conditions, to get reliable and comparable data. In standard conditions, between the first contact of the electrodes with the electrolyte and the beginning of the galvanostatic cycling, a maximum time span of 20 min was allowed in order to keep the self-discharge phenomena and its effects on the cell performance as small as possible. Furthermore, the test cells were placed in climatic chambers to keep the temperature during cycling at a constant temperature of 25°C. Before the cells were galvanostatically cycled, impedance spectra were measured with a multi potentiostat (VMP3, Biologic), from 500 kHz to 100 mHz with an amplitude of 10 mV at OCV, to determine if the cells had a short circuit or if the high frequency resistance was not in the expected range, which can be caused from insufficient wetting of the separator or the electrode. When the test cell showed a normal impedance behavior, it was cycled galvanostatically with a battery cycler from MACCOR (Figure 23).

Figure 23: Battery test cycler with 64 channels and climatic chambers for a constant temperature during galvanostatic cycling

To investigate the complete electrochemically active region, the cells were cycled in a potential window from 1.5 V to 3 V vs. Li/Li$^+$. The used current was calculated on the basis of the S loading on the cathode, which was determined for every single electrode by weighing it with a semi-micro balance (Cubis MSA, error ratio ±0.00001 g Satorius) before it was placed in the cell, the specific capacity of S (1670 mAh/g_{Sulfur}) and the area of the cathode:

$$I_{spec.} = C_{spec.} \cdot S_{load} \cdot A_{cathode} \tag{3.16}$$

For example, the current for a round S/C-composite cathode with an S loading of 2 mg/cm^2 and a diameter of 5 mm can be calculated as followed:

$$I_{spec.} = 1670\ \frac{mAh}{g_{Sulfur}} \cdot 2\ \frac{mg}{cm^2} \cdot (\pi \cdot 0.5^2)\ cm^2$$
$$I_{spec.} = 2.62\ mAh \tag{3.17}$$

This current corresponds to a C-Rate of 1 C, which means that a test cell with the above mentioned specifications needs 1 h for a total discharge or charge, when a current of 2.62 mA is applied. The C-Rate is the quotient of the applied current to the specific current and has the unit 1/h.

$$C - Rate = \frac{I_{applied}}{I_{spec.}} \tag{3.18}$$

In Li/S batteries the commonly used C-Rate is C/10, which corresponds in theory to a total discharge or charge time of 10 h. Because the S loadings are varying between the cathodes,

the resulting currents are converted and given as C-Rate. In this way, cells with cathodes of different S loading but the same C-Rate can be easily compared. For practical applications, high C-Rates are desirable, because it allows a fast charge of the battery or high performance can be provided immediately ($P = U \cdot I$).

With the coulombic efficiency η_{CE} the reversibility of the cell reactions could be proved. It can be calculated by dividing the discharge capacity through the charge capacity and is given in percent.

$$\eta_{CE} = \frac{C_{discharge}}{C_{charge}} \cdot 100\% \tag{3.19}$$

A coulombic efficiency of 100% would represent a battery with totally reversible anode and cathode reactions, without losses due to side reactions of the active material with the electrolyte or the degradation of the electrode material. In Li/S batteries, we have different phenomena, which are influencing the coulombic efficiency and the ideal value of 100% is not obtainable. The shuttle mechanism during charge of a Li/S battery (explained in Chapter 2.3.3) lowers the coulombic efficiency, because it can lead to an overcharge of the battery and C_{charge} is getting greater than $C_{discharge}$. If an additive is used to suppress the side reactions of the polysulfides with the Li anode, the coulombic efficiency can rise above 100% in the first cycle, because a part of the active material will take place in the SEI formation and the charge step is shorter than the discharge step. For state-of-the art Li ion batteries the coulombic efficiency lies at 99.9%.[HBB]

Table 5: Trend of coulombic efficiency at the three possible scenarios

	η_{CE} [%]	e.g.
$C_{discharge} = C_{charge}$	100	Ideal battery
$C_{discharge} > C_{charge}$	> 100	Li/S battery with shuttle suppresion additive
$C_{discharge} < C_{charge}$	< 100	Shuttle current higher than charge current

4. Results & Discussion

4.1. Characteristics of the S/C-composite

4.1.1. X-ray diffraction analysis

At first X-ray diffraction was chosen for the analysis of the samples, because it is a very quick and easy method to figure out, if crystalline S is on the surface of the carbon black support. Also, if there are residues from $Na_2S_2O_3$ or $NaNO_3$ from the synthesis, they can be visible in the pattern, as long as they are in the detection range of the instrument (≤ 2 wt%).

In Figure 24, a representative pattern of an S/C-composite powder is shown. In the range of 15° to 30° 2θ, an amorphous background from the carbon black support can be noticed, but compared to other pattern with an amorphous component the hill is strongly suppressed. The reflexes from the S are clearly visible and the analyses of the pattern shows, that the S is in its orthorhombic crystal structure with the space group Fddd(70).[68] With the information from the XRD-pattern, it can be concluded that the S is successfully precipitated on the carbon black surface and no reflexes from impurities could be detected.

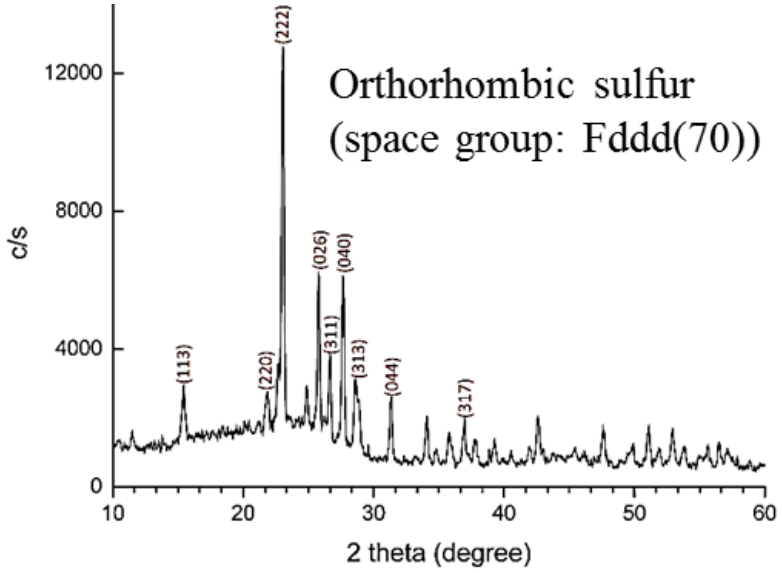

Figure 24: Representative XRD-pattern of a S/C-composite based on a Vulvan XC72 with a S/C-ratio of 52.7 wt% S and 47.3 wt% C synthesized by the standard route (Chapter 3.1.1).[46]

4.1.2. Scanning electron microscopy and energy dispersive X-ray mapping

To get a more detailed insight on the morphology of the S/C-composite, the powder was studied by scanning electron microscopy. With this technic, it is possible to examine the surface morphology of the S/C-composites. In Figure 25 [a] and [b] two sections of the S/C-composite sample with different magnification are shown. In [a] a general view on the S/C-

composite powder is shown and the typical carbon black host structure can be identified. This indicates that the synthesis method is non-destructive and the structure of the carbon support was maintained. Furthermore, no bigger particles or agglomerates on the surface can be assigned. A close-up view (Figure 25 [b]) of the S/C-composite powder showed a nice round shape of the primary carbon black particles, but the edges between them are blurry and not sharp as it would be for a pure carbon black sample. At the basis of these findings, it was assumed that the carbon black surface is covered by a smooth and homogenously distributed S-layer. To prove this assumption, energy dispersive X-ray (EDX) mapping of carbon and S was done. The sector, where the EDX-mapping was taken, is shown in Figure 25 [c] and in the following two pictures ([d] and [e]) the characteristic radiation of carbon ([d]) and S ([e]) were mapped. In both cases a homogenous distribution of both elements in the analyzed sector can be observed and there are no indications of bigger particles or agglomerates of S. This proves the assumption, which was made on the basis of the SEM pictures, that the S is homogenously distributed on the carbon black surface.

On the basis of the SEM and EDX results, an estimation of the thickness of a hypothetical S-layer on a carbon black support can be done and could be roughly calculated with the following equation:

$$t = \frac{m_{S_8}}{\rho_{S_8} \cdot A_{carbon}} \tag{4.1}$$

Where m_{S_8} is the mass of the Sulfur in the S/C-composite powder, ρ_{S_8} is the density of Sulfur ($2.07 \frac{g}{cm^3}$) and A_{carbon} is the external surface area of the carbon black.

The calculation will be done on the basis of the S/C-composite, which is shown in Figure 25. The external surface area of the Vulcan XC72 is $96 \frac{m^2}{g}$ (**Fehler! Verweisquelle konnte nicht gefunden werden.**). To simplify the calculation, it is assumed, that 1g of S/C-composite is available and with the weight ratio of 52.7 wt% S and 47.3 wt% C this results in a total S mass of 0.53 g and a total carbon mass of 0.47 g. With this values a total carbon area of

$$A_{carbon} = 96 \frac{m^2}{g_{Carbon}} \cdot 0.47\ g_{Carbon} = 45.12\ m^2_{carbon} \tag{4.2}$$

can be calculated. Afterward the hypothetical thickness of the S-layer could be calculated with equation (4.1)

$$t = \frac{0.53\ g_{S_8}}{2.07\ \frac{g}{cm^3} \cdot 45.12\ m^2_{Carbon}} = 5.7\ nm \tag{4.3}$$

The resulting S-layer thickness of 5.7 nm seems to be relatively low, but the value for the thickness is dependent on the surface area of the carbon black support and on the weight ratio between S and C. So, if the surface area of the carbon increases the thickness of the S-layer decreases. So, for a Ketjen Black carbon with an external surface of $713\ \frac{m^2}{g}$ and the same S/C-ratio of 52.7 wt% S to 47.3 wt% C the S-layer thickness will decrease to only 0.9 nm. But if the weight percentage of S increases from 52.7 wt% to ≈ 66 wt%, the S-layer thickness increases also and lies at approximately 9.8 nm and for a Ketjen Black based S/C-composite at roughly 1.3. These calculations show that the surface area plays an important role on the resulting thickness of the S-layer and a high surface area on the carbon result in thin S-layers also when the weight percentage of S increases. (The surface area data were measured via nitrogen absorption analysis, details in Chapter 4.1.4, measured values in Table 7)

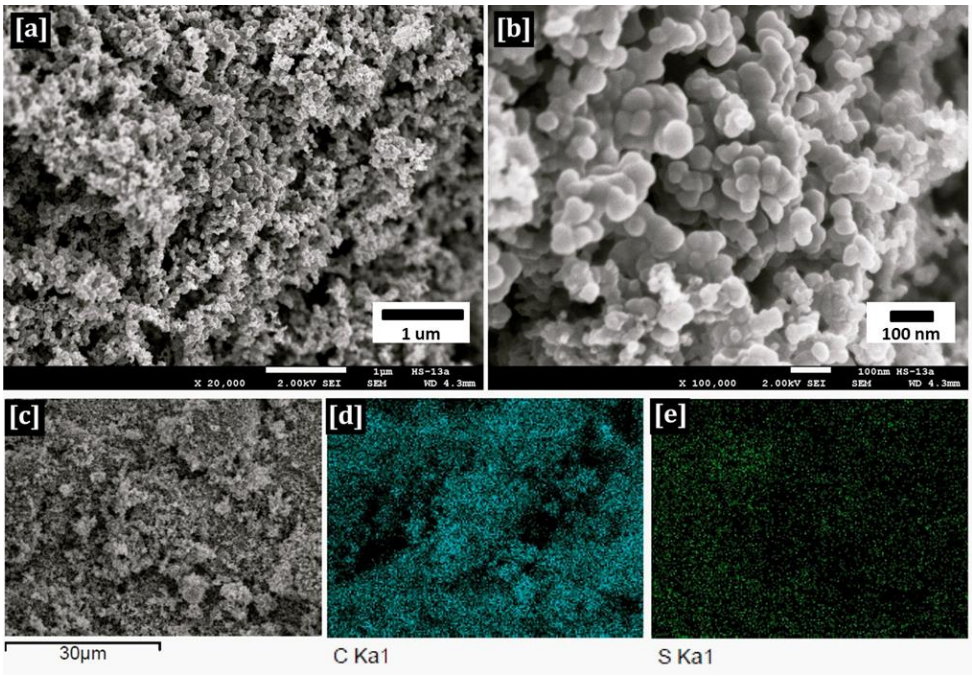

Figure 25: SEM-picture of a S/C-composite powder based on a Vulcan XC72 carbon with a weight ratio of 52.7 wt% S and 47.3 wt% C at low [a] and high magnification [b]. In [d] and [e] the EDX-mapping of carbon and S is shown within the area of [c].[11]

4.1.3. Thermal gravimetric analysis

For electrochemical studies of S/C-composite cathodes, the exact amount of S on the respective cathode is needed to calculate the current for galvanostatic cycling and for analysis of the measured data to get the discharge and charge capacities of the test cells. Therefore, the amount of S in all synthesised S/C-composite batches was measured by TGA. Figure 26 shows four TGA-curves, exemplary for S/C-composites on different carbon supports, which were used in this study (Table 7). All curves exhibit two steps at around 350°C and 550°C, which can be assigned to the S evaporation and the carbon oxidation. In detail, the S/C-composite shows different burning behavior, due to the carbon black, which was used in as support for the S. The S/C-composites based on Super C65 or Vulcan XC72 show a defined first step at 330°C, where the evaporation point of S lies. If Ketjen Black or Black Pearls were used as carbon support for the S/C-composite the step, which is identified for the S evaporation, is slightly bent at the bottom. This behavior can be attributed to the micropores in Ketjen Black and Black Pearls, which are able to absorb small molecules. Before the S evaporates from the carbon support, it first melts at 120-125°C. In the liquid phase, it can be partially absorbed by the micropores of the carbon black. The amount of S, which can be absorbed, is dependent on the pore volume of the micropores. If the burning process now reaches the evaporation point of 330°C, the S on the external surface and in the mesopores evaporates immediately. But the S in the small micropores is apparently stabilized by capillary forces in the small pores, which results in a higher evaporation temperature for the S in these pores and leads to a more gradual desorption of S over a wider temperature range compared to Vulcan XC72 or Super C65. On the Super C65 and Vulcan XC72 the micro porosity is negligible and essentially all Sulfur is on the external surface of the carbon support. For this reason only a sharp step is visible.[90,139,146]

The second step represents the carbon combustion in pure oxygen. Depending on the type of carbon support used, the carbon combustion started between temperatures of 460°C to 620°C (Table 6). The combustion temperature is related to the surface area of the carbon black. High surface areas can have catalytic properties and accelerate the reaction of the carbon with oxygen to carbon dioxide. Here, Black Pearls with $1509 m^2/g_{carbon}$ has the highest surface area of the different used carbon supports, also showing the lowest combustion temperature of 460°C. For several carbons, the trend of specific surface areas versus oxidation temperature is given in Table 6.

Table 6: Surface areas of the different carbon supports and their combustion temperature in pure oxygen at a heating rate of 20°C/min. (BP = Black Pearls, KB = Ketjen Black, VC = Vulvan XC72, SC = Super C65)

$1509\,m^2/g_{BP}$	>	$834\,m^2/g_{KB}$	>	$240\,m^2/g_{VC}$	>	$68\,m^2/g_{SC}$
$460°C$	<	$500°C$	<	$590°C$	<	$620°C$

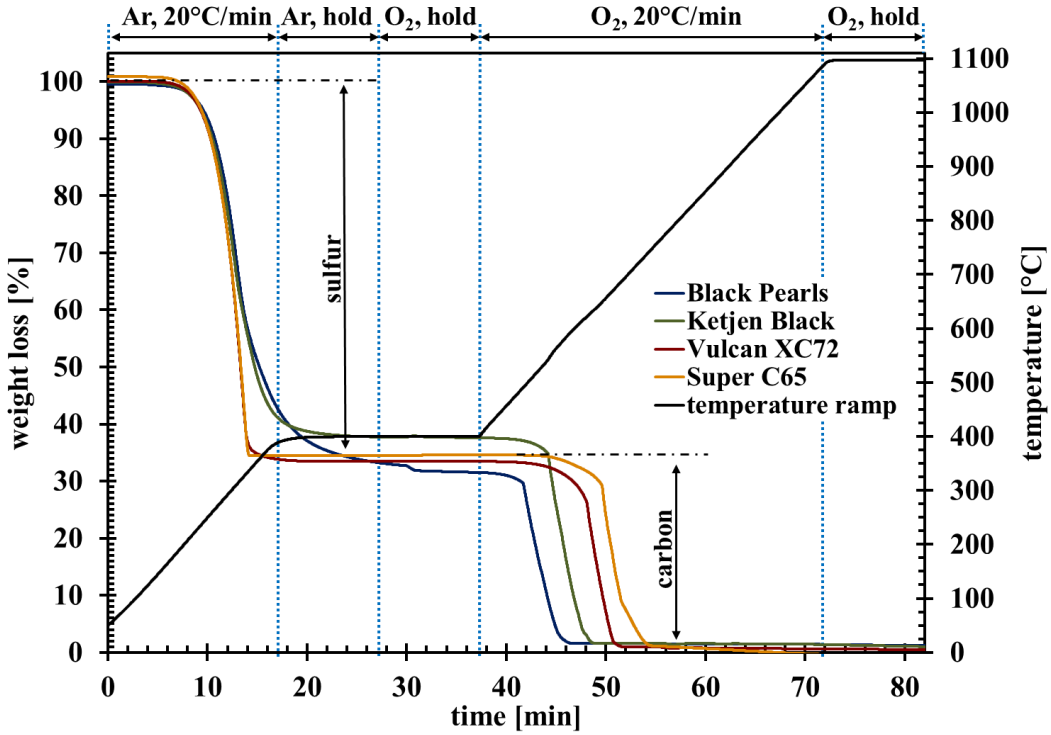

Figure 26: TGA analysis of the synthesised S/C-composites with different carbon blacks as support. The S/C-composite samples were heated from 25°C to 1100°C at a heating rate of 20°C/min with a heating break of 20 min at 400°C. To burn only Sulfur, in the first heating step the furnace was purged with Ar till 400°C was reached. During the rest period the temperature was kept at 400°C for 20 min and the gas was switched from Ar to O_2. In the second heating step, the sample was heated up to 1100°C at a heating rate of 20°C/min and kept at 1100°C for additional 10 min to make sure that the Carbon was fully burned.

4.1.4. Nitrogen absorption analysis

As support for the S-particles different high-structure carbon blacks were used. Carbon blacks are generally produced in oxygen free environments and consist of spherical primary particles (ø ≥ 50 nm), which are coalesced to agglomerates (~250 nm) with high structural properties. The material source as well as the process of its thermal treatment, influences the particle size distribution and the surface area of the resulting carbon black.[127] The carbon blacks we used as support for the S/C-composite synthesis belong to two different categories. Super C65 is a member of the acetylene black family. In general, they consist of graphitic primary particles with no or only little amount of micro porosity and have low surface areas. In contrast, we used furnace blacks like Ketjen Black and Black Pearls, which were built up from partially graphitic micro porous primary particles and exhibit high surface areas. Also, the particle surfaces are covered with a significant amount of oxygen-containing surface groups.[128]

The values for the pore size, pore volume and the surface area (internal and external) of the different carbon blacks were measured with the nitrogen absorption method.[129] The exact numbers are important to compare the different surface areas, the different pore volumes and sizes and their influence on the electrochemical performance of the S/C-composite cathodes (Chapter 4.2.4). In Figure 27 the pore size distributions of the used carbon blacks is plotted and in Table 7 the values are listed. It can be easily seen, that the measured curve for Super C65 is nearly flat and shows only a small peak at the beginning, which is in the range of the measurement error. For the high surface area carbon blacks, two main peaks can be assigned. Ketjen Black shows a peak in the micro porous area and in the meso porous area, which are lying close together. Due to the small pore sizes the total pore volume is relatively low and the main part of the volume is related to the mesopores. In contrast, Black Pearls has very tiny micropores and large mesopores and the pore volume nearly doubled compared to the Ketjen Black, but the fraction of the small pore volume is slightly smaller.

Also, the comparison of the surface areas of the different carbon blacks shows great differences between them. As described above, Super C65 consists of dense spheres without any micro- and meso porosity. Because of this morphology, Super C65 has mostly external surface area and offers no internal surface area inside the primary particles, which results in a very small allover surface area of 68 m^2/g_{carbon}. Compared to the Super C65 carbon, Vulcan XC72 exhibits some micro pores and due to that offers a small amount of pore volume in the small pores. If we have a look at the numbers of Ketjen Black and Black Pearls, which are listed in Table 7, we can see that they have nearly similar external surface areas, but the overall surface area of Black Pearls is almost doubled. This can be simply explained by the pore sizes of the mesopores. In the Black Pearls carbon the mesopores have a diameter of 15.4 nm compared to 3.4 nm in Ketjen Black and deliver in this way a great amount of internal surface area.

Table 7: Surface analysis date for the different carbon supports used for the S/C-synthesis. (Pores were classified by IUPAC: micropores >2 nm, mesopores 2-50 nm, macropores <50 nm)

Carbon type	Brand name	Surface area		Pore volume			Pore size	
		total	external	total	small pores	V_{micro}/V_T	micro	meso
		[m^2/g]	[m^2/g]	[cm^3/g]	[cm^3/g]	[%]	[nm]	[nm]
Super C65	Super C65	68	68	0.145	-	-	-	-
Vulcan XC72	V-Type	240	96	0.616	0.033	5.4	0.6 – 1.1	-
Ketjen Black	E-Type	834	713	1.270	0.176	13.9	1.2 – 2.2	2.6 – 4.0
Black Pearls	B-Type	1509	703	2.040	0.114	5.6	0.6 – 0.7	14.1 – 16.8

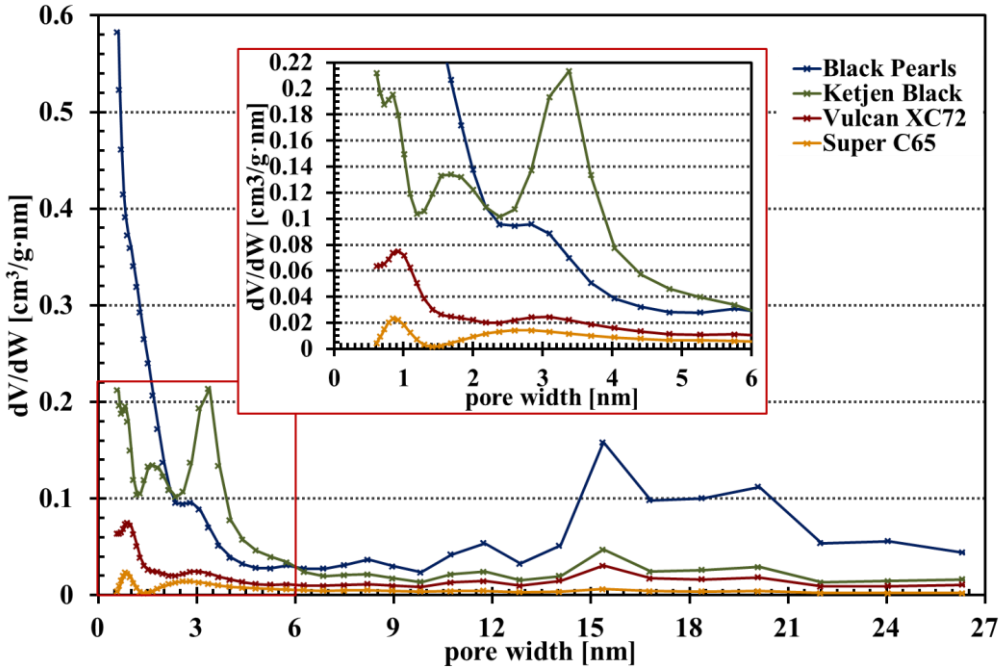

Figure 27: Pore size distribution measured with nitrogen adsorption of the different carbon black types used as support for the S/C-composites. Inset shows the magnification of the red rectangle on the left side of the graph.

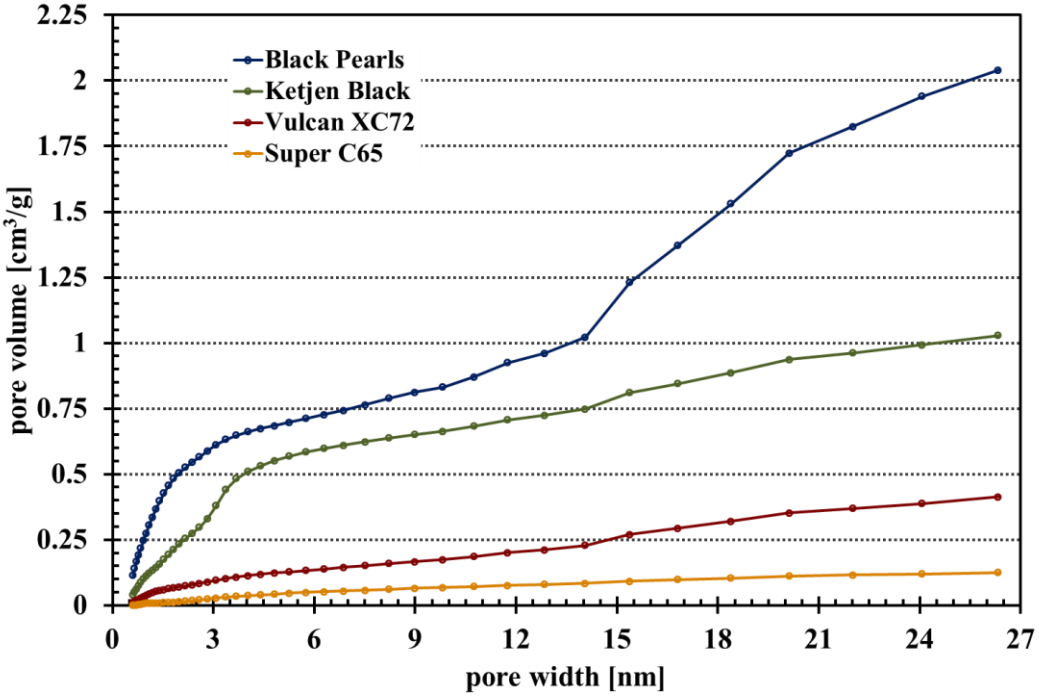

Figure 28: Total pore volume of the different carbon black types used as support for the S/C-composites determined by DFT.

4.2. Electrochemical investigation of S/C-cathodes

4.2.1. Comparison of S/C-cathodes made of S/C-composite powder from the standard and alternative synthesis route

As shown in the experimental part of this work, it is possible to synthesis the S/C-composite by two different routes (Chapter 3.1). Theoretically, we expect no big difference between the two S/C-composites, because in both ways colloidal S is precipitated and settled on the chosen carbon black surface. Also, a homogenous distribution of the S on the carbon black surface should be reached, due to the continuous sonication of the aqueous synthesis mixture during the whole synthesis process. In Figure 30, SEM pictures of an S/C-composite powder based on a Vulcan XC72 synthesised by the standard route (Chapter 3.1.1), which had an S/C-ratio of 66.5 wt%/33.5 wt%, on the left side (Figure 30 [a]-[d]) and an S/C-composite powder by the alternative route (Chapter 3.1.2), which had an S/C-ratio of 65.1 wt%/34.9 wt%, on the right side are shown (Figure 30[e]-[h]). In both cases, no bigger particles or agglomerates can be detected and the surface shows a smooth appearance at low and high magnifications. The carbon structure of the Vulcan XC72 can be preserved on either routes and the Sulfur encloses the primary particles homogenously (Figure 30 [d] and [h]). Additionally, an EDX-mapping of S and C for the two different synthesised S/C-composite powders was made. In Figure 29 the mapped areas of both S/C-composite powders are shown on the left. On the pictures in the middle the EDX-spectra of C is represented and it shows a homogenous distribution of the

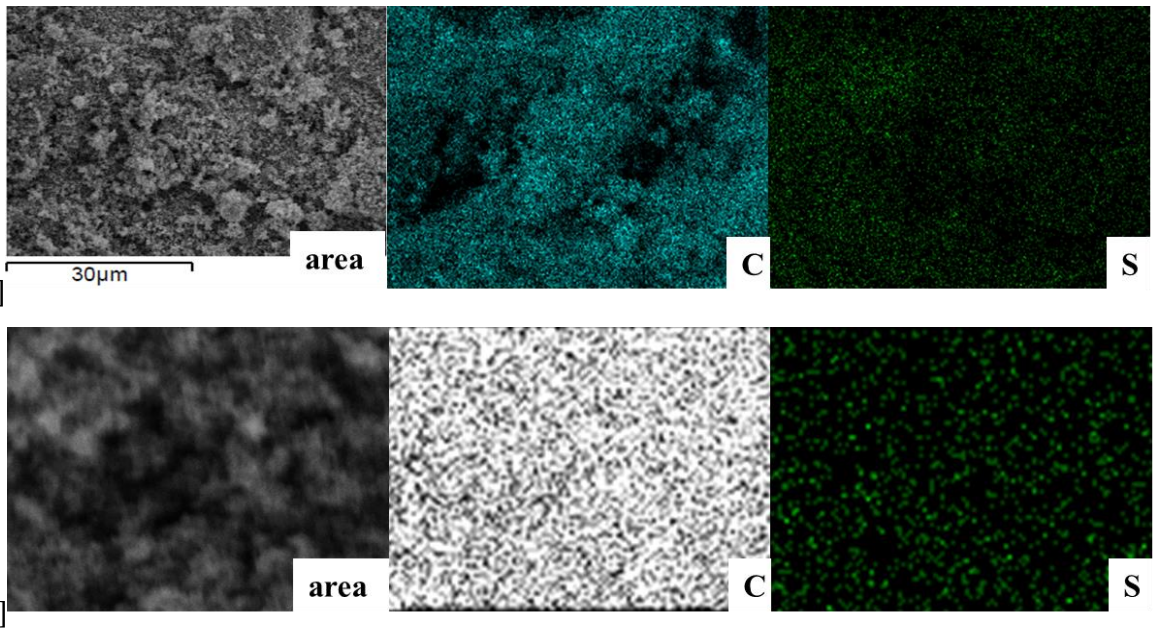

Figure 29: EDX-mapping of C and S of a Vulcan XC72 based S/C-composite powders made by the standard (Chapter 3.1.1) [a] and the alternative synthesis route (Chapter 3.1.2) [b] within the area at the left.

measured component C. The pictures on the right side, represent the EDX-spectra of S and no local accumulation of Sulfur within the mapped area could be detected. So, the observations from the SEM pictures and the EDX-mapping, confirmed the theoretical estimation, that there will be no visual difference between the unequally synthesised S/C-composite powders.

To figure out, if the S/C-composites from both synthesis routes show the same electrochemical behavior or if there are differences in the discharge capacity as well as the long-term cycling performance, the two S/C-composite powders were further processed to cathodes. The cathodes made of the powder from the standard synthesis route had an average S loading of 0.88±0.002 mg_{Sulfur}/cm^2 and for the cathodes made of the powder from the alternative synthesis route an average S loading of 0.86±0.02 mg_{Sulfur}/cm^2 could be achieved. For both cathode types the preparation method 1 was used, which is described in detail in Chapter 3.3.1 (Figure 15).

In Figure 31, a representative first discharge/charge cycle of both S/C-composite cathodes is shown. It is clearly visible that the S/C-composite cathode prepared with the standard synthesis route powder, achieved a higher discharge capacity, which lied in average at 558±55 mAh/g_{Sulfur} (blue lines, Figure 31) for the measured test cells. With the S/C-composite cathodes made from the powder of the alternative synthesis route, only 421±35 mAh/g_{Sulfur} (red lines, Figure 31) can be reached, which equates to 137 mAh/g_{Sulfur} less capacity in the first discharge step. The better discharge capacity of the standard S/C-composite cathodes indicates that the precipitated S has a better contact to the carbon support in the S/C-composite powder compared to the composite synthesised by the alternative route and so more S can take part in the electrochemical reaction.

The comparison of the cycling performance of the different test cells showed that the discharge capacity drop between the first and the second cycle is about 78% in both cases, but the decline in the following cycles for the discharge capacity of the alternative S/C-composite cathode is a little bit smaller and the discharge capacities after 50 cycles converged. Nevertheless, the discharge capacity of the standard S/C-composite cathodes is still 30 mAh/g_{Sulfur} higher. Because of the better behavior of the standard S/C-composite cathodes, only S/C-composite powders from the standard synthesis route were used for further electrochemical experiments.

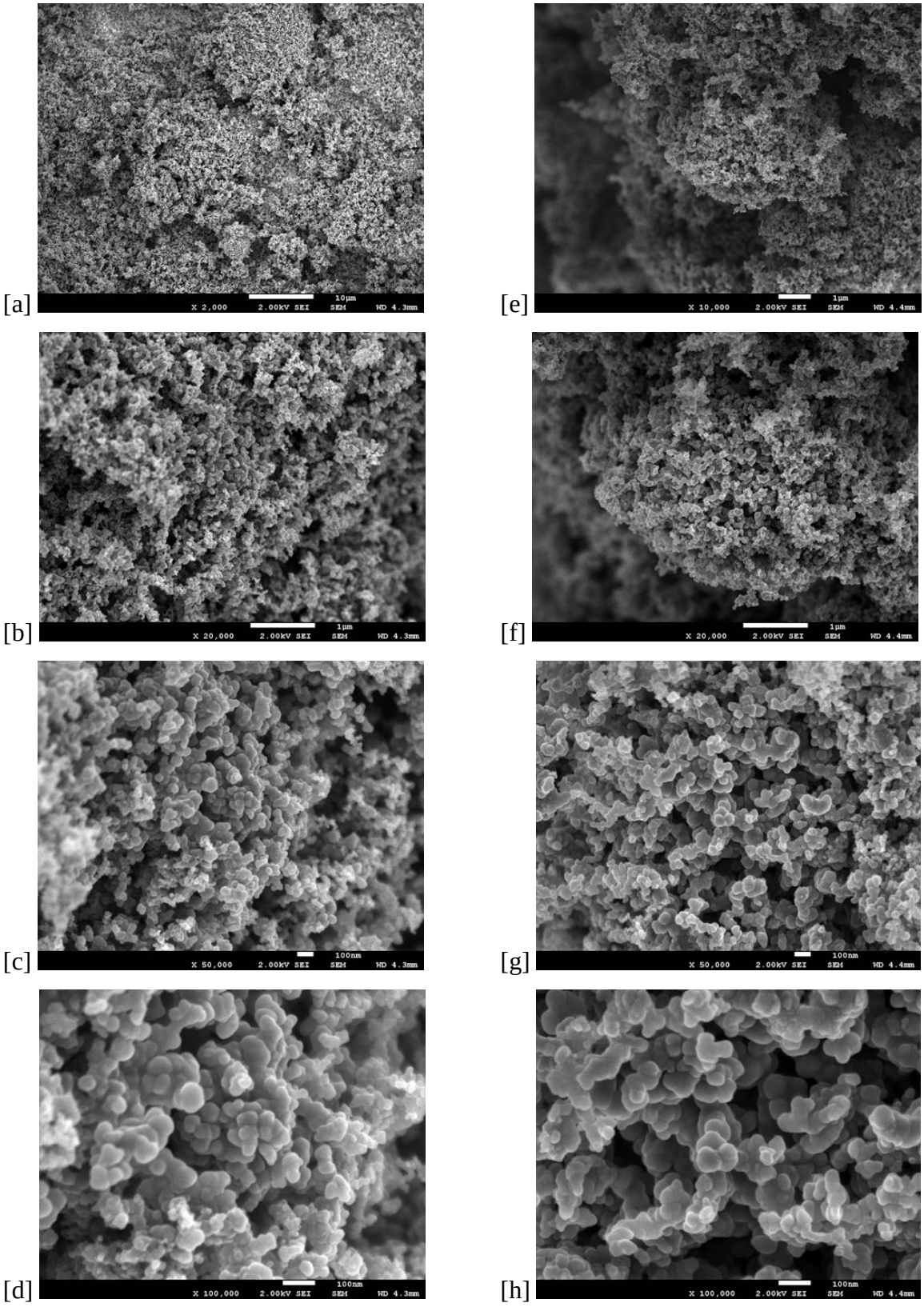

Figure 30: SEM of S/C-composite synthesised by different synthesis routes. [a] to [d] S/C-composite powder made from standard route (Chapter 3.1.1), [e] to [h] S/C-composite powder made from alternative route (Chapter 3.1.2). Both S/C-composites are based on a Vulcan XC72 carbon type and contain ~65wt% Sulfur.

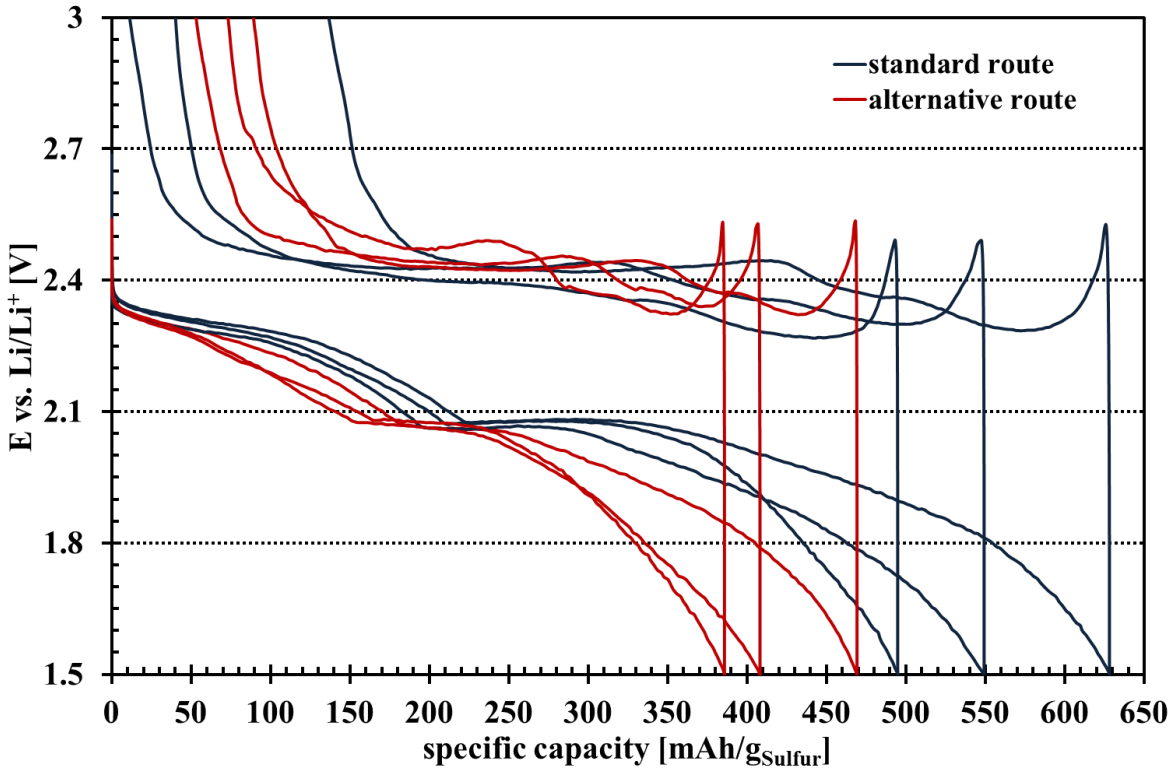

Figure 31: First discharge charge profile of S/C-composite cathodes based on a Vulcan XC72 carbon made by electrode preparation method 1 (Figure 15) with S/C-composite powder from the standard (blue lines) or the alternative (red lines) synthesis route. The average S loading for the electrodes made with the standard route powder was 0.88mg$_{Sulfur}$/cm^2 and for electrodes made with the alternative route powder was 0.86mg$_{Sulfur}$/cm^2. The cells were cycled at a C-rate of C/12 between cut off voltages of 3 V$_{Li/Li+}$ and 1.5 V$_{Li/Li+}$. As electrolyte 30 µL of DOL:DME + 1 M LiTFSI/0.5 M LiNO$_3$ was used.

In Figure 33 the coloumbic efficiency of both test conditions is shown. In both cases the coulombic efficiency of the first two cycles are slightly over 100% (Chapter 3.6, eq. 3.19). In the first cycles the SEI on the Li-anode will be formed in assistance of $LiNO_3$, which is used as additive in the electrolyte solution. This leads to an incomplete charge of the test cells, because of the consumption of S species due to the formation of the surface layer. The principle of operation of the $LiNO_3$ on the Li-surface is described in detail in Chapter 2.3.3. When the SEI is properly built the test cells can be completely recharged and the coloumbic efficiency will be 100% for the rest of the cycling time. This behavior is representative for all following measurements and due to this, no further coloumbic efficiency plots will be shown as long as they did not differ dramatically.

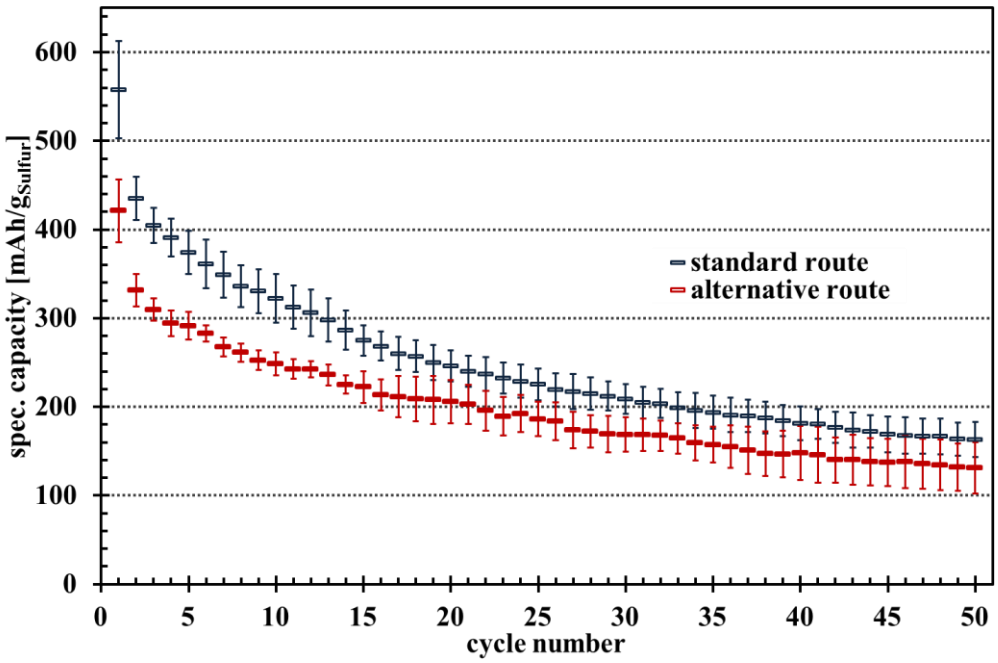

Figure 32: Comparison of discharge capacity over cycle number between S/C-composite cathodes based on a Vulcan XC72 carbon made by electrode preparation method 1 with S/C-composite powder from the standard (blue symbolss) or the alternative (red symbols) synthesis route. The average S loading for the electrodes made with the standard route powder was 0.88mg$_{Sulfur}$/cm^2 and for electrodes made with the alternative route powder was 0.86mg$_{Sulfur}$/cm^2. The cells were cycled at a C-rate of C/12 between cut off voltages of 3 V$_{Li/Li+}$ and 1.5 V$_{Li/Li+}$. As electrolyte 30 µL of DOL:DME + 1 M LiTFSI/0.5 M LiNO$_3$ was used. The standard deviation of both measurements was obtained from 3 repeated measurements.

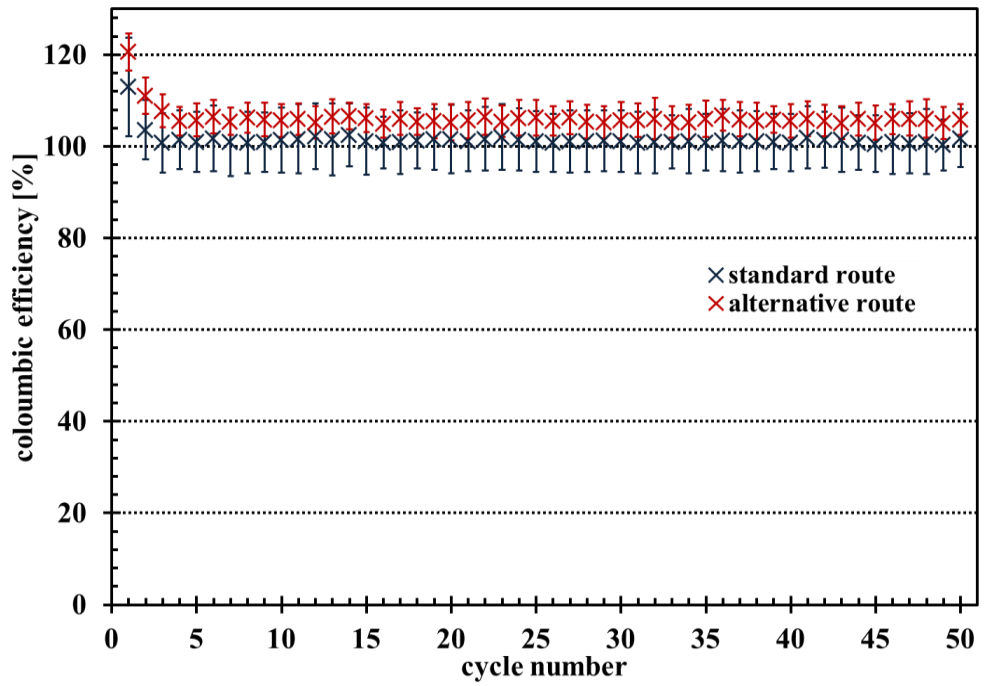

Figure 33: Coloumbic efficiency over cycle number for the measured S/C-composite cathodes based on a Vulcan XC72 carbon made by electrode preparation method 1 with S/C-composite powder from the standard (blue symbols) or the alternative (red symbols) synthesis route. The average S loading for the electrodes made with the standard route powder was 0.88 mg$_{Sulfur}$/cm^2 and for electrodes made with the alternative route powder was 0.86 mg$_{Sulfur}$/cm^2. The cells were cycled at a C-rate of C/12 between cut off voltages of 3 V$_{Li/Li+}$ and 1.5 V$_{Li/Li+}$. As electrolyte 30 µL of DOL:DME + 1 M LiTFSI/0.5 M LiNO$_3$ was used. The standard deviation of both measurements was obtained from 3 repeated measurements.

4.2.2. Influence of storage on cycling performance of Li-S test cell

In Li-ion batteries, a standard procedure is to store the test cells for a certain time span before they get electrochemically cycled. This should help the system to build up a good SEI on the electrodes at OCV and the dry cell components have time to get properly wetted. In this way, the cell resistance should be lowered and the capacity loss between the cycles gets minimized, which leads to higher capacities over cycle number and an increasing cycle life. This issue raised the question, if a defined storage time before cycling of a Li-S battery can also help to build up a better SEI on the anode side and thereby improve shelf life and lower the polysulfide shuttle phenomenon during charge step.

Therefore, defined storage times were assigned and two cells for each resting time were built. Also, two cells, which were started immediately after assembly, were built to compare the results and to see if the storage has a benefit on the discharge capacity, the cell performance over cycle number and/or the coloumbic efficiency of the cell. As S/C-composite cathodes, made with Methode 1 (Figure 15), a Super C65 based S/C-composite with a ratio of 66 wt% S and 34 wt% Super C65 was chosen with S loadings between 4.16 mg_{Sulfur}/cm^2 and 4.62 mg_{Sulfur}/cm^2. More details are listed in Table 8.

Table 8: Storage conditions, S loading on the S/C-composite cathodes (two cells for each condition) and used electrolyte composition.

Electrolyte	Storage time	Sulfur loading [mg_{Sulfur}/cm^2]	Average discharge capacity [mAh/g_{Sulfur}]
DOL:DME + 1 M LiTFSI/0.5 M $LiNO_3$	started immediately	4.26±0.05	789±65
	13 hours	4.16±0	1042±63
	48 hours	4.16±0	1111±11
DOL:DME + 1 M LiTFSI	started immediately	4.62±0.002	884±62
	48 hours	4.50±0	408±6

First of all, cells with a DOL:DME + 1 M LiTFSI/0.5 M $LiNO_3$ electrolyte were built, stored and electrochemically tested. The cells were assembled as described in Chapter 3.5.1 and straight after assembly of the cells impedance spectroscopy was used to measure their high frequency resistance (HFR). Because none of them showed an unexpected high resistance, two cells were immediately started, while the other four were placed in a climatic chamber for the storage times specified in Table 8. Afterwards, they were also connected to the battery cycler. All cells were cycled galvanostatically at a C-Rate of C/12 with cut off voltages of 1.5 $V_{Li/Li+}$ for the discharge and 3.0 $V_{Li/Li+}$ for the charge.

In Figure 34 [a] the representative first discharge charge profiles of the cells with different storage times are visible. The cells with no storage time (blue line) showed a typical discharge curve with two plateaus at 2.28 $V_{Li/Li+}$ and 2.0 $V_{Li/Li+}$. The discharge capacity of 789±65 mAh/g_{Sulfur} in average fits to the value which one expected for S/C-composite cathodes with this type of carbon and S loading. Also, the charge curve showed a typical shape for a Li-S battery system and the charge process stops at approximately the same capacity, which was reached in the discharge step, with steep potential increase towards the cut off potential at the end of charge. So, no overcharge of the cell can be observed, which is successfully suppressed because of the use of $LiNO_3$ as additive. The discharge profiles of the cells, which were stored for a defined time (red line for 13 h storage time and green line for 48 h storage time), present also the two typical discharge plateaus at the same potentials as for the non-stored test cells. Compared to the immediately started cells, it is clearly visible that the first discharge capacity rose up and average discharge capacities of 1042±63 mAh/g_{Sulfur} for the cells with 13 h storage time (red line) and 1111±11 mAh/g_{Sulfur} for cells with 48 h storage time (green line) can be achieved. This equals to an average increase of 24% after 13 h and 29% after 48 h in discharge capacity. But the charge curves revealed an undesired behavior. The charge potential did not rise up after the value of the discharge capacity was reached and the charge process instead went on, till the cells were manually stopped. This indicates that the polysulfide shuttle mechanism in the cell could take place unhindered and the cell can be charged infinitely, if the cells were rested before galvanostatic cycling. Also, the overpotential of the stored cells is slightly higher compared to the immediately started cells.

During the resting time of the test cells, polysulfides are created on the cathode side and an SEI on the anode side can be formed. Over the resting time, one would expect that the SEI on the Lithium will be properly built up and the loss of active material towards the Li-anode in the following galvanostatic cycling should be minimized. But in a Li-S battery system, the creation of polysulfides starts immediately after the contact with the electrolyte, because small amounts of S are getting dissolved, which in turn will react with the Li^+-ions of the solution. The long chain polysulfides which will appear in the first instance can now diffuse to the Li-anode and get reduced to polysulfides with shorter chain length. So, the shuttle mechanism and the SEI formation take place at the same time and the mechanism of the SEI formation differs from the passivation of the Li-anode in the first discharge. Holding the test cells at OCV for extended amounts of time versus discharging the cells obviously leads to a different

structure of the protective SEI layer, which is not sufficiently protective to prevent a large polysulfide shuttle and leads to a large or even endless overcharge of the test cells.

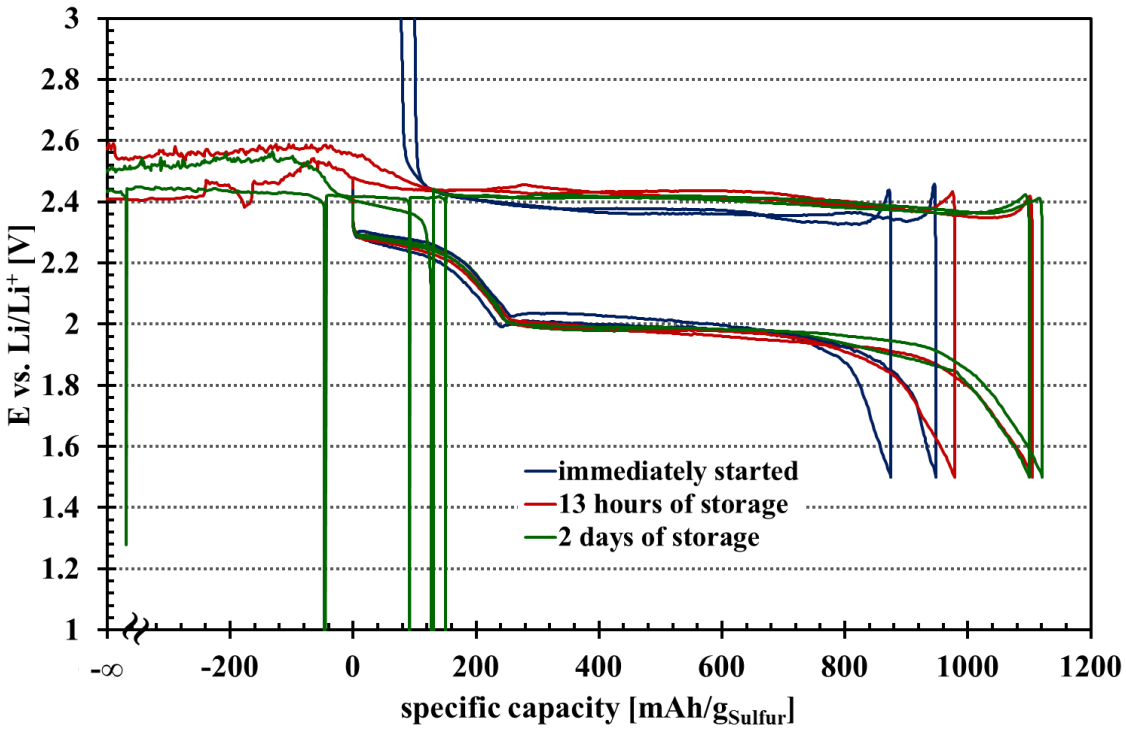

[a]

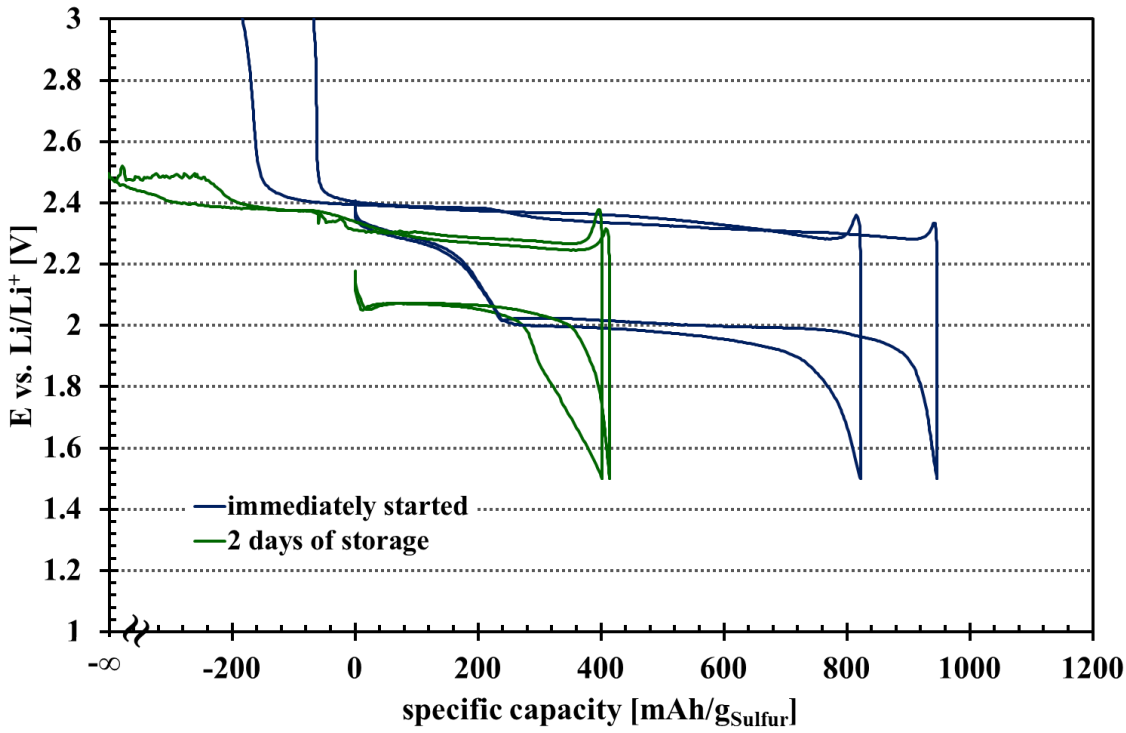

[b]

Figure 34: First galvanostatic cycle of the test cells at C/12 after the different storage scenarios with [a] DOL:DME + 1 M LiTFSI/0.5 M LiNO3 and [b] DOL:DME + 1 M LiTFSI as electrolyte (Table 8). The used S/C-composite cathodes are based on a Super C65 carbon black with a weight ratio of 66 wt% S/34 wt% C, the S loadings range between 4.16 to 4.62 mg_{Sulfur}/g and 30 µL of the specific electrolyte per test cell was used. (Color code: blue –test cells, which were immediately started after assembly; red – test cells after 13 h storage; green – test cells after 48 h of storage)

Also, a higher saturation of the electrolyte with polysulfides can be expected, because the solubility of them are very high and the large time frame promoted the dissolution.[25] But, the loss of active material in the test cell with the resting time did not influence the discharge capacity, because compared to the high S loading on the S/C-composite cathode the amount of S species, which are involved in the reaction on the Li-anode is small.

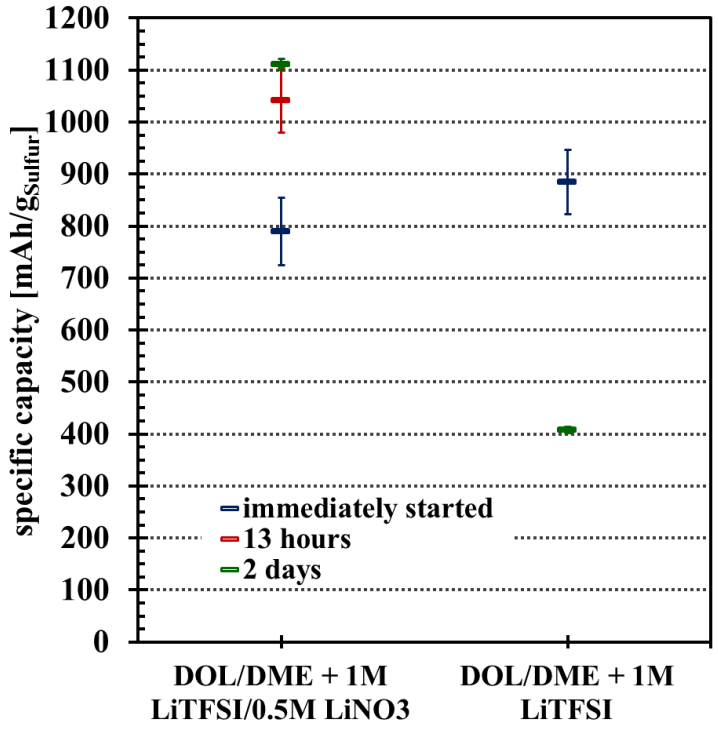

Figure 35: Comparison of the average first discharge capacity for the different storage conditions (Table 8) of S/C-cathode test cells, cycled at C/12. The used S/C-composite cathodes are based on a Super C65 carbon black with a weight ratio of 66 wt% S/34 wt% C, the S loadings range between 4.16 to 4.62 mg$_{Sulfur}$/g and 30 µL of the specific electrolyte per test cell was used. The standard deviation was calculated from 2 cells for each testing condition. (Color code: blue – test cells, which were immediately started after assembly; red – test cells after 13 h storage; green – test cells after 48 h of storage)

In Li/S-batteries, the additive $LiNO_3$ had shown a positive effect on the suppression of the overcharge due to its chemical reactions on the Li-surface, which help to build up a proper SEI and so it was established in standard electrolyte solutions. The reaction of $LiNO_3$ on the Li-surface is described in Chapter 2.3.3 and one can see that it also reacts with polysulfide species. To exclude that the overcharge is triggered by the additive salt $LiNO_3$, cells without the additive salt in the electrolyte under the same test conditions were studied (Figure 34 [b]). Here, only the extreme storage condition of 48 h was tested, because the cells with storage times of 13 h and 48 h did not show differences in the discharge charge profile and during the longer storage time the S in the cathode had more time to get dissolved to create polysulfide species, which can benefit the shuttle mechanism during charge. The immediately started cells without $LiNO_3$ additive (blue line, Figure 34 [b]) demonstrated a similar discharge behavior as the cells with $LiNO_3$ additive. The first average discharge capacity of 884±62 mAh/g$_{Sulfur}$ is about 100 mAh/g$_{Sulfur}$ higher compared to the average discharge capacity of the immediately started cells with $LiNO_3$ additive (blue symbols, Figure 35). The charge step showed a nice

smooth curve and only a slight overcharge of the cell. This can be referred to the weaker SEI on the Li-anode, due to the absences of the $LiNO_3$ additive. Thereby, the long polysulfides can reach the Li-anode more easily and the shuttle mechanism is promoted. For the stored test cells without $LiNO_3$ in the electrolyte (green line, Figure 34 [b]) a big change in the discharge profile occurred. Already, the OCV potential of the test cells was different and with 2.16 $V_{Li/Li+}$ 250 mV lower compared to all other test cells at the various conditions. When the test cells were started, the potential dropped immediately to 2.06 $V_{Li/Li+}$, at which predominantly short polysulfides are represented in the electrolyte solution. This indicates that during the storage time, the created polysulfides can be transformed from S over the long chain species to short chain polysulfides. Due to this, the discharge capacity of the test cells can only be gained from reactions, which occur at the second plateau and thus only 408±6 mAh/g_{Sulfur} can be achieved. The recharge of the test cells is also not possible under these conditions and they were overcharged till they were manually stopped as well. So, the claim that $LiNO_3$ have a negative effect on the charge behavior of a stored test cell can be ruled out.

Closing this topic, one can say that storage of a Li-S battery improved its first discharge capacity, but it led to a primary battery cell, because the system cannot be recharged anymore. The use of $LiNO_3$ did not affect the overcharge of the test cells and had more a beneficial impact on the first discharge capacity of the measured test cells. Due to the fact that commercial available test cells have longer resting times at OCV when the device is switched off, a more effective passivation layer on the Li-anode has to be created or a diffusion barrier in the battery cell has to be implemented to stop the shuttle mechanism during the resting time.

4.2.3. Impact of Sulfur loading on the discharge capacity and cycling performance

For the commercial use in electrical vehicles, the areal capacity (mAh/cm^2) of the electrode is a key factor.[96] To realize high areal capacities without increasing the weight of the battery, high S loading as well as a high S content in the S/C-composite is necessary. Also, an easy manufacturing of a Li-ion battery is a big issue for the industry, because the cost for the production of commercial devices has to be in a range that it is affordable for the consumer. So, the influence of the S loading on the discharge/charge behavior was tested with an S/C-composite on a Super C65 basis. With this carbon black, it is relatively easy to get S/C-composite cathodes up to roughly 5 mg_{Sulfur}/cm^2 with an S/C-ratio of 65.2 wt%/34.8 wt%.

A view in the literature showed, that other research groups also tried to increase the S ratio in the S/C-composite, the S loading on the electrode or both. With low S loadings between 0.42 mg_{Sulfur}/cm^2 and 0.84 mg_{Sulfur}/cm^2 and a S content of 45 to 60 wt% in the raw material they got discharge capacities of over 1000 mAh/g_{Sulfur}, but for higher S loading and/or higher S weight percentage in the S/C-composite, the discharge capacities predominately drop (Table 9). The highest reported S loading of 7 mg_{Sulfur}/cm^2 was reported by Wei et al.[134], but they are not able to cycle the cell with a reasonable discharge capacity. The best result showed S.S. Zhang and Read[131] with a S loading of 3 mg_{Sulfur}/cm^2 and 77 wt% S in the S/C-composite. They reached a first discharge capacity of approximately 950 mAh/g_{Sulfur} (2.85 mAh/cm^2), but around 48% of the initial discharge capacity was lost after 20 cycles[132]. In all the studies, compared here, a Super P carbon support was used. However, a comparison of the Super P and the Super C65 carbon black showed that the two types only differ in the grid content and for Super C65 carbon black a higher purity of the powder is given (Table 10). But these small variations have no impact on the cycling performance of the S/C-composite cathodes so that a comparison is still possible.

To go into detail, a reason for the poor capacity and cycle life of the reviewed S/C-composite cathodes with high S loading and/or high S weight percentage could be the mixing of the inks used for the electrode preparation. In most cases, when detailed information was given, the S powder and carbon black were only mixed as received with the binder and some solvent[74,85,133,134], before the ink was casted onto an aluminum current collector. Only in two of the chosen articles, the use of a ball mill to mix the cathode ingredients was reported[73,96] and one described a milling step of the S particles before it was mixed with the carbon black and the binder[50]. With these methods, a good connection between the S particles and the carbon black support is not necessarily given and the S particles will be relatively big, especially when they were used as-received. But to get high discharge capacities, a good connection between the carbon host and the active material is very important. With the synthesis method described here (Chapter 3.1), these issues can be addressed and an S/C-composite with well distributed nano-S particles on the carbon surface and a good electrical connection between S and carbon black can be generated.

Table 9: Literature data on S/C-composite cathodes based on a Super P carbon black

Carbon type	Discharge capacity	Sulfur		Current	Literature
	1st	loading	in composite	C-rate	
	[mAh/g_{Sulfur}]	[mg_{Sulfur}/cm^2]	[wt%]	-	
Super P	1100	0.42	45	C/10	[85]
	685	2.00	50	C/10	[73]
	1135.6	0.65	56.7	C/4	[50]
	1035.4	1.49	56.7	C/10	[50]
	584.5	3.12	56.7	C/10	[50]
	1000	0.84	60	C/10	[85]
	720	1.5 – 2	60	C/10	[74]
	1150	1.5 – 2	60	C/10	[133]
	700	0.88	70	C/16	[96]
	900	1.01	70	C/10	[85]
	42.6	7.00	70	C/2	[130]
	420	1.5 – 2	70	C/11	[74]
	610	2.40	77	-	[131]
	950	3.00	77	-	[132]
	790	1.97	80	C/10	[85]

Table 10: Comparison of the specifications of Super P and Super C65 carbon black (product specification found on http://www.xuxtl.com (2016))

Super P		Super C65	
Volatile Content	0.15%	Volatile Content	0.15 % max.
Toluene Extract	0.10%	Toluene Extract	0.10% max.
Ash content (600C)	0.05%	Ash content (600C)	0.025% max.
Grit content > 45 microns	5 ppm	Grit content > 45 microns	< 2ppm
Grit content > 20 microns	25 ppm	Grit content > 20 microns	12 ppm
BET Nitrogen surface area	$62m^2/g$	BET Nitrogen surface area	$62m^2/g$
Adsorption stiffness value	32ml/5g	Adsorption stiffness value	32ml/5g
Moisture	0.10%	Moisture	0.10%
Density	$160kg/m^3$	Density	$160kg/m^3$
Sulfur Content	0.02%	Sulfur Content	0.02%
PH	10	PH	10
Iron	5ppm	Iron	2ppm
Nickel	1ppm	Nickel	1ppm
Vanadium	1ppm	Vanadium	< 1ppm
		Chromium	< 1ppm
		Copper	< 1ppm

To prove this assumption, an S/C-composite on basis of a Super C65 carbon black was synthesised with a final S/C-ratio of 65.2 wt%/34.8 wt%. From this powder, cathodes with different S loadings between 1.03 mg_{Sulfur}/cm^2 and 4.63 mg_{Sulfur}/cm^2 were made and test cells were galvanostatically cycled with a C-rate of C/12. 30 µL of DOL:DME + 1 M LiTFSI/0.5 M $LiNO_3$ electrolyte was used.

In Figure 36 a representative first discharge/charge cycle of S/C-composite cathodes is shown with the different S loadings (Table 11). In the discharge step both plateaus are nicely pronounced and can be assigned to the reaction of S_8 to Li_2S_x ($6 < x \leq 8$) at the higher voltage plateau and the reaction of long chain polysulfides to Li_2S_x ($2 < x \leq 6$) in the lower voltage plateau.[18,53,74] For all S loadings, the first discharge plateau had a similar length and

delivered a discharge capacity of ~ 250 mAh/g_{Sulfur}, which correlates very well with the proposed reaction equation.[18,131,132]

$$S_8 + 2e^- \rightarrow S_8^{2-} \rightarrow S_6^{2-} + {}^1/_4\, S_8 \qquad (4.1)$$

When S_6^{2-} is assumed as final polysulfide product in the solution at the end of the first discharge plateau, a theoretical capacity of ≈279 mAh/g_{Sulfur} can be expected. This is consistent with the measured value, and the slight difference can be explained by the fact that other longer and shorter polysulfides are likely produced to a minor extent, but S_6^{2-} is the predominate polysulfide species at this point of the discharge.

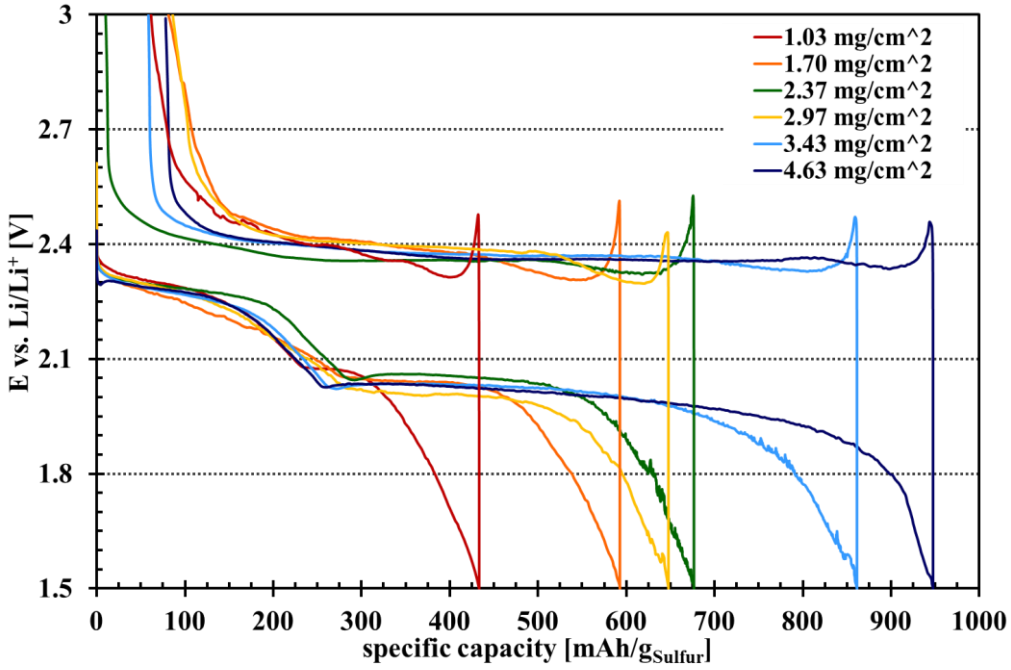

Figure 36: Representative first discharge/charge cycle of S/C-composite cathodes based on a Super C65 carbon black with different S loadings at C/12 (Table 11). The measurements were carried out in modified Swagelok T-fittings (Chapter 3.5). The area of the cathode as well as the anode was 0.785 cm^2, as electrolyte 30µL of DOL:DME + 1M LiTFSI/0.5 M $LiNO_3$ were used and the cells were galvanostatically cycled between 3 and 1.5$V_{Li/li+}$.

In the second plateau a gain in length with increasing S loading on the S/C-composite cathode can be observed. During the first discharge step the electrolyte is getting saturated with polysulfide species and as described earlier, a fraction of the S will be lost in side reactions, like the SEI formation or the polysulfide shuttle mechanism. With a low S loading on the S/C-composite cathode, the percentage of S, which takes place in the side reactions, is much higher compared to cathodes with a high S loading. So, if the S amount on the S/C-composite cathode is increased, the overall percentage of S loss is getting negligible and more active material will be present for the reversible cell reactions, leading to an increase of the discharge capacity. Interestingly, it showed a linear trend (Figure 38, dashed purple line),

when the first discharge capacities of the test cells were plotted against the S loading of the S/C-composite cathodes. So, based on this trend, a further increase in S loading on the cathode side could still improve the discharge capacity and the cycling performance of the test cells. Also, after 30 cycles the linear trend can be still observed (Figure 38, light purple dashed line).

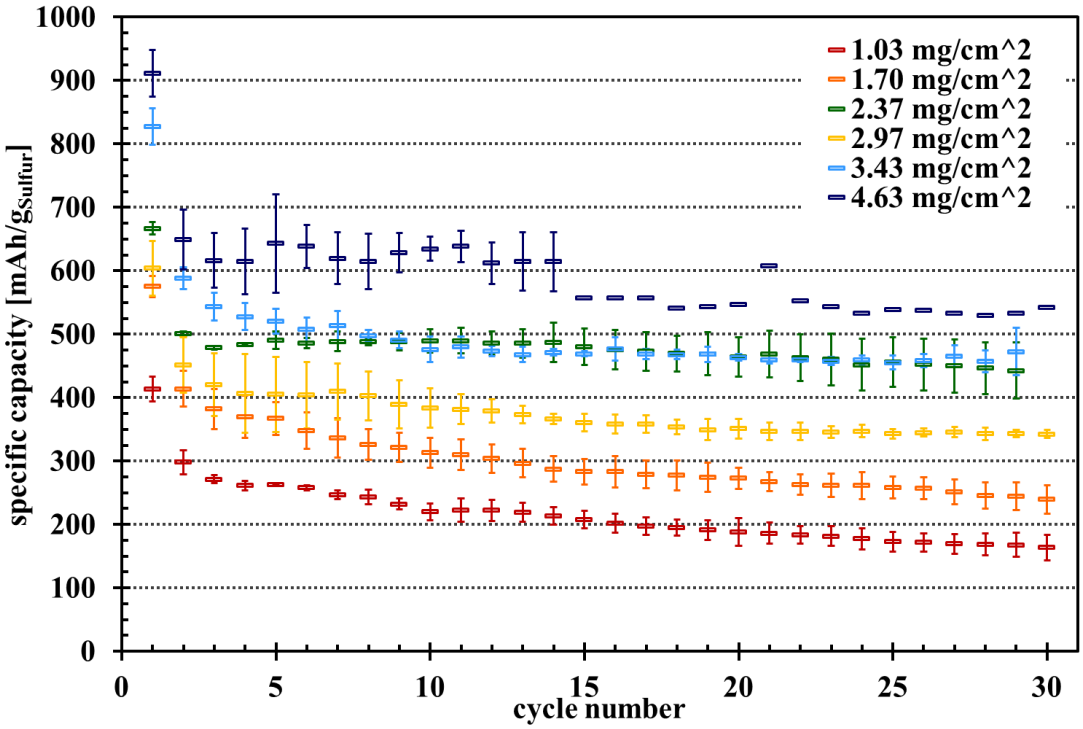

Figure 37: Discharge capacity over cycle time of all measured S/C-composite cathodes based on a Super C65 carbon black with different S loadings at a C-rate of C/12 (Table 11). The measurements were carried out in modified Swagelok T-fittings (Chapter 3.5). The area of the cathode as well as the anode was 0.785 cm^2, as electrolyte 30µL of DOL:DME + 1M LiTFSI/0.5 M LiNO3 were used and the cells were galvanostatically cycled between 3 and 1.5VLi/li+.The standard deviation was calculated from 2 to 3 test cells.

Between the first and the second discharge cycle, the normal capacity loss can be observed (Figure 37). Also here, the loss can be attributed to irreversible side reactions between polysulfide species and the Li-anode or the loss of electrical contact of S-particles during the first cycle.[51,54] For S/C-composite cathodes with a low S loading, these phenomena will be the major reasons for the active material loss, but in test cells with high S loading cathodes, a further effect can influence the capacity drop. Because of the thickness of the S/C-composite cathode (70-80 µm$_{cathode}$ for high S loadings vs. 20-25 µm$_{cathode}$ for low S loadings), the change in the cathode structure will be more significant. During the first discharge, the solid S will be transformed to polysulfide species and is getting dissolved in the electrolyte.

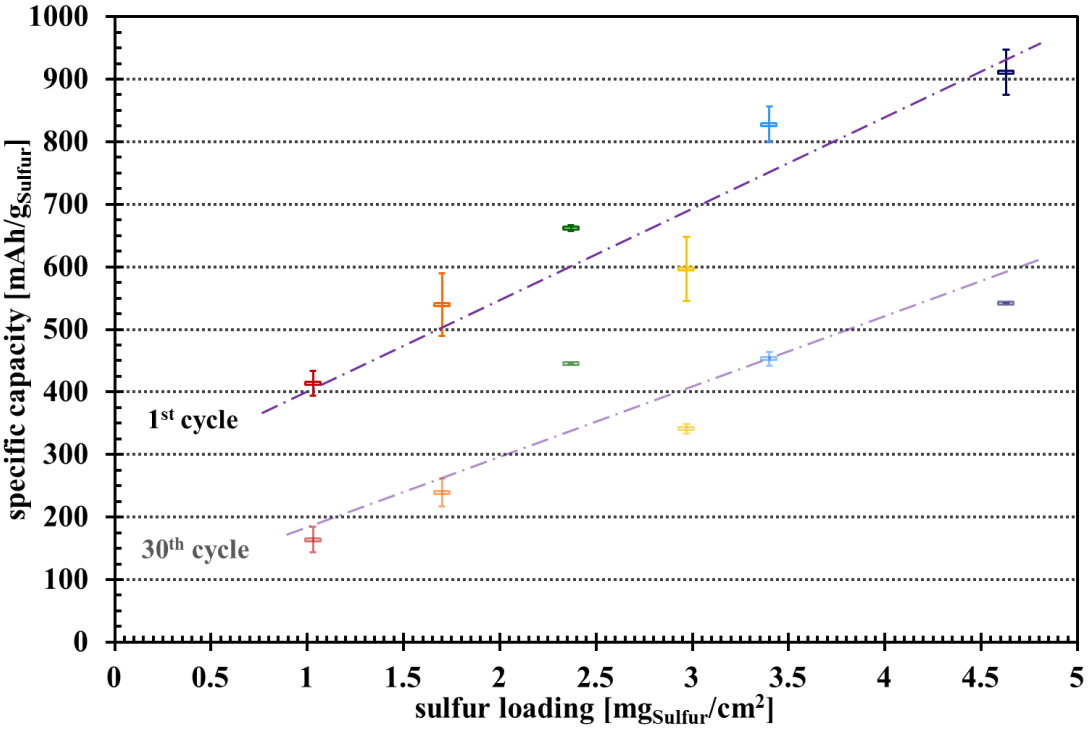

Figure 38: 1st and 30th discharge capacity of all measured S/C-composite cathodes based on a Super C65 carbon black with different S loadings at a C-rate of C/12 (Table 11). The measurements were carried out in modified Swagelok T-fittings (Chapter 3.5). The area of the cathode as well as the anode was 0.785 cm^2, as electrolyte 30µL of DOL:DME + 1M LiTFSI/0.5 M $LiNO_3$ were used and the cells were galvanostatically cycled between 3 and 1.5$V_{Li/Li+}$. The standard deviation was calculated from 2 to 3 test cells and the dashed lines are inserted as a guide for the eye.

In the following charge, the cell reaction will be reversed and the polysulfides will be precipitated as S on the carbon matrix at the end. The deposition of S can lead to bigger agglomerates or thick S film. In the next discharge, these agglomerates or films can be isolated from the carbon matrix. The S which is in direct contact to the carbon matrix will be reacting first, because the resistance for the electrons is the smallest at this region. This can lead to a separation of the agglomerates or films from the cathode and an irreversible loss of active material, which is not available for the cell reactions in further cycles.[13,50,56,85] In the subsequent cycles, the decrease in discharge capacity is much lower, because of the SEI on the Li-anode, which hinders undesired side reaction of the polysulfide species during charge, and no significant changes in the cathode structure will take place anymore. But the discharge capacity loss between the discharge cycles in S/C-composite cathodes with low S loadings is higher compared to middle and high S loadings (Table 11). The absolute amount of irreversibly lost active material is in all test cells comparable, but with a high S loading on the S/C-composite cathode the ratio of lost S to the total S amount is not as significant as compared to a cathode with a lower S mass and a more stable cycling performance can be obtained.

But with high S loading on the cathode other problems occurred. One problem was to produce a stable cathode film with a high S amount, which was did not crack or peeled off from the current collector during the drying process and did not break when the cathodes were cut out. Another problem occurs during cycling of the S/C-composite cathodes. The electrochemical tests of all cathodes with different S loading were done with the same amount of electrolyte. When the amount of electrolyte was calculated in relation to the S amount on the cathode, a cathode with a low S loading of 1.03 mg_S/cm^2 and the standard amount of 30µL of 37µl/mg_S are available for the cell reactions. Compared to this value a cathode with 4.63 mg/cm2 has only 8.25 µL/mg_S available. If cathodes with a high S loading were used, the amount of electrolyte could be not sufficient to wet the electrode properly. Also the consumption of electrolyte during cycling is higher because of the higher amount of S and the bigger surface

Table 11: S loadings of the different S/C-composite cathodes, 1st average discharge capacities and capacity loss between the 1st and 2nd cycle as well as the average capacity loss for subsequent cycles*. The S/C-composite cathodes were made with Method 2 (Figure 15) and the standard deviation was calculated from 2 to 3 test cells.

Carbon type	Sulfur loading	Discharge capacity	Capacity loss	
	on electrode	1st cycle	between 1st & 2nd cylce	Ø supsequent cycles*
	[mg_{Sulfur}/cm^2]	[mAh/g_{Sulfur}]	[%]	[%]
Super C65	1.03	432±20	28	2.1
65.2wt% Sulfur	1.70	575±50	28	2.0
	2.37	667±5	25	0.5
	2.97	604±51	25	1.0
	3.43	828±29	29	0.8
	4.63	911±35	29	0.4[a]

*** average capacity loss between discharge cycle 2 and 30**

[a] average capacity loss between discharge cycle 2 and 16

area on the electrode, which is reported in literature, and was not considered when the test series was measured.[135] This could lead to the shorter cycle life of test cells with high S loading cathodes and due to the coating difficulty the cycling data were hard to get.

The results of this investigation has proven that it is possible to get high discharge capacities as well as a good cycling performance with a S/C-composite cathode, which has a high S-content in the S/C-composite and a high S loading. The important point for these results can be mainly referred to the good connection between the S and the carbon black, is the case for nano-sized S deposits produced by our synthesis method.

4.2.4. Investigation of different carbon supports and their impact on the discharge capacity and cycling stability

The choice of the carbon black support for the S can play an important role for the performance of a battery. High surface area supports can increase the discharge capacity drastically, because more active sites for the cell reactions are available. If additionally mesopores and/or micropores are offered by the carbon black, the decay of S loss over cycle time can be decreased, because these pores have the ability to capture and retain polysulfides.[49,87,90,91,92,136,137]

Based on this knowledge, four different carbon black types (Table 12) were used to prepare S/C-composite cathodes, and the performance of the test cells were compared. In the beginning of this work Vulcan XC was used as the standard carbon black support for the S/C-composite powders. It has a total specific surface area of 240 m^2/g, whereof 96 m^2/g are contributed by the external surface area and the rest contributed by micro pores. The second carbon black, which was used earlier in this work, was a Super C65 carbon black. This one had a very low surface area of 68 m^2/g with essentially no micro or meso porosity. As contrasting samples, two carbon blacks with a high surface area were chosen: Ketjen Black with a total specific surface area of 838 m^2/g and Black Pearls with 1509 m^2/g. Both have a similar external surface area of ~700 m^2/g[129], but the size of the pores, pore size distribution and total pore volume of these carbon blacks differ to a great extent (**Fehler! Verweisquelle konnte nicht gefunden werden.**). During the synthesis of the S/C-composite powder, the S can only precipitate on the external surface of the carbon black support, because the particles are too big to access the micro pores. So, in this step only the external surface of the carbon black is decisive for the "film thickness" of the precipitated S. A calculation[IV] of the thickness of the S film on the different carbon supports showed, that the S film on Ketjen Black (~1.2 nm) or Black Pearls carbon support (~1.5 nm) is 8 times thinner compared to a Vulcan XC support (~9.9 nm) and an order of magnitude thinner compared to a Super C65 support (~13.5 nm). Because of the very small electronic conductivity of S ($5x10^{-30}$ Scm^{-1} [67]), the reaction from S_8 to Li_2S_x will preferably take place at the S carbon interface. Here, the diffusion path for the electrons is small and thereby the transfer resistant will be minimized. Due to a thin S

[IV] The thickness t was calculated with $t = \frac{m_{S_8}}{\rho_{S_8} \cdot A_{carbon}}$, where m_{S_8} is the mass of the Sulfur on the S/C-composite cathode, ρ_{S_8} is the density of Sulfur ($2.07 \frac{g}{cm^3}$) and A_{carbon} is the external surface area of the carbon black. It was assumed that the Sulfur will be homogeneously distributed over the surface of the carbon and no bigger particles will be formed during the synthesis.

"film" on the high surface area carbon blacks, the reaction sites between support and S is enlarged and the contact resistance is smaller.[56,86,138]

Table 12: S loading of the S/C-composite cathodes based on different carbon black supports, first discharge capacity and capacity loss between 1st and 2nd cycle as well as an average for the subsequent cycles. The standard deviation value was obtained from 2-3 repeated measurements.

Carbon type	Sulfur		Discharge capacity	Capacity loss	
	loading	in composite	1st cycle	between 1st & 2nd cylce	Ø supsequent cycles*
	[mg_{Sulfur}/cm^2]	[wt%]	[mAh/g_{Sulfur}]	[%]	[%]
Super C65	1.03	65.2	432±20	28	2.1
	2.97	65.2	604±51	25	1.0
Vulcan XC72	1.05	66.5	558±55	22	2.3
Ketjen Black	1.14	67.6	1275±17	33	2.1
	3.05	67.6	1177±28	21	1.0
Black Pearls	1.41	69.2	1012±1	2.4	1.3

*** average capacity loss between discharge cycle 2 and 30**

On this basis a high utilization rate of the S on the S/C-composite cathode during the discharge step should be reached, which led to high discharge capacities. Furthermore, a higher external surface area offers more space for the discharge product Li_2S, which will precipitate on the carbon black at the end of the discharge cycle. On the larger area, the Li_2S precipitate will be better distributed and thinner films or particles will be generated. Therefore, it is expected, that test cells with high surface carbon black cathodes show a better long term performance compared to test cells with low surface area carbon black cathodes.

To check this hypothesis, S/C-composite powders with all four carbon supports were synthesised and S/C-composite cathodes with an S loading between 1.03 mg_{Sulfur}/cm^2 and 1.41 mg_{Sulfur}/cm^2 were produced using Method 2 (Figure 15). The S contents of the different S/C-composites as well as the specific S loadings are listed in Table 12. The test cells were galvanostatically cycled with a C-rate of C/12 and 30 µL of DOL:DME + 1 M LiTFSI/0.5 M $LiNO_3$ was used as electrolyte.

In Figure 39 a first representative cycle of S/C-composite cathodes with the different carbon supports are shown. S/C-composite cathodes, which are based on a high surface area carbon support showed significantly higher discharge capacities compared to the low surface area carbon black based S/C-composite cathodes. The best first discharge capacity of over 1200 mAh/g_{Sulfur} can be reached with a Ketjen Black support, which is roughly 87% of the practical available discharge capacity of 1461 mAh/g_{Sulfur} in a DOL:DME electrolyte[18].

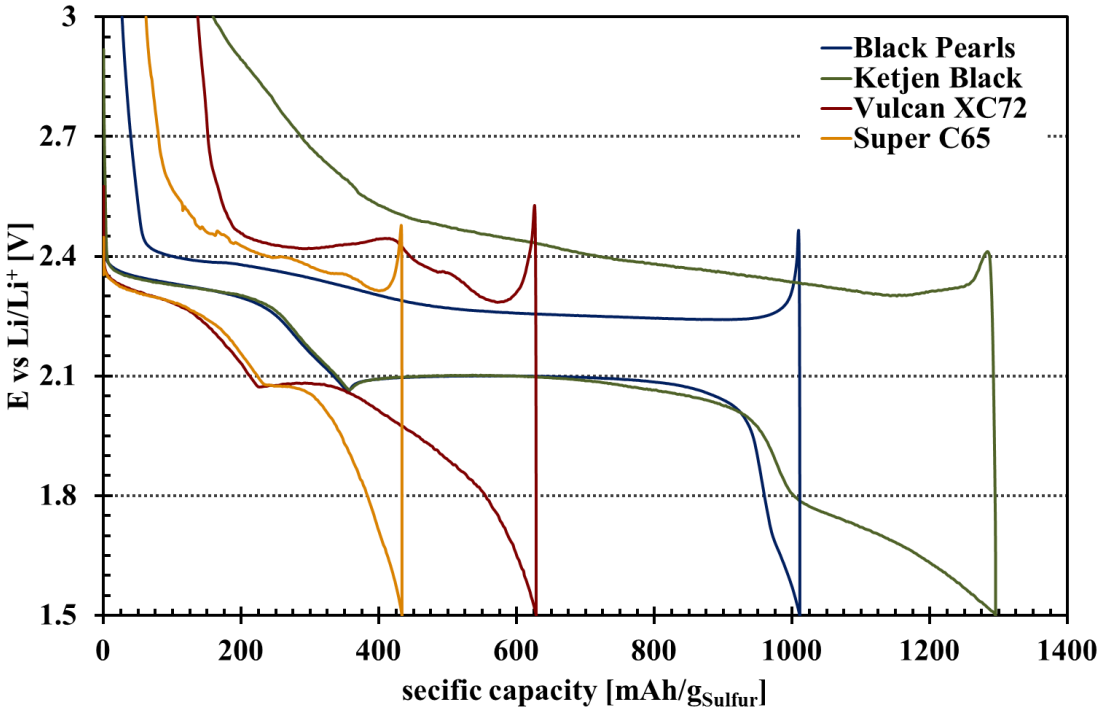

Figure 39: First representative cycle profile of S/C-composite cathodes based on different carbon black supports with an S loading between 1.03 and 1.41 mg_{Sulfur}/cm^2 (Table 12). As test cells modified Swagelok T-fittings were used and cycled at C/12 rate between 3 and 1.5$V_{Li/Li+}$ and 30 µL of DOL:DME + 1 M LiTFSI/0.5 M $LiNO_3$ was used as electrolyte.

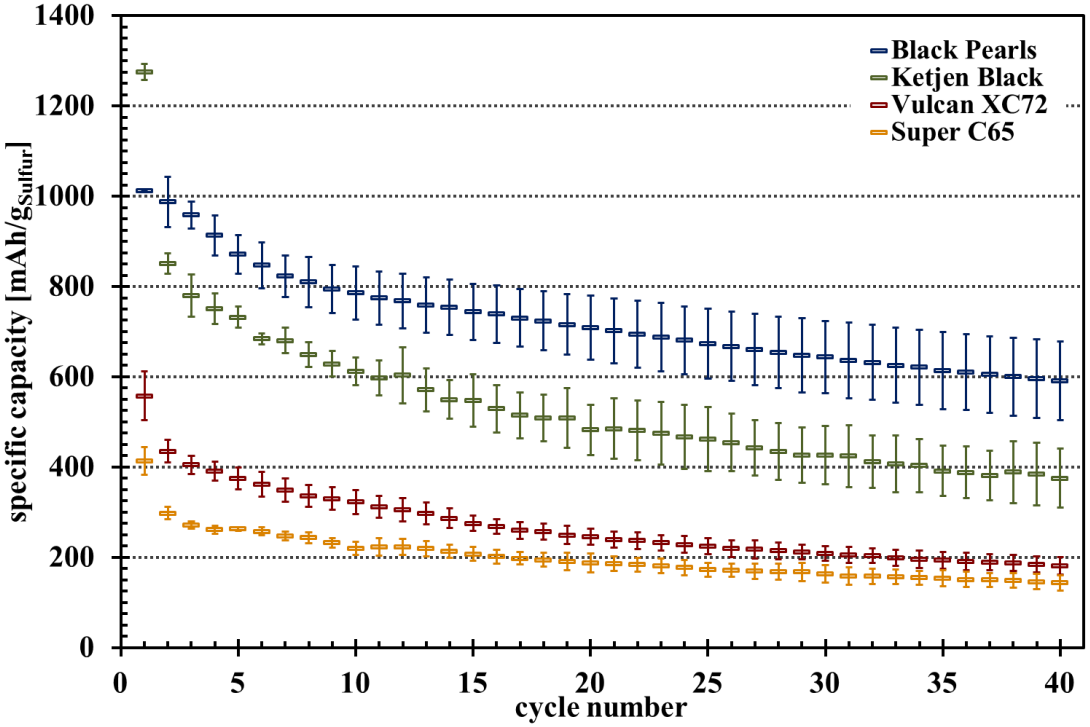

Figure 40: Comparison of the cycling performance over cycle number of S/C-composite cathodes based on different carbon black support with an S loading between 1.03 and 1.41 mgSulfur/cm2 (Table 12) at a C-rate of C/12 using 30 µL of DOL:DME + 1 M LiTFSI/0.5 M LiNO3 as electrolyte. As test cells modified Swagelok T-fittings were used and cycled at C/12 rate between 3 and 1.5VLi/Li+. The standard deviation values were obtained from 2-3 repeated measurements.

Remarkable discharge behavior of this carbon type was, that the discharge curve of the Ketjen Black based cathodes differed from the other discharge curves, because of a “third” plateau at the end, which were attributed to the small micro pores on the support.[137] These pores have the ability to absorb polysulfides from the electrolyte solution and so the reaction area of the cathode is expanded by the surface area of the small pores and in this way the discharge capacity were increased at the end of the cycle. The lowest discharge capacity of 413.5 mAh/g_{Sulfur} was delivered from the Super C65 based S/C-composite electrode, as one expected from the theory, because of its low specific surface area. But the small pores of the Ketjen Black carbon had the most beneficial effect on the first discharge capacity. In further cycles, the best overall cycling performance was reached with S/C-composite cathodes on the basis of a Black Pearls carbon support (Figure 40). Between the first and the second cycle the loss of discharge capacity is only 2.4% and 1.3% in subsequent cycles. After 40 cycles a discharge capacity of 590 mAh/g_{Sulfur} was left and thus remained ~200 mAh/g_{Sulfur} higher compared to a Ketjen Black based cathode.

The better cycling behavior of the Black Pearls based S/C-composite cathodes could be attributed to the high total pore volume and the interaction of big mesopores and small micropores (Table 6). We hypothesize that during the first discharge step polysulfides species are formed, which can diffuse in to the small micro pores of the Black Pearls carbon and get trapped inside. The big mesopores (14.1 – 16.8 nm, Figure 27) enhance the Li^+-transport and act as a kind of reservoir for electrolyte and polysulfides. The combination of both likely reduces the shuttle mechanism during charge and the related side reactions, leading to less S loss [24,91,92,93,94,139,140,141].

Furthermore, the ability to bind the polysulfides inside the pores stabilized the structure of the carbon through the solid discharge products Li_2S_2 and Li_2S and the discharge capacity drop between the first and second cycle is strongly reduced.[85]The highest discharge capacity drop of 33% between first and second cycle was recorded for the Ketjen Black based S/C-composite cathodes. The high discharge capacity drop in between the first and second discharge cycle of the Ketjen Black based S/C-composite cathode could be explained through a partial collapse in the carbon matrix, because the carbon skeleton can be very fragile after the S is dissolved.[50] A more reliable possibility for the capacity drop could be the building of S islands or S films during the first charge step, which can be disconnected from the carbon matrix and get inactive.[13,50,56,85] Due to the fact, that the pores of the Ketjen Black carbon are relatively small, the outer surface area would be more preferred for the precipitation of the S

at the end of the charge cycle. In a Black Pearl carbon the meso pores are bigger and the accessibility for the polysulfides during the charge step is much easier. So, the precipitation of S at the end will be more uniform and the building of big agglomerates or films will be partially suppressed, which leads to a lower capacity loss in between the first two cycles.

In the subsequent cycles, the average loss of discharge capacity is again comparable to the low surface area based cathodes. Because of the small differences between micro and meso pores the ability to absorb the polysulfides and to stabilize the capacity retention in further cycles, the effect is getting insignificant. For the Vulcan XC and the Super C65 based S/C-composite cathodes, the discharge capacities in the first cycle as well as the cycling performance looked as expected and both showed discharge capacities under 200 mAh/g_{Sulfur} after 40 cycles.

To investigate if the discharge capacity over cycle time in a Ketjen Black supported S/C-composite cathode can be improved, the S loading was increased from 1.14 mg_{Sulfur}/cm^2 to 3.05 mg_{Sulfur}/cm^2. In Figure 41 the first discharge curve of an S/C-cathode based on a Ketjen Black carbon with a high S loading and a low S loading is presented. Compared to the Super C65 based S/C-composite cathode, in the first discharge capacity no further enhancement with the higher S loading for Ketjen Black based S/C-cathodes could be achieved (Table 12). But the test cells with the three times higher S loading, showed only a discharge capacity loss of 21% between the first and the second cycle, which is a decrease of 12% compared to the low S loading and in subsequent cycles the average decay went down to 1% (Figure 42). By the way, these results approved the findings with the Super C65 S/C-composite cathodes with different S loadings, which indicate that a higher S loading improved the cycling performance of the test cells significantly (Chapter 4.2.3).

At the end one can say that the surface area of the carbon support plays a significant role on the first discharge capacity and the cycling performance of the S/C-composite cathode. A high surface area can deliver high first discharge capacities and in case of Black Pearls S/C-composite cathodes decrease the discharge capacity loss of the test cells with a low S loading. An increase in S loading on the Ketjen Black S/C-composite cathodes also lead to an improvement in the cycling performance, consistent with the previous reported results with Super C65 carbon support and different S loadings.

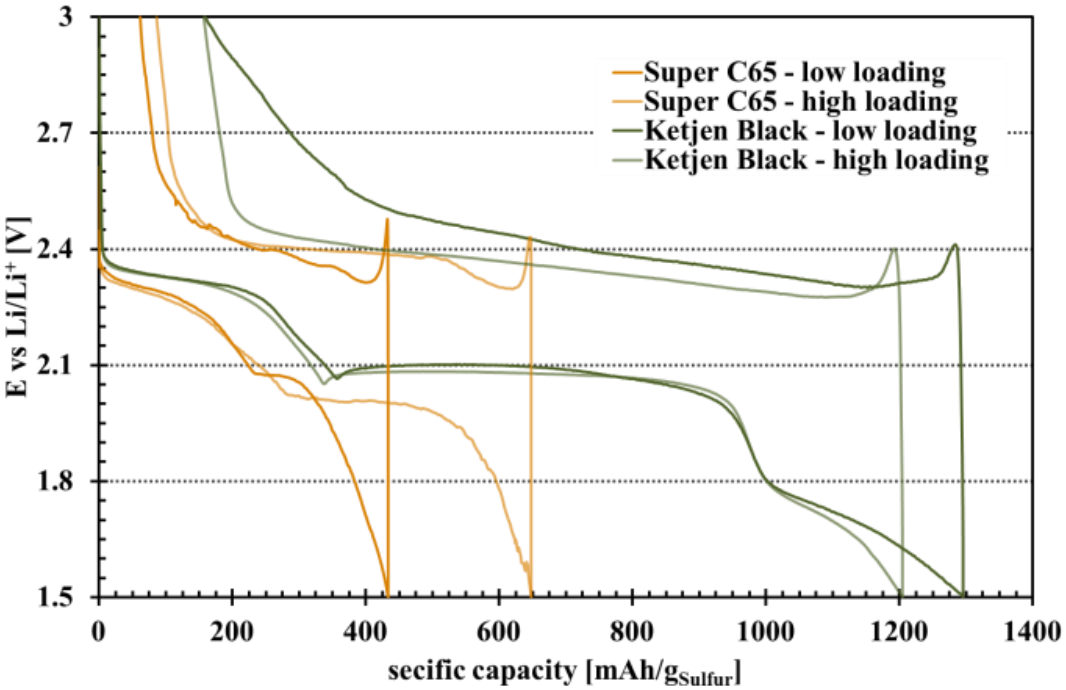

Figure 41: First representative cycle profile of S/C-composite cathodes based on a Super C65 or Ketjen Black carbon support with a high or a low S loading. The here plotted discharge curves were obtained with Super C65 based cathodes, which had a S loading of 1.03 mg_{Sulfur}/cm^2 (dark yellow) and 2.97 mg_{Sulfur}/cm^2 (light yellow) and with a Ketjen Black based cathode, which had a S loading of 1.14 mg_{Sulfur}/cm^2 (dark green) and 3.05 mg_{Sulfur}/cm^2 (light green). The test cells were cycled at C/12 rate using 30 µL of DOL:DME + 1 M LiTFSI/0.5 M $LiNO_3$ as electrolyte.

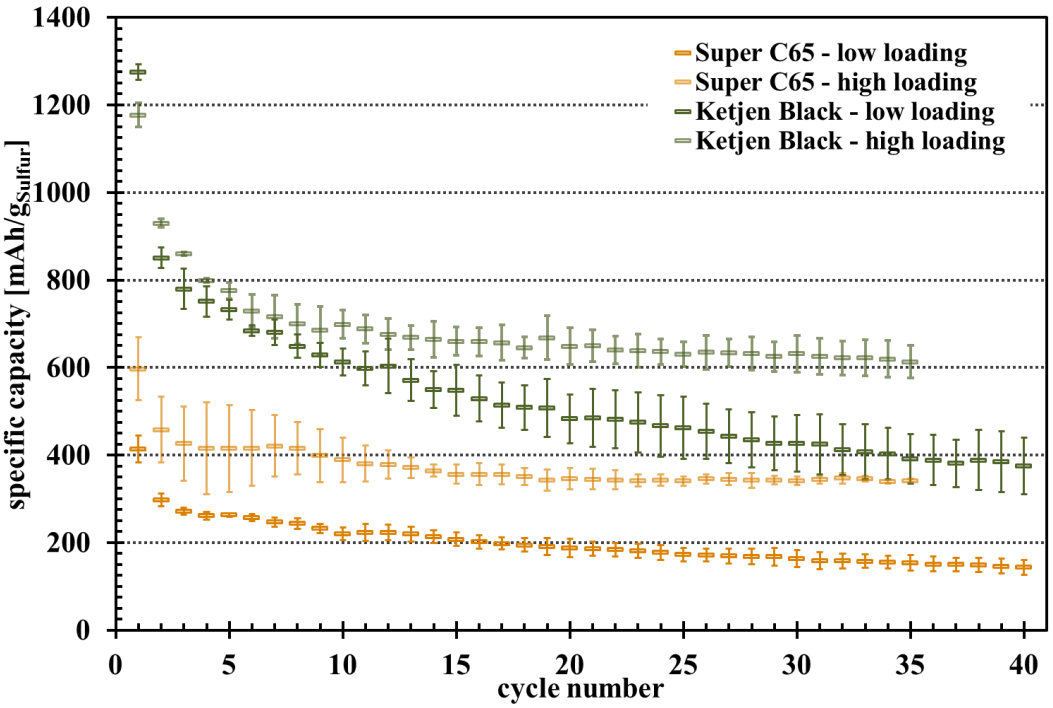

Figure 42: Cycling performance of S/C-composite cathodes based on a Super C65 or Ketjen Black carbon support with a high or a low S loading. The here plotted discharge curves were obtained with Super C65 based cathodes, which had a S loading of 1.03 mg_{Sulfur}/cm^2 (dark yellow) and 2.97 mg_{Sulfur}/cm^2 (light yellow) and with Ketjen Black based cathodes, which had a S loading of 1.14 mg_{Sulfur}/cm^2 (dark green) and 3.05 mg_{Sulfur}/cm^2 (light green). The test cells were cycled at C/12 rate; 30 µL of DOL:DME + 1 M LiTFSI/0.5 M $LiNO_3$ were used as electrolyte. The standard deviation value was obtained from 2-3 repeated measurements.

4.2.5. Verification of lifetime enhancement by using a polysulfide enriched electrolyte

Examining the Li-S battery research literature of the last few years, one can find a lot of published papers, where the use of a polysulfide enriched electrolyte is described and its benefits in terms of lifetime enhancement and active material loss reduction are illustrated.[142,143] To see if the cycling performance of an S/C-composite cathode can also be improved by enriching the electrolyte with polysulfides, tests with a polysulfide enriched standard electrolyte (DOL:DME + 1 M LiTFSI/0.5 M $LiNO_3$) were done.

Therefore, the polysulfide enriched electrolyte was prepared as described in Chapter 3.4.2 and electrochemical tests were conducted. To receive information about the improvement by using a polysulfide enriched electrolyte, test cells with a standard electrolyte were built and the results were compared. Here, a Ketjen Black based S/C-composite powder was used for the cathode preparation, with a S to Ketjen Black ratio of 67.6 wt%/32.4 wt% and a loading of S on the cathodes of 1.02±0.01 mg_{Sulfur}/cm^2 for test cells with polysulfide saturated electrolyte and 1.03±0.01 mg_{Sulfur}/cm^2 for test cells with standard electrolyte. The S/C-composite cathodes were made by Method 2 (Figure 15) and test cells were built as described in Chapter 3.5.1 and then cycled galvanostatically with a C-rate of C/10 for 60 cycles or a C-rate test was done. For the C-rate test, the cells were cycled for 3 cycles at C/10, C/5, C/2, C, 2C and then went back to C/5 for 10 cycles to see if the capacity could be regained. For each test scenario, two test cells were measured and if the results were not clear enough, a third test cell was assembled and measured to ascertain the data.

At first the measured capacities with and without polysulfide enriched electrolyte were analyzed on basis of the S amount only from the S/C-composite cathode and the S in the electrolyte was not taken into account, as mostly seen in literature.[135,143,149] In chapter 3.4.3 the amount of S was calculated to be 0.7 mol_{Sulfur}/L and at the end of this chapter the translation of this value into mg_{Sulfur}/cm^2 (equation 4.2) is given. With the real S loading, the cycling data of the test cell with polysulfide enriched electrolyte were re-analyzed and the effect on the capacity is shown in Figure 46 and the consequences of the results are described in the text below.

Immediately after connecting with the potentiostat a difference between the test cells can be recognized. Quite obviously, on the OCV potential of the polysulfide containing test cells is much lower than the normal OCV value, i.e., ≈ 2.3 $V_{Li/Li+}$ vs. 2.8 $V_{Li/Li+}$ - 3 $V_{Li/Li+}$, to (Figure

43). The value of the polysulfide containing test cells corresponded very well with the potential, which was recorded at the end of the polysulfide synthesis (Chapter 3.4.2) and so the drop of the OCV potential can be easily related to the presence of the synthesised polysulfide mixture of Li_2S_8, Li_2S_6 and Li_2S_4 in the electrolyte.

In Figure 43 a representative first discharge charge profile of a test cell with polysulfide enriched electrolyte (brownish line) and one with a standard electrolyte (dark green line) at a C/10 C-rate is shown. The test cell with the standard electrolyte showed the normal cycling behavior with two nicely defined plateaus and the typical slope at the end of the discharge step. The average discharge capacity of the standard electrolyte cells is 1019±18 mAh/g_{Sulfur}, which is the expected value for S/C-composite cathodes with a Ketjen Black carbon support and an S loading of approximately 1 mg_{Sulfur}/cm^2. This value can be increased by 180 mAh/g_{Sulfur} to 1199±9 mAh/g_{Sulfur} if the test cells contain an electrolyte, which is enriched with polysulfides. If one compares the shape of the discharge profiles, a difference between the slopes and the potential of the plateaus can be seen. When the test cell contained polysulfides the first discharge plateau is about 50 mV lower, but did not influence its length. The lower potential can be explained by the already existing polysulfide mixture in the test cell. The difference between a cell which contains polysulfides and a cell without is that in a standard cell the discharge products have to be electrochemically formed. So, according to the proposed reaction (Chapter 2.1), in a Li-S test cell initially long polysulfide species like Li_2S_8 and Li_2S_6 are formed at a voltage plateau of ca. 2.31 $V_{Li/Li+}$. To get shorter polysulfides, the potential of the cell has to drop or the system needs more time to create shorter chain length via disproportionation reactions. During the synthesis of the polysulfide enriched electrolyte, the time frame for the reaction is much longer compared to the time in a test cell. So, after the concentration of long chain polysulfides in the electrolyte has reached a critical limit, Li_2S_8 and Li_2S_6 start to disproportionate to Li_2S_4 accompanied by a shift in the potential to ca. 2.26 $V_{Li/Li+}$. The length of the plateau is influenced by the cathode and not by the electrolyte. In both types of cells, a certain amount of S on the cathodes has to be transformed to polysulfides before the potential of the cathode can drop. Also, in the second plateau a difference in the appearance can be recognized. For the test cells with a standard electrolyte, the plateau is flat and lies at a potential of 2 $V_{Li/Li+}$ and at the end of the discharge the typical "third plateau" can be observed (described in Chapter 4.2.4). The second plateau of the cells with polysulfides in the electrolyte started at the same potential like the cells without polysulfides, but the curve did not show a flat plateau. The potential of the plateau decreased

slowly from the beginning and after 2/3 it started to drop faster, so that a bent curve is formed and the discharge is not finished by a sharp potential drop. Also, the "third plateau" is missing. Therefore, two issues can be possible. Due to the high amount of polysulfides in the electrolyte, the viscosity of it must be higher compared to a standard electrolyte and so the small pores of the Ketjen Black carbon may not be accessible for existing polysulfides, which in turn might influence the slope as well as the pore structure of the carbon support and, so that the appearing discharge curve would be a superposition of both characteristics.

In the charge step, the curve for the test cells with the standard electrolyte showed the typical behavior with one plateau and a sharp potential step at the end. The charge curve of the test cells with the polysulfide enriched electrolyte looked a bit different. Compared to the charge plateau of the standard test cell, the potential drop after the peak at the beginning is smaller and the increase in potential during charge is about 50 mV lower. Also, a full recovery of the discharge capacity can be reached, if polysulfides are initially added to the electrolyte. The amount of polysulfides in the electrolyte at the end of the discharge step plays a big role for the shape of the subsequent charge curve. After the discharge, Li_2S is precipitated as discharge product on the S/C-composite cathode. In a standard cell, most of the S will be precipitated as discharge product Li_2S on the electrode and the concentration of polysulfides in the electrolyte goes towards zero. In the subsequent charge step, the small amount of polysulfides is sufficient to break up the Li_2S particles on the electrode and only a slight overshoot of the potential to 2.4 $V_{Li/Li+}$ is necessary to start the recharge of the cell. But the concentration in the electrolyte is still low and the balance of polysulfide species is on the side of the ones with a short chain length. This results in a potential drop to 2.25 $V_{Li/Li+}$ after the initial overshoot. During the charge, the potential raises slowly to 2.4 $V_{Li/Li+}$, because the length of the polysulfide chains are growing and at the end S will be precipitated again on the electrode. The polysulfide concentration in the test cells with the enriched electrolyte will also decrease at the end of the discharge, but the amount will be still higher compared to the standard test cells. So, when the test cells went to the charge step, the potential of the charge plateau after the initial peak will be higher due to the fact that the chemical balance of the solution the polysulfide species will push immediately to a longer chain length, which results in a higher potential of the charge plateau of 2.28 $V_{Li/Li+}$ after the initial overshoot and only a slight increase of the potential during the charge process. Also, the complete recovery of the capacity can be linked to the added amount of polysulfides to the test cells. During the first

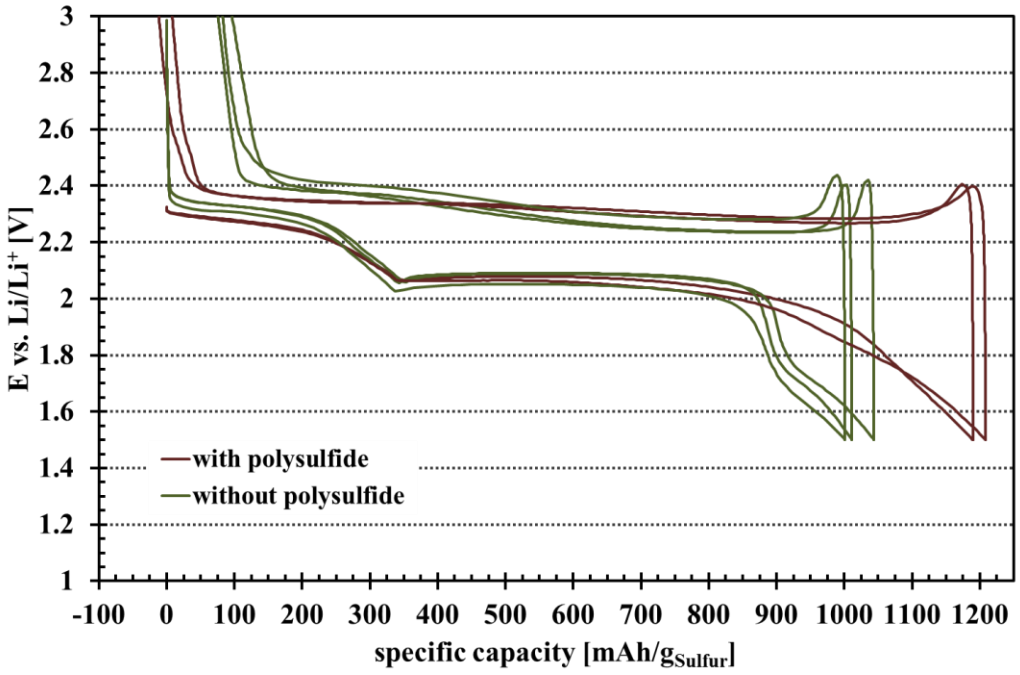

Figure 43: First discharge charge cycle of tests cells at C/10 with (brownish curve) and without (dark green curve) the addition of polysulfides in the standard electrolyte (DOL:DME + 1 M LiTFSI/0.5 M $LiNO_3$). The used S/C-composite cathodes are based on a Ketjen Black carbon, made by Method 2 (Figure 15) and the S loading for both test conditions was ≈1 mg_{Sulfur}/g. The measurements were performed in modified Swagelok T-fittings in a potential window of 3 to 1.5$V_{Li/Li+}$. For both cases 30µL of electrolyte was used.

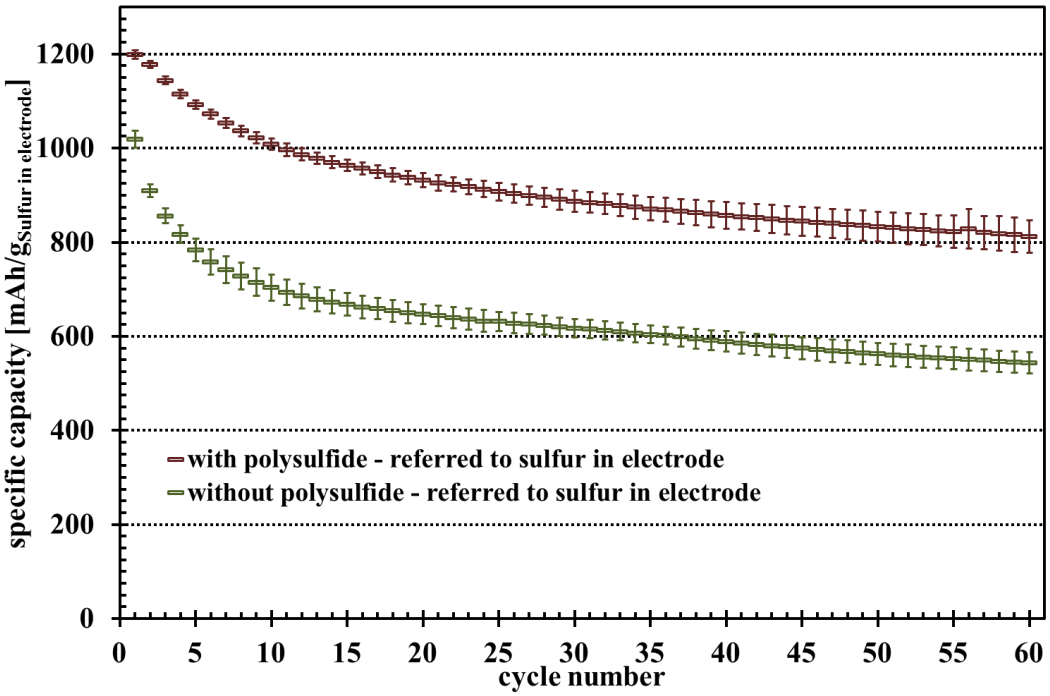

Figure 44: Discharge capacity vs. cycle number at a C-rate of C/10 (calculated on the basis of the cathode S loading) using 30µL of a standard electrolyte (DOL:DME + 1 M LiTFSI/0.5 M LiNO3; dark green symbols) or 30µL of a standard electrolyte enriched with polysulfide (brownish symbols). The used S/C-composite cathodes are based on a Ketjen Black carbon, made by Method 2 (Figure 15) and the S loading for both test conditions was ≈1 mgSulfur/g. The measurements were performed in modified Swagelok T-fittings in a potential window of 3 to 1.5VLi/Li+. The standard deviation value is obtained from 2 to 3 repeated measurements.

discharge, the SEI will be formed on the Li-anode and in this reaction also polysulfide species are involved (Chapter 2.3). In the standard cell this amount of S will be missing in the first charge step and a capacity loss in the first cycle will be unavoidable. Did the test cell contain an additional amount of S in the form of the polysulfides, which is not taken into account by the calculation of the active material amount in the test cell, the loss towards the SEI formation will not be recognized, because the S for the reaction will be taken from the additionally added S and not from the calculated active S source and will so lead to the total recovery of the cell capacity.

After the first discharge, normally the biggest capacity loss can be observed and can be clearly seen in the cycle performance of the standard test cells (Figure 43, dark green symbols). The capacity loss between the first and the second discharge is over 100 mAh/g_{Sulfur}, which equates to roughly 11% of the initial discharge capacity of the test cell. For the test cells with the polysulfide enriched electrolyte (brownish symbols), the capacity loss between the first and the second cycle is only 21 mAh/g_{Sulfur} (2%) in average. But after 15 cycles the effect of the polysulfides began to get negligible and the loss of active material in both types of test cells is around 0.4-0.2% between the following discharge charge cycles. A look at the overall capacity loss after 60 cycles led to the result that test cells with the standard electrolyte lose 475 mAh/g_{Sulfur} and test cells with the polysulfide enriched electrolyte 386 mAh/g_{Sulfur} in average. The difference of only 89 mAh/g_{Sulfur} in discharge capacity between the two test cell types showed that the effect over cycle time decreases and the addition of polysulfides had only a beneficial effect on the initial capacity loss due to the SEI formation, but over time the side reactions like the polysulfide shuttle and other undesired side reactions cannot be inhibited.

After measuring the test cells with a constant C-Rate of C/10, a C-Rate test was performed to see what effect the polysulfides in the electrolyte have on the discharge capacity at higher currents, which usually drops in standard test cells. At the end, the test cells were set back to a C-rate of C/5 for 10 cycles to proof if the discharge capacity of the test cells can be regained or if there are irreversible reactions at higher C-rates.

The first three cycles were performed with a C-rate of C/10 to see if the test cells show the right discharge capacities and to form a proper SEI on the Li-anode. The first discharge capacity of both cell types is in the accepted range, for this kind of cathodes (Figure 45). Also, the usual trend is visible. One can see that the capacity drop between the first and the second

cycle in the standard test cells is relatively big compared to the discharge capacity decay in the polysulfide enriched test cells, which is very small. Also, at C/5 the test cells with the polysulfide enriched electrolyte show a higher discharge capacity compared to the standard cell and the decrease in discharge capacity is still low. But, when the current raised to a C-rate of C/2, the discharge capacity of the polysulfide enriched test cells break down. Interestingly it seems to be a temporary issue, because the discharge capacity of the test cell with the additional S amount rose between the three cycles for about 100 mAh/g_{Sulfur}. At higher currents the ionic conductivity of the electrolyte becomes a bigger issue, because the fast transport of the Li^+-ions is decisive for the reachable capacity of the test cell. If one compare the amount of ions in both electrolytes, in the enriched electrolyte are definitely more solved species than in the standard electrolyte. This leads to a higher viscosity of the electrolyte solution and also the conductivity of the electrolyte can be decreased. Conductivity measurements of DOL/DME with different amounts of LiTFSI and $LiNO_3$ showed that solutions with a high amount of salt show a decreasing Li^+ conductivity[V]. So, one can expect that the ionic conductivity in the polysulfide enriched electrolyte is lower than in the standard electrolyte, because of the high amount of dissolved ions in the solution. So, at a current of C/2 the lower ionic conductivity of the polysulfide enriched electrolyte is coming into effect and the discharge capacity breaks down, because the Li^+-ion transport is too slow and leads to a lack of Li^+-ions on the cathode side. From this it follows that the reaction from S to Li_2S is speeded up, because only the polysulfides near the cathode can take part in the reaction, which results in a low discharge capacity.

Due to the high amount of ions in solution, it is much more viscose compared to the standard electrolyte and if now a high current is applied, the system shows some kind of inertia, which contributed the discharge capacity drop in the first cycle as well. In the next cycles of the test cells, the retardation in the polysulfide solution can be overcome and the discharge capacity raises, because the cell reaction is getting more and more dependent on the ionic conductivity of the solution. At higher C-Rates (C, 2C) this phenomenon cannot be seen any more and the discharge capacity of the test cells with a polysulfide enriched electrolyte stays low.

The test cells with the standard electrolyte show the typical capacity decay between each C-rate step, and at 2C still 347±28 mAh/g_{Sulfur} can be achieved. When the applied current is cut back to C/5, the test cells with and without additional S can recover the discharge capacity,

[V] Conductivity of DOL/DME + 1M LiTFSI/xM $LiNO_3$: x=0 ⇨ σ=0.0123 S/cm; x=0.5 ⇨ σ=0.0113 S/cm; x=1 ⇨ σ=0.0101 S/cm

which was achieved in cycle 6. Concluding, one can say that the polysulfides in the electrolyte had a beneficial effect on the discharge capacity at slow C-rates, but at higher C-rates the high viscosity and low ionic conductivity hinder the cell reaction and the discharge capacity decreases significantly.

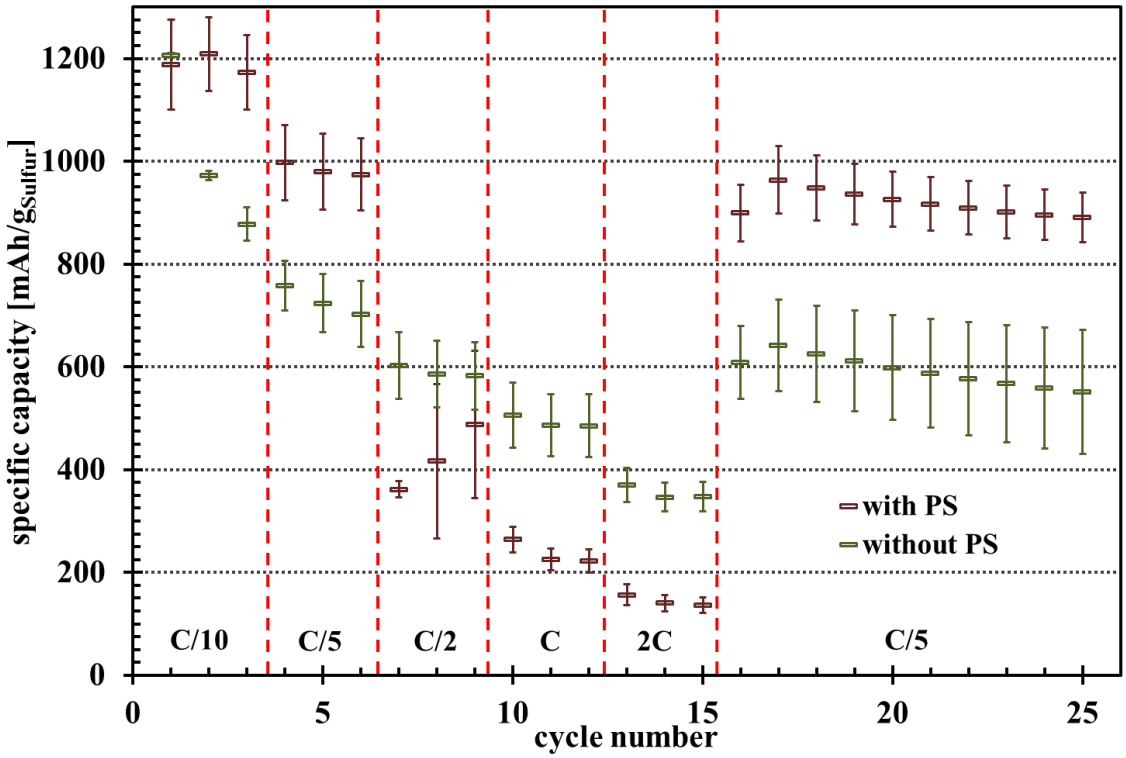

Figure 45: C-rate performance of test cells with 30 µL of a standard electrolyte (dark green symbols) (DOL:DME + 1 M LiTFSI/0.5 M $LiNO_3$; dark green symbols) or 30µL of a standard electrolyte enriched with polysulfide (brownish symbols). The used S/C-composite cathodes are based on a Ketjen Black carbon, made by Method 2 (Figure 15) and the S loading for both test conditions was ≈1 mg_{Sulfur}/g on which the current for the cycling test was calculated. The measurements were performed in modified Swagelok T-fittings in a potential window of 3 to 1.5$V_{Li/Li+}$. The standard deviation value is obtained from 2 to 3 repeated measurements.

In the previous section the amount of S in the electrolyte was not taken into account in the analysis of the data. But the S in the electrolyte takes also part in the electrochemically active steps during the cycling of the cell and therefore it has to be included in the calculation of the capacity of the test cells. In Chapter 3.4.2 it is explained how the amount of the S in the polysulfide enriched electrolyte was determined and the resulting value was calculated to be 0.7 mol_{Sulfur}/L. So, the amount of additional S in the test cell can be easily calculated:

$$m_{Sulfur} = V_{electrolyte} \cdot c_{Sulfur} \cdot M_{Sulfur} \quad (4.2)$$

$$m_{Sulfur} = 0.67 mg_{Sulfur} \quad (4.3)$$

where $V_{electrolyte}$ is the volume of added electrolyte to the test cells ($3 \cdot 10^{-5} L$), c_{Sulfur} is the S concentration in polysulfide enriched electrolyte, and M_{Sulfur} is the molar mass of S ($32 \frac{g}{mol}$).

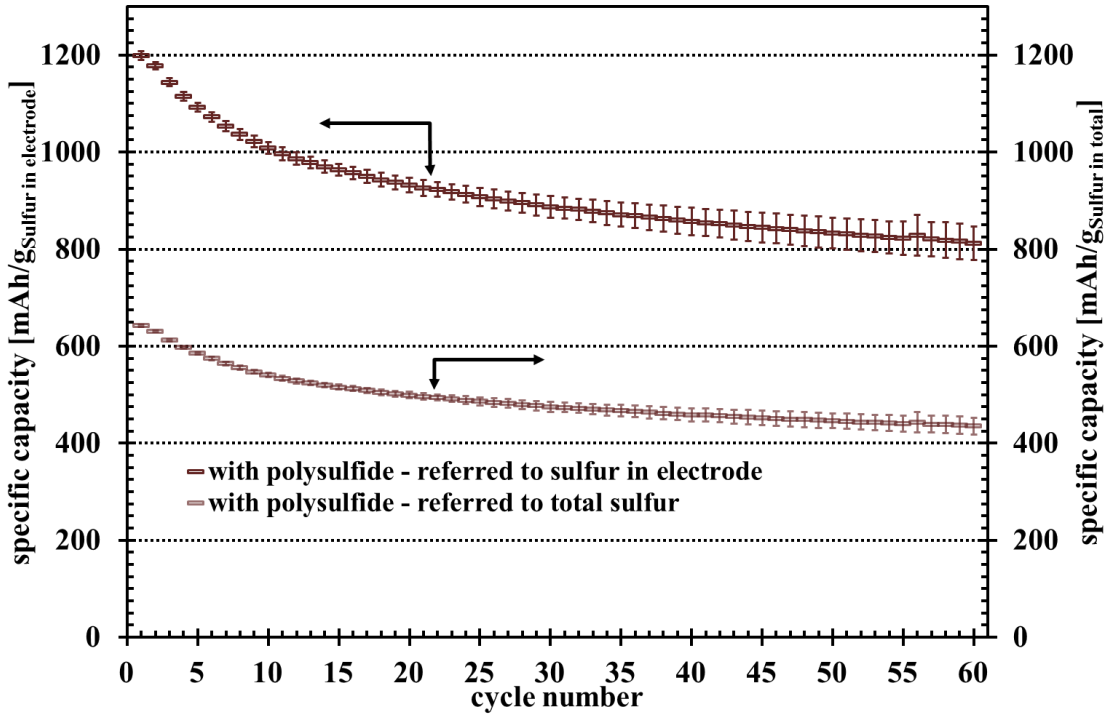

Figure 46: Discharge capacity vs. cycle number at a C-rate of C/10 (calculated on the basis of the cathode S loading) in a potential window of 3 to 1.5V$_{Li/Li+}$. As electrolyte 30µL of a polysulfide enriched standard electrolyte (DOL:DME + 1 M LiTFSI/0.5 M LiNO$_3$) was used. The S/C-composite cathodes are based on a Ketjen Black carbon, made by Method 2 (Figure 15) and the S loading was ≈1 mg$_{Sulfur}$/g. The brownish symbols represent the specific discharge capacity calculated on basis of the cathode S loading, whilst the light brownish symbols represent the specific discharge capacity calculated on basis of the total S amount contained in the test cell. The standard deviation value is obtained from 2 to 3 repeated measurements.

Together with the S loading of 1.03 mg$_{Sulfur}$/cm^2 on the cathode with an area of 0.785 cm^2, the total S amount in the test cell with the polysulfide enriched electrolyte adds up to 1.48 mg$_{Sulfur}$, which equals to an S loading of 1.89 mg$_{Sulfur}$/cm^2. Compared to a standard test cell, which contains only 0.8 mg$_{Sulfur}$, the S-content of these test cells is 1.85 times higher. When the measured capacity of the tests cells with the polysulfide electrolyte are normalized by the total S in both electrolyte and cathode rather than just by the S in the cathode, the discharge capacity dropped from 1199±9 mAh/g$_{Sulfur}$ to 642±3 mAh/g$_{Sulfur}$ and so the first impression of improvement of the cell capacity through additional S via an enriched electrolyte is wrong. But there are also beneficial aspects, when the S amount in the test cells is increased trough the enrichment of the electrolyte with polysulfides. The more obvious aspect is that the capacity decay in the beginning of the cycling, especially between the first and the second cycle, is much lower compared to a standard test cell. Furthermore, with the

addition of S via the electrolyte the Wh/kg_{cell} can be increased. If one wants to increase the Wh/kg_{cell} via a higher S-loading on the cathode, also the amount of carbon has to be taken into account and so the weight of the cell increases. With the increase of the S-loading through the polysulfide enriched electrolyte, the additional amount of carbon is omitted and the weight of the cell increases only by the weight of the amount of active material in the electrolyte.

4.2.6. Use of solvent with different donor numbers and their influence on the cell performance

In the chapters, before, the main focus was set on the improvement of the S/C-composite cathode to increase the discharge capacity and the cycling performance of a Li-S battery. But the solvents, which were used for the electrolyte and their properties have an influence on the cycling behavior of the test cell, too.

A rotating-ring disk electrode study by Y. Lu et al.[18] examined the electrochemical behavior of S in DOL:DME and DMSO, and showed that the cell reactions are not exclusively of electrochemical nature. For the measurements, the S was dissolved in both solvents and the reactions were studied using a glassy carbon working electrode and a gold ring. For DOL:DME, only one reduction step was recorded, which corresponds to approximately 5 electrons. In DMSO, two waves could be detected and the analysis gave a total of 4 electrons for this reaction. But with this method, only reactions with fast kinetics could be measured. Therefore, further tests with catholyte cells at different C-rates were done, which showed that for DMSO and DOL:DME a real discharge capacity of 100% at slow rates could be achieved, indicating that indeed 16 electrons had to be involved in the whole process. Based on the RRDE and the cycling results, a different reaction route has to be taken into account and a mechanism with possible reactions was drawn (Figure 5). In the first part of the mechanism, the cell reactions were dominated by electrochemical reactions from S_8 over S_8^{2-} to S_4^{2-}, which are judged to be very fast. But the further steps to break down the polysulfides to the final discharge product are redox or chain-growth reactions. The results showed also that solvents with a high dielectric constant like DMSO ($\kappa = 46.5$)[144] stabilize the polysulfide species in contrast to solvents with a low dielectric constant like DOL ($\kappa = 7.13$)[144] or DME ($\kappa = 7.075$)[144]. The destabilizing effect in solvents with a low dielectric constant accelerates the disproportionation or chain-growth reactions of the polysulfide species. In this way, also at higher C-rates more reducible species can be generated, which enhances the rate capability of the catholyte test cells.[18]

Based on this theory, an electrolyte solvent with a lower dielectric constant than DOL or DME should further improve the rate capability. Because of the very low dielectric constant of $\kappa = 2.21$[144], 1,4-Dioxone (DiOX) was selected to test the above hypothesis. The electrochemical tests were made with S/C-composite cathodes based on an S/C-composite powder with a Ketjen Black carbon support made by Method 2 (Figure 15). The S content in the S/C-composite powder was 69.5 wt% S/30.5 wt% C and the S loading ranged from 0.82 mg_{Sulfur}/cm^2 and 1.02 mg_{Sulfur}/cm^2 (more details in Table 13). In each test cell, 30 µL of the respective electrolyte was added. The electrochemical tests were done with a C-rate of C/10 to investigate the cycling stability in each solvent and a C-rate test to examine the rate capability of the different solvents.

In the first attempt, it was tried to dissolve 1 M LiTFSI in pure DiOX. Unfortunately, the solubility product for LiTFSI in DiOX is very low and no significant amount of the salt could be dissolved in the solvent. Also, the try to dissolve $LiClO_4$ or $LiNO_3$ failed. To increase the solubility of the conducting salt, DiOX was mixed with DME. Therefore, the volume fraction of DME was continuously increased and at a ratio of 6:1 by volume, 0.5 M LiTFSI could be dissolved successfully and first galvanostatic measurements were done. In the first cycle an average discharge capacity of 417±68 mAh/g_{Sulfur} could be reached (Figure 47, green line), which was less than half of the discharge capacity an S/C-composite cathode based on a Ketjen Black carbon can achieve in a standard test cell assembly in the first discharge step. An inspection of the shape of the discharge curve showed that the first plateau started at around 2.3 V as expected, but the second plateau did not exist anymore and the curve dropped down to the "third" plateau, which is typically observed in Ketjen Black based S/C-composite cathodes. During the first charge, the cell voltage got very noisy and also a high overcharge of the test cells could be observed. In further cycles, the discharge capacity dropped below 200 mAh/g_{Suflur} extremely fast and after 40 cycles only 100 mAh/g_{Suflur} could be reached (Figure 48, green symbols). Due to these observations and especially the high noise in the charge step, it was assumed that the Celgard® separator was not wetted enough. A quick test, where a piece of Celgard® was placed on a tissue and a drop of electrolyte was placed on it, showed that the white Celgard® only in a few small spots changed its color from white to greyish, but the major amount of solvent stayed as drop on top of the surface. After a waiting time of approximately 10 min the appearance of the Celgard® did not change and so the before mentioned assumption was proven (test was done in an Ar-filled glovebox).

In the next step, the Celgard® was exchanged by a Glasfibre separator and the volume fraction of DME in the solvent mixture of DiOX:DME was increased from 6:1 to 3:1, because in this mixture ratio the molar amount of LiTFSI could be increased from 0.5 M to 1 M, which improved the conductivity of the electrolyte and made the results more comparable to data measured with the standard electrolyte. To see if the electrochemical behavior of the cathode could be improved with these changes, initially one test cell was assembled and measured. The modification of the electrolyte composition had a positive influence on the discharge capacity of the test cell and it could be nearly doubled to 777 mAh/g_{Sulfur} (yellow line, Figure 47). Now, the second plateau could be observed in the discharge step, but the length of it was very short and had the shape of a bump instead of the typical flat line. However, due to the high porosity of the Glasfiber separator the polysulfide shuttle in the charge step increased significantly and an enormous overcharge was observed. An addition of $LiNO_3$ to hinder the reaction of the polysulfides with the Li-anode was not possible, because of the near zero solubility of the additive salt in the electrolyte solvent.

To prevent the overcharge, the Li-anode was pre-passivated in a carbonate electrolyte.[145] As solvent, propylene carbonate (PC) was used, because from Li-ion research it is known that PC in combination with a salt has the ability to build a stable SEI layer on Li. To avoid contamination of the test cell set up with a different salt, LiTFSI was picked and 1 M of it was dissolved in PC. Before the Li was placed in the electrolyte solution, the anodes were punched out to the desired size of 10 mm. For a proper SEI formation, the disks had to stay for 24 h in the PC electrolyte solution. Then, they were removed and left-over solvent was removed with a clean tissue. Afterwards, the Li-anodes were washed 3 times in the same electrolyte, which will be used in the test cells (here: DiOX:DME (1/3; v/v) + 1 M LiTFSI). With the so prepared Li-anodes new test cells were built and measured under the same condition as before. The shape of the discharge curve and the discharge capacity showed no significant change compared to the test cell with a fresh Li-anode (orange line, Figure 47). But in the charge step, the overcharge was successfully suppressed and also the loss of discharge capacity between the first and the second step could be lowered. In further cycles, the decrease of discharge capacity showed a linear trend with an average loss of 1.3% between each cycle (orange symbols, Figure 48).

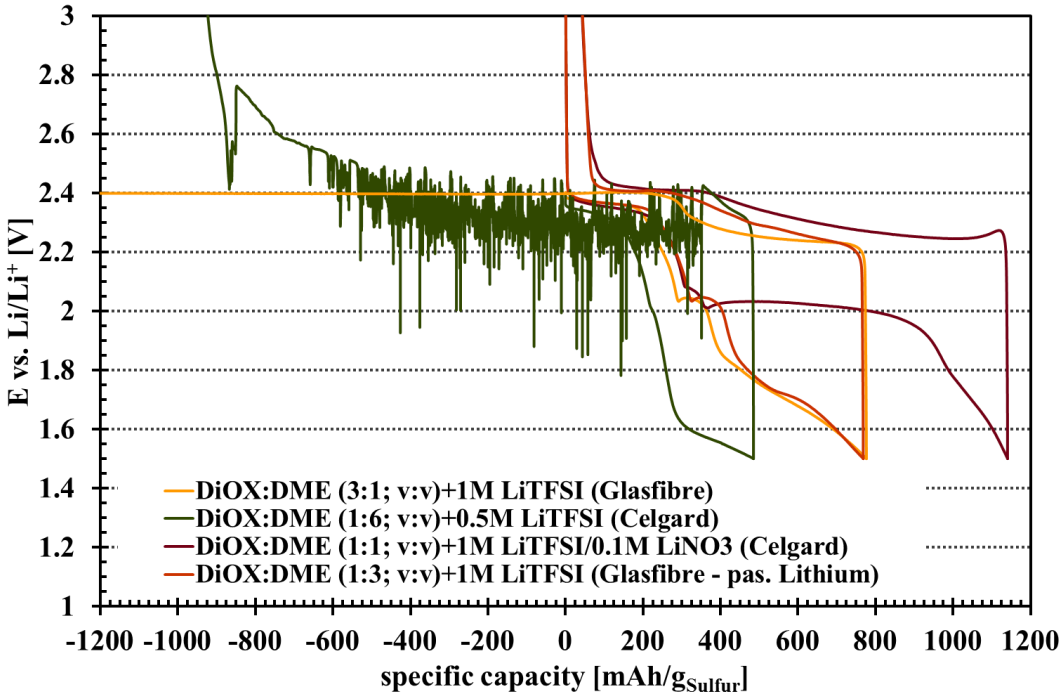

Figure 47: Representative first discharge charge cycle of test cells with DiOX:DME as solvent in different electrolyte compositions (details about volume fractions, amount of conducting salt and additive in graph or Table 13). The used S/C-cathodes are based on a Ketjen Black carbon with a S/C-ratio of 69.5 wt% S/30.5 wt% C and the S-loadings ranged from 0.82 – 1.02 mg_{Sulfur}/cm^2. The cells were cycled with C/10 between 3 – 1.5 $V_{Li/Li+}$.

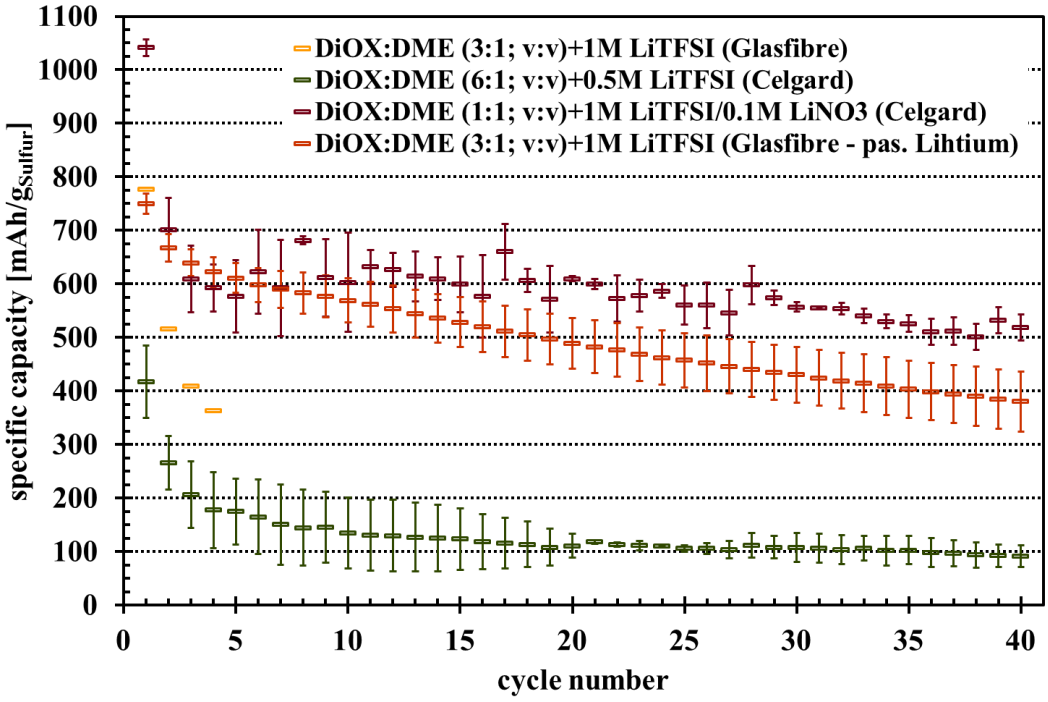

Figure 48: Discharge capacity vs. cycle number for test cell measurements with DiOX:DME as solvent in different electrolyte compositions (details about volume fractions, amount of conducting salt and additive in graph or Table 13). The used S/C-cathodes are based on a Ketjen Black carbon with a S/C-ratio of 69.5 wt% S/30.5 wt% C and the S-loadings ranged from 0.82 – 1.02 mg_{Sulfur}/cm^2. The cells were cycled with C/10 between 3 – 1.5 $V_{Li/Li+}$. The standard deviation value is obtained from 2 to 3 repeated measurements.

The measurements with the pre-passivation of the Li-anode showed that test cells could be successfully cycled with an acceptable discharge capacity, but the preparation of the SEI layer with a carbonate electrolyte has also some risk in terms of contamination and associated undesired side reactions, which can lead to an early cell death. So, it was decided to increase the DME volume to a final DiOX:DME-ratio of 1:1, in which fortunately a small amount of 0.1 M $LiNO_3$ could be dissolved, so that a pre-passivation was unnecessary. Furthermore, the Glasfibre separator could be exchanged by the Celgard® one, which is also beneficial for the cell performance, due to the lower porosity. Measurements with the final electrolyte composition and the use of the Celgard® separator showed that the discharge capacity of the first cycle could be raised by around 260 mAh/g_{Sulfur} to an average first discharge capacity of 1037±18 mAh/g_{Sulfur} (maroon line, Figure 47). In this test cell set up, the shape of the discharge curve had its common characteristics. Additionally, to the usual plateaus, a small plateau, which appeared at 2.07 $V_{Li/Li+,}$ cannot be clearly assigned till now.

Because of the potential of the small plateau, it was assumed that it will be generated by the S_4^{2-} polysulfide. Due to the use of the additive $LiNO_3$, the cell could be successfully charged, without further difficulties. After the first cycle the discharge capacity dropped dramatically to approximately 700 mAh/g_{Sulfur}, but then the value fluctuated slightly around 600 mAh/g_{Sulfur} after the 3rd cycle till the 30th cycle. Afterwards, the discharge capacity declined further and after 40 cycles a residual discharge capacity of slightly over 500 mAh/g_{Sulfur} was left. The big drop of discharge capacity between the first and the second cycle indicates that a lot of active material might get consumed by undesired side reactions. There are two probable scenarios for the capacity loss. First, the active material could be consumed or incorporated irreversibly during the SEI formation on the Li-anode or, second isolated S islands might be created during the charge step. Because of almost complete regain of the discharge capacity in the first charge step, the second assumption seemed to be more reliable and suggested that in DiOX:DME the formation of big S crystals is favored.

Interestingly, the cycling data of DIOX:DME in Figure 48 showed a better cycling behavior compared to the older cycling data in Figure 42 with a Ketjen Black based S/C-composite electrode and DOL:DME+1M LiTFSI/0.5M $LiNO_3$ as electrolyte. One difference between the measurements was the fabrication of the used cathodes. The results in Figure 42 were obtained with cathodes, which were made with coating method 1 (Figure 15), but the cycling data in this chapter were made with cathodes, which were made with the second method. Due

to the better distribution of the coating ingredients in the planetary centrifugal mixer, better cathodes could be produced and also better cycling could be the result.

A comparison of the new electrolyte with the standard electrolyte solution and electrodes, which were made with the same coating procedure (Figure 15), showed that the first discharge capacity of the DIOX:DME electrolyte is only 125 mAh/g_{Sulfur} below. In Figure 49 the representative first cycle with either DiOX:DME (1:1; v:v) with 1 M LiTF SI+0.1 M $LiNO_3$ or DOL:DME (1:1; v:v) with 1 M LiTFSI+0.5 M $LiNO_3$ is shown. The potential for the first discharge plateau is in both cases at 2.35 $V_{Li/Li+}$. The additional small plateau in DiOX:DME at 2.07 $V_{Li/Li+}$ had a similar potential compared to the long second plateau in DOL:DME, which is at 2.1 $V_{Li/Li+}$, but for the second long plateau in DiOX:DME, the potential dropped to 2.02 $V_{Li/Li+}$. This indicated that in DiOX:DME in the second discharge step the polysulfide mixture consists of more short chain polysulfide species compared to the standard electrolyte. The so called “third plateau”, which is a characteristic of S/C-composite electrodes based on Ketjen Black, was not as defined as in the standard electrolyte solution, but still visible.

In the curve of the first charge the slight over shoot of potential in the beginning of the charge process is missing for the test cells cycled with DiOX:DME (maroon line, Figure 47), which also showed two plateaus compared to the standard DOL:DME electrolyte. The missing peak at the beginning of the charge indicates that during the discharge step a nice and smooth layer of Li_2S with a good contact to the carbon black surface is formed, so that the overpotential to start the reaction of Li_2S back to polysulfides is kept small. The cycling performance comparison in both electrolytes shows that the discharge capacity drop in DOL:DME after the first cycle is much lower compared to DiOX:DME (Figure 50). In subsequent cycles, in DOL:DME, a constant decay in discharge capacity was observed, whereas in DiOX:DME an enormous drop of discharge capacity after the first cycle and afterward a slow decay was noticed. At cycle 30 the discharge capacities of the two test cell with the different electrolyte solutions converged and overlapped afterwards. Also, the decay in between the cycles was similar after that point and the discharge capacity of both was slightly over 500 mAh/g_{Sulfur} at the 40^{th} cycle.

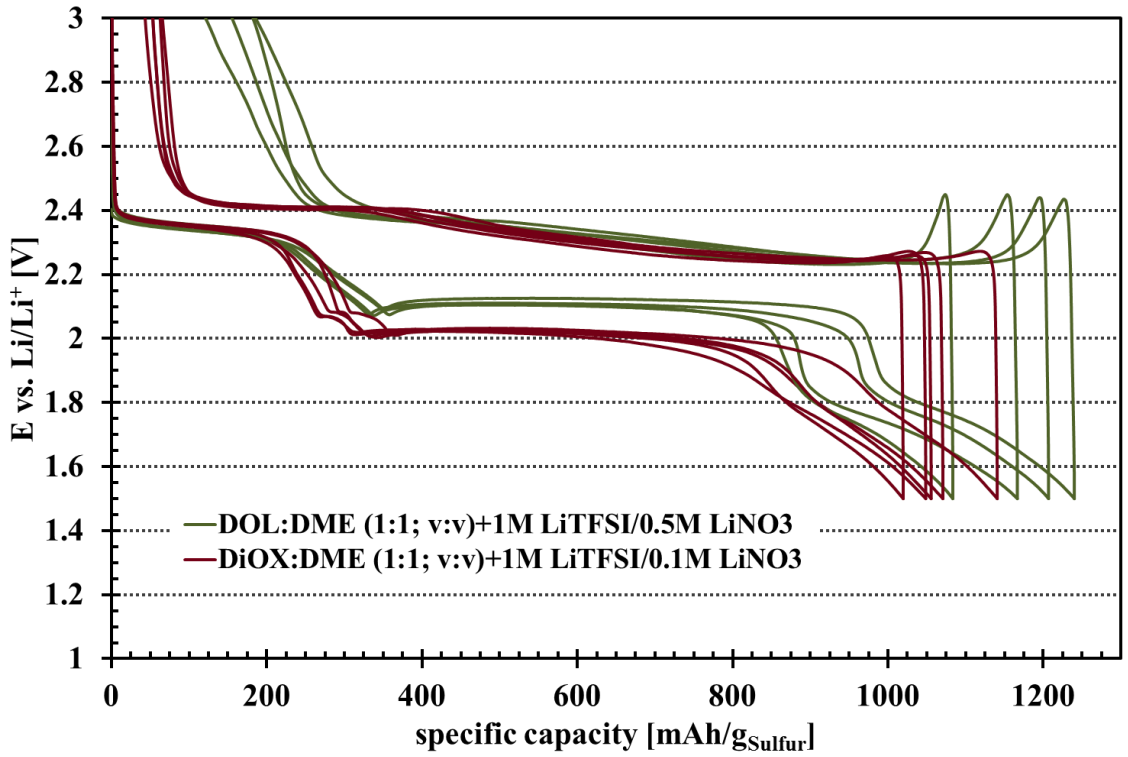

Figure 49: First discharge charge cycle of tests cells with 30 µL of DiOX:DME + 1 M LiTFSI/0.5 M LiNO3 (maroon curve) or DOL:DME + 1 M LiTFSI/0.5 M LiNO3 (green curve) at a C-rate of C/10 with cut off voltages of 3 $V_{Li/Li+}$ and 1.5 $V_{Li/Li+}$. The S/C-composite cathodes based on a Ketjen Black carbon with S-loadings between 0.86 – 0.87 mg_{Sulfur}/cm^2.

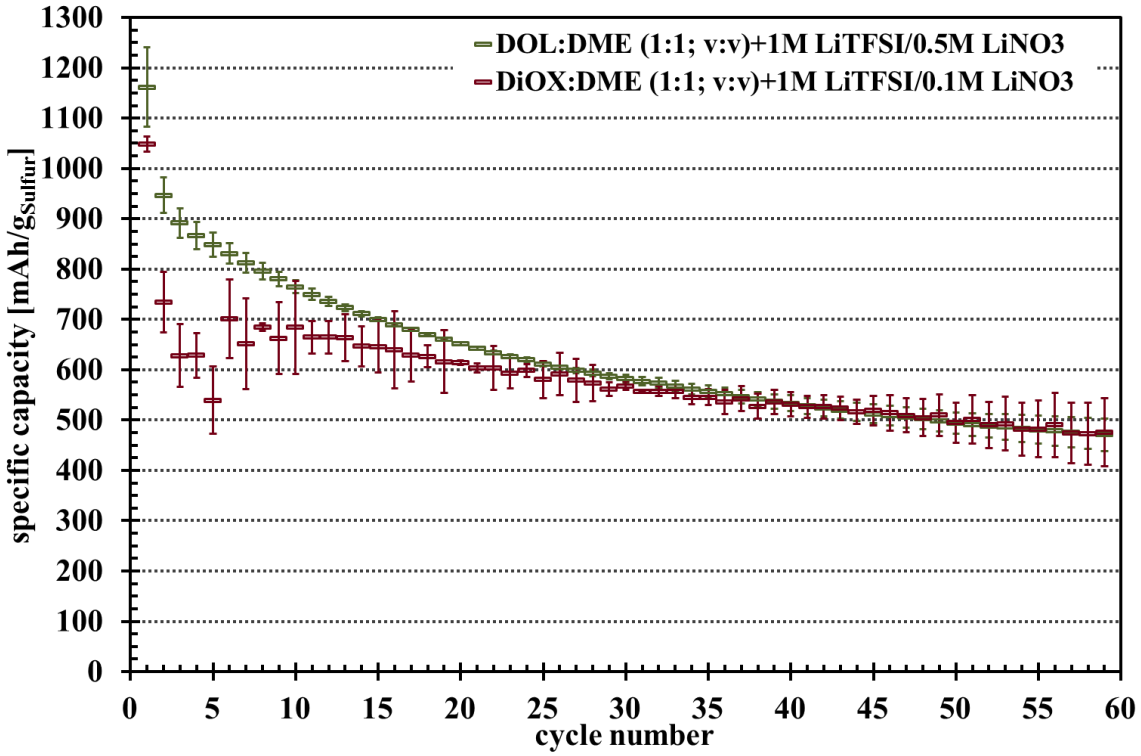

Figure 50: Discharge capacity vs. cycle number at a C-rate of C/10 using 30 µL of DiOX:DME + 1 M LiTFSI/0.5 M $LiNO_3$ (maroon symbols) or DOL:DME + 1 M LiTFSI/0.5 M $LiNO_3$ (green symbols). The cut off voltages were 3 $V_{Li/Li+}$ and 1.5 $V_{Li/Li+}$ and the S/C-composite cathodes based on a Ketjen Black carbon with S-loadings between 0.86 – 0.87 mg_{Sulfur}/cm^2. The standard deviation value is obtained from 4 to 5 repeated measurements.

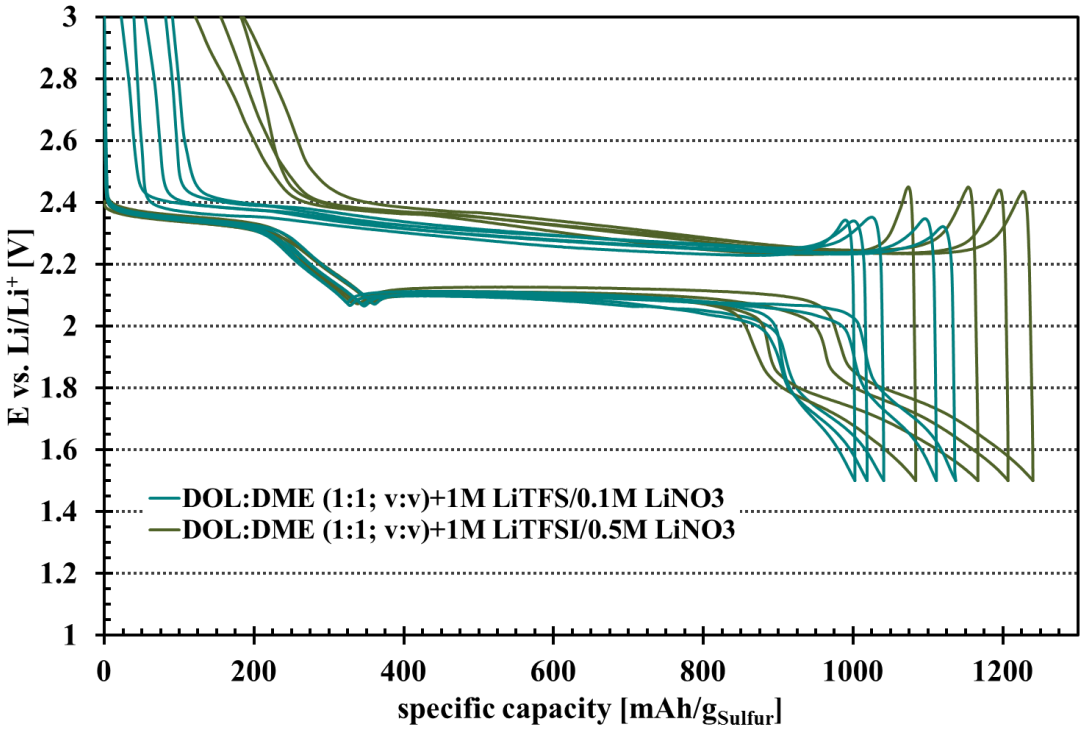

Figure 51: First discharge charge cycle of tests cells with 30 µL of DOL:DME (1:1; v:v) + 1 M LiTFSI/0.5 M $LiNO_3$ (green curve) or DOL:DME (1:1; v:v) + 1 M LiTFSI/0.1 M $LiNO_3$ (turquoise curve) as electrolyte. The cells were cycled with a C-rate of C/10 and the cut off voltages were 3 $V_{Li/Li+}$ and 1.5 $V_{Li/Li+}$. For the cathodes an S/C-composite based on a Ketjen Black carbon with a S/C-ratio of 69.5 wt% S/30.5 wt% C was used and the S-loadings ranged from 0.85 – 0.86 mg_{Sulfur}/cm^2.

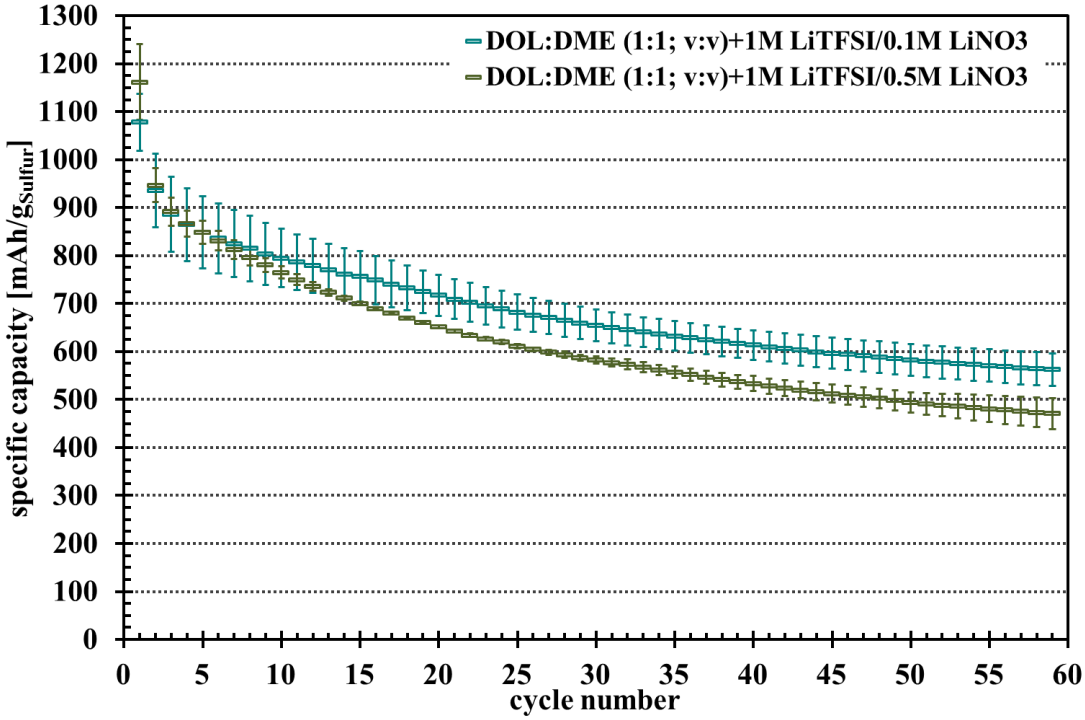

Figure 52: Discharge capacity vs. cycle number of test cells containing 30 µL of DOL:DME + 1 M LiTFSI/0.5 M $LiNO_3$ (green symbols) or DOL:DME + 1 M LiTFSI/0.1 M $LiNO_3$ (turquoise symbols) as electrolyte solvent. The measurements were done at a C-rate of C/10 between 3 $V_{Li/Li+}$ and 1.5 $V_{Li/Li+}$. For the cathodes an S/C-composite based on a Ketjen Black carbon with a S/C-ratio of 69.5 wt% S/30.5 wt% C was used and the S-loadings ranged from 0.85 – 0.86 mg_{Sulfur}/cm^2. The standard deviation value is obtained from 4 to 5 repeated measurements.

To make sure that the $LiNO_3$ amount in the electrolyte solution does not influence the cycling behavior of the test cells too much, a standard electrolyte solution with 0.1 M $LiNO_3$ instead of 0.5 M was made. As average first discharge capacity 1078±59 mAh/g_{Sulfur} could be obtained for DOL:DME (1:1; v:v) with only 0.1 M $LiNO_3$, which is only a bit lower compared to the average discharge capacity obtained with the standard electrolyte (DOL:DME (1:1; v:v) + 1 M LiTFSI/0.5 M $LiNO_3$) (Figure 51). In further cycles the discharge capacity decreased as usual for both electrolyte, but the loss with only 0.1 M $LiNO_3$ is lower compared to test cells with the standard electrolyte and after 40 cycles over 600 mAh/g_{Sulfur} of discharge capacity was left (Figure 52). It seemed that the lower amount of $LiNO_3$ is beneficial for the test cell cycle life, but from literature it is known that the additive will be consumed over cycle time. In each discharge step, Li will be dissolved from the anode side and diffuse into solution as Li^+. During this process, the SEI layer on the Li can burst and the bare surface is exposed to the electrolyte solution. When the test cell will be recharged after a complete discharge step, the SEI formation will take place on the bare Li spots and in this mechanism the additive $LiNO_3$ is involved. So, the higher amount of $LiNO_3$ is necessary to ensure a stable long term performance.

After the electrochemical investigation of the different electrolytes at a constant C-rate of C/10, the rate capabilities of them were examined with a C-rate test. Therefore, test cells with the three different electrolytes were assembled and cycled at C/10, C/5, C/2, C, 2C for three cycles and then went back to C/5 for additional 10 cycles to see if the discharge capacity from the first C/5 cycling could be regained or if some irreversible side reactions take place during the fast C-rates, which leads to a decrease in discharge capacity. Additional to the three electrolytes, a fourth mixture with the composition DME + 1 M LiTFSI/0.5M $LiNO_3$ was incorporated in the measuring matrix (Table 13). Pure DME was chosen because it is part of all three electrolytes and so it can be investigated how the addition of the co-solvent DiOX or DOL (solvent ratio co-solvent:DME was 1:1 by volume) influences the behavior of the pure electrolyte solvent DME and if the co-solvents have a beneficial or a negative effect on the rate capability of the test cells. The first discharge capacities of the test cells with the solvent mixtures were comparable to the value, which was obtained in the cycling measurements with a constant C/10-rate and with the electrolyte, which contains only DME, an average discharge capacity of 1162±9 mAh/g_{Sulfur} could be obtained (Figure 53). This value lies in the range of the other electrolytes and thus there was no benefit on the first discharge capacity by using the pure solvent itself. At C/10 the discharge capacities of all electrolytes were in a similar

margin, but already at C/5 the performance of the electrolytes began to split up. While DOL:DME and DME showed still a similar performance, DiOX:DME had a higher decay in discharge capacity in the first discharge cycle with C/5 (Figure 54). But the discharge capacity could be regained within the three cycles and at the 3rd cycle with C/5 the value for the discharge capacity converged to the values of the other electrolytes. Here, similar phenomena were active as in the polysulfide enriched electrolyte (Chapter 4.2.5). At C/2 or higher C-rates this could not be observed anymore and the discharge capacity of the test cells with DiOX:DME completely broke down to zero at 2C. The best C-rate performance was exhibited by DOL:DME with the low amount of $LiNO_3$ (turquoise symbols, Figure 54). Due to the lower amount of $LiNO_3$ the conductivity of the electrolyte is higher and so S/C-composite cathodes could obtain better discharge capacities at higher C-rates compared to the cathodes, which were cycled with the standard electrolyte solution.[VI]

Till a C-rate of C/2, DOL:DME with high $LiNO_3$ amount and DME showed a similar performance, but at 1 C the discharge capacities began to go apart and at 2C the discharge capacity for DME went below 200 mAh/g_{Sulfur} Fortunately, when the C-rate went back to C/5 the discharge capacities of all test cells with the different electrolyte compositions could be recovered after the second cycle. To conclude this chapter, it seems that the solvent DiOX had rather a more negative effect on the cell performance than a positive one. In the electrolyte composition DiOX:DME (1:1; v:v) + 1 M LiTFSI/0.1 M $LiNO_3$, no higher discharge capacities in the first cycle could be obtained and during the cycling with a constant C-rate only the same value after 40 cycles as with the standard electrolyte was reached. It also seemed that between the first and the second cycle additional side reactions take place, which lead to a higher loss of discharge capacity at that point. Furthermore, the proposed theory that DiOX should have a beneficial impact on the rate capability of an S/C-composite cathode is hereby disproved. The electrolyte with it showed the worst discharge capacities at high C-rates and had a total break down at 2C, but fortunately there were no irreversible reactions and when the current went back to C/5 the discharge capacity could be regained.

To summarize the results for the other electrolytes, the measurements showed that for batteries cycled with low and medium C-rates the addition of DOL to DME is not necessary to obtain good discharge capacities, but at high C-rates the mixture of both solvent can deliver the better results. Also, here the lower amount of $LiNO_3$ was beneficial for the rate dependent

[VI] Conductivity of DOL/DME + 1M LiTFSI/xM $LiNO_3$: x=0 ⇨ σ=0.0123 S/cm; x=0.5 ⇨ σ=0.0113 S/cm; x=1 ⇨ σ=0.0101 S/cm.

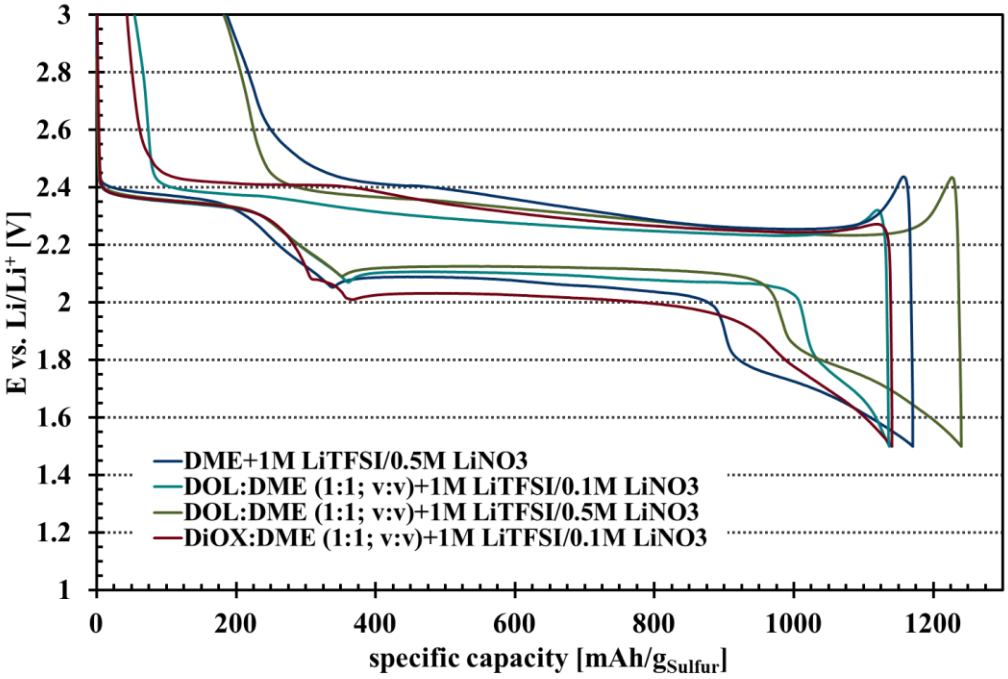

Figure 53: Comparison of representative first discharge charge cycles of tests cells with DiOX:DME + 1 M LiTFSI/0.5 M $LiNO_3$ (maroon curve), DOL:DME + 1 M LiTFSI/0.5 M $LiNO_3$ (green curve) or DME + 1 M LiTFSI/0.5 M $LiNO_3$ (blue curve) and DOL:DME + 1 M LiTFSI/0.1 M $LiNO_3$ (turquoise line) at a C-rate of C/10 and cut off voltages of 3 $V_{Li/Li+}$ and 1.5 $V_{Li/Li+}$. The used S/C-composite for the cathode preparation based on a Ketjen Black carbon with an S/C-ratio of 69.5 wt% S/30.5 wt% C and the S loadings range from 0.83 – 0.88 (Table 13).

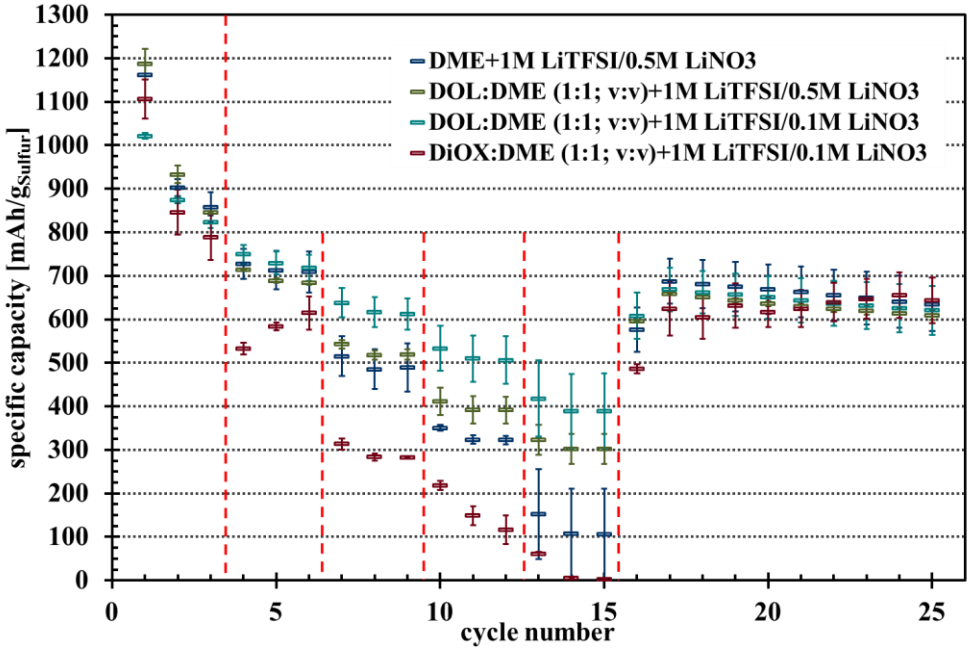

Figure 54: Discharge capacity vs. cycle number at different C-rate from C/10 to 2C and cut off voltages of 3 $V_{Li/Li+}$ and 1.5 $V_{Li/Li+}$ using DiOX:DME + 1 M LiTFSI/0.5 M $LiNO_3$ (maroon symbols), DOL:DME + 1 M LiTFSI/0.5 M $LiNO_3$ (green symbols), DOL:DME + 1 M LiTFSI/0.1 M $LiNO_3$ (turquoise symbols) or DME + 1M LiTFSI/0.5M $LiNO_3$ (blue symbols). The used S/C-composite for the cathode preparation based on a Ketjen Black carbon with an S/C-ratio of 69.5 wt% S/30.5 wt% C and the S loadings range from 0.83 – 0.88 (Table 13). The standard deviation value is obtained from 5 repeated measurements for DiOX:DME, 4 repeated measurements for DOL:DME with 0.5 M $LiNO_3$, 5 repeated measurements for DOL:DME with 0.1 M $LiNO_3$ and 2 repeated measurements for DME.

Table 13: Average S loading of the S/C-cathodes in the different test cell set ups and comparison of the average discharge capacity for the tested electrolyte solutions. The S/C-cathodes are all based on a Ketjen Black Carbon with a weight ratio of 69.5wt% S to 30.5wt% C.

Electrolyte	C/10		C-rate test (C/10, C/5, C/2, C, 2C, C/5)	
	Sulfur loading [mg_{Sulfur}/cm^2]	Average discharge capacity [mAh/g_{Sulfur}]	Sulfur loading [mg_{Sulfur}/cm^2]	Average discharge capacity [mAh/g_{Sulfur}]
DiOX:DME (1/6; v/v) + 0.5 M LiTFSI	1.01±0.01	417±68		
DiOX:DME (1/3; v/v) + 1 M LiTFSI (Glasfibre)	1.03±0	777±0		
DiOX:DME (1/3; v/v) + 1 M LiTFSI (Glasfibre – pas. Lithium)	1.02±0.01	749±19		
DME + 1 M LiTFSI/0.5 M LiNO3			0.88±0.02	1162±9
DOL:DME (1/1; v/v) + 1 M LiTFSI/0.5 M $LiNO_3$	0.86±0.01	1162±78	0.84±0.02	1187±20
DOL:DME (1/1; v/v) + 1 M LiTFSI/0.1 M $LiNO_3$	0.85±0.02	1078±59	0.83±0.01	1022±19
DiOX:DME (1/1; v/v) + 1 M LiTFSI/0.1 M $LiNO_3$	0.87±0	1037±18	0.87±0	1106±35
DME + 0.5 M TBATFSI/0.5 M LiTFSI/0.5 M $LiNO_3$			0.82±0	1203±31
DOL:DME (1/1; v/v) + 0.5 M TBATFSI/0.5 M LiTFSI/0.5 M $LiNO_3$	0.85±0.01	1199±31	0.86±0.01	1219±80
DiOX:DME (1/1; v/v) + 0.5 M TBATFSI/0.5 M LiTFSI/0.1 M $LiNO_3$			0.88±0.01	778±41

performance of the S/C-composite cathode and could be linked to the higher conductivity in this electrolyte. As already mentioned above, for long term performance a higher $LiNO_3$ amount in a test cell is necessary, because of the constant consumption of it during each charge step.

4.2.7. Effect of TBA^+-cation and its impact on the discharge capacity and cycling stability

For a better understanding of the reaction mechanism of Li-S batteries, RRDE[VII] measurements were done with various electrolytes. Also, electrolyte solutions, which contain the solvents DiOX and DME or DOL and DME, should be examined with this method. Therefore, the plain solvents were mixed by a ratio of one-to-one by volume and in both solutions a millimolar amount of polysulfides were generated by adding Li_2S and S[VIII]. The so generated polysulfide solutions were divided into two parts and the conducting salt LiTFSI was added or TBATFSI as salt was used to examine the stability/kinetics of discharge or charge products in the absence of Li^+-ions. During the preparation of the DiOX:DME electrolyte after the addition of TBATFSI a color change from colorless to light blue within a few minutes could be observed, which indicates the formation of the $S_3^{\cdot-}$ radical[25,33]. Due to this observation a few tests with different electrolyte solutions were done, to see if the color change only happens in DiOX:DME with TBATFSI or if it could be observed in DOL:DME, too. The results showed that in both solvent mixtures with TBATFSI the color changed to blue, but within different time frames. If LiTFSI was added to the solutions, the color changed from colorless in the beginning to yellow after a short resting time, which indicates the appearance of long chain polysulfides like Li_2S_8 or Li_2S_6.[25]

In theory, the stabilization of the $S_3^{\cdot-}$ radical should help to increase the discharge capacity of a Li-S battery, because of the equilibrium between $S_3^{\cdot-}$ and S_6^{2-}. The proposed reaction mechanism in Figure 5 shows that S will be reduced to S_8^{2-} in the first electrochemical step, followed by a second step to S_4^{2-} via the short living intermediate $S_8^{4-\cdot}$ If the solution is able to stabilize the S_6^{2-} or $S_3^{\cdot-}$ respectively, S_8^{2-} can disproportionate to S_6^{2-} and generate "new" S, which can be reduced again. In this way, more active material can take place in the electrochemical reaction step and more discharge capacity could be gained.

[VII] Measurements were done by Qi He, PHd student at the TU Munich (Chair Technical Electrochemistry)
[VIII] Detailed description of the preparation of a polysulfide solution for RRDE measurements published by Lu et al.[69]

To prove if the theory matches with the reality, three electrolyte solutions with 0.5 M TBATFSI, 0.5 M LiTFSI and 0.5 M $LiNO_3$ in the cases of DOL:DME or DME and 0.1 M $LiNO_3$ in the case of DiOX:DME were prepared. Because the assumption showed that the radical should have a beneficial effect on the rate capability of Li-S batteries, the electrochemical tests were focused on this issue and C-rate test with test cells, which contain one of the three electrolytes were done.

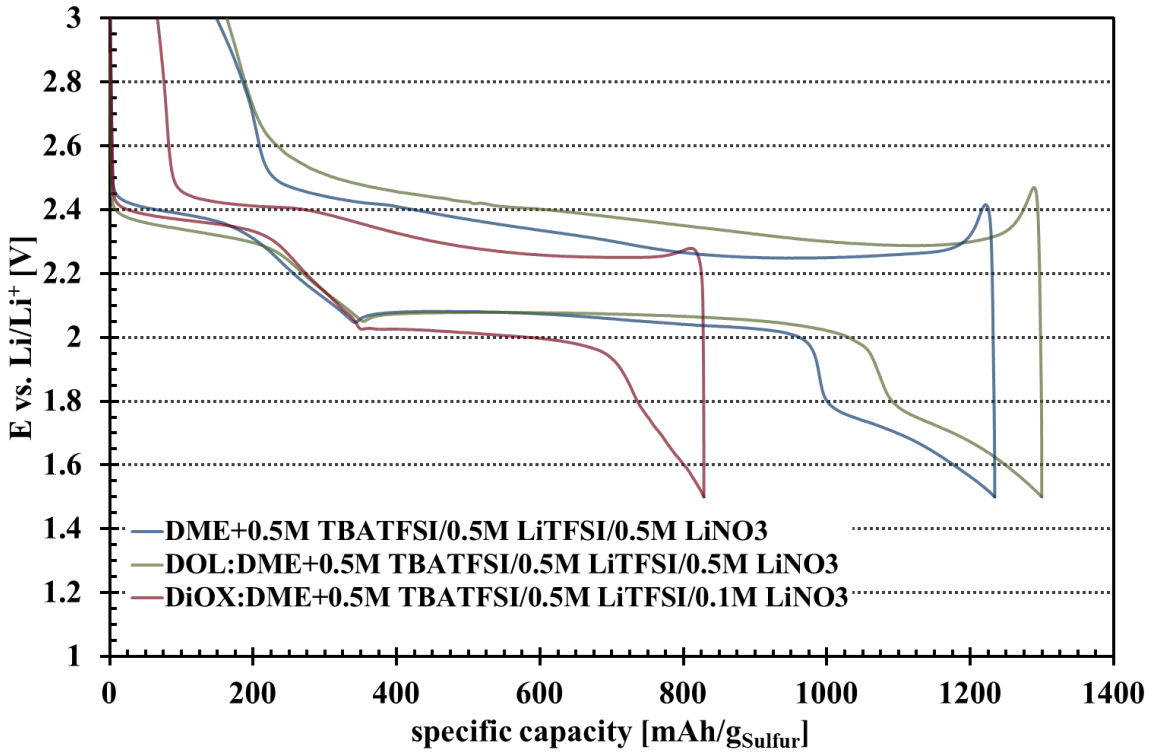

Figure 55: Representative first discharge charge cycle of test cells with three different electrolyte solvent compositions and the addition of TBATFSI salt at C/10. All cells contain 30µL of electrolyte and were cycled between 3V to 1.5V. The used S/C-composite electrodes are based on a Ketjen Black carbon with a weight ratio of 68wt% S to 32wt% C. The average S loadings of the used electrodes range from 0.82 to 0.88 mg_{Sulfur}/cm^2 (more details in Table 13).

In Figure 55 one representative first cycle of the three electrolytes is shown and in Figure 56 a comparison to the first cycle without TBATFSI in the electrolyte solution is displayed. The discharge and charge curves with the TBA^+-cation electrolytes possessed the typical shape with two distinct plateaus and the "third" one at the end of the discharge step. The first plateau had the same length and was located at the same potential in all three cases. Also, no difference to the discharge plateaus from the test cells without TBATFSI in the electrolyte could be observed. In the second discharge step, the TBATFSI did not influence the plateau for test cells with DOL:DME and DME and the usual shape and potential for it could be noticed. Also, the average discharge capacity in both cases was similar to the average one without TBATFSI (Figure 57). But the discharge profile of DiOX:DME showed a different

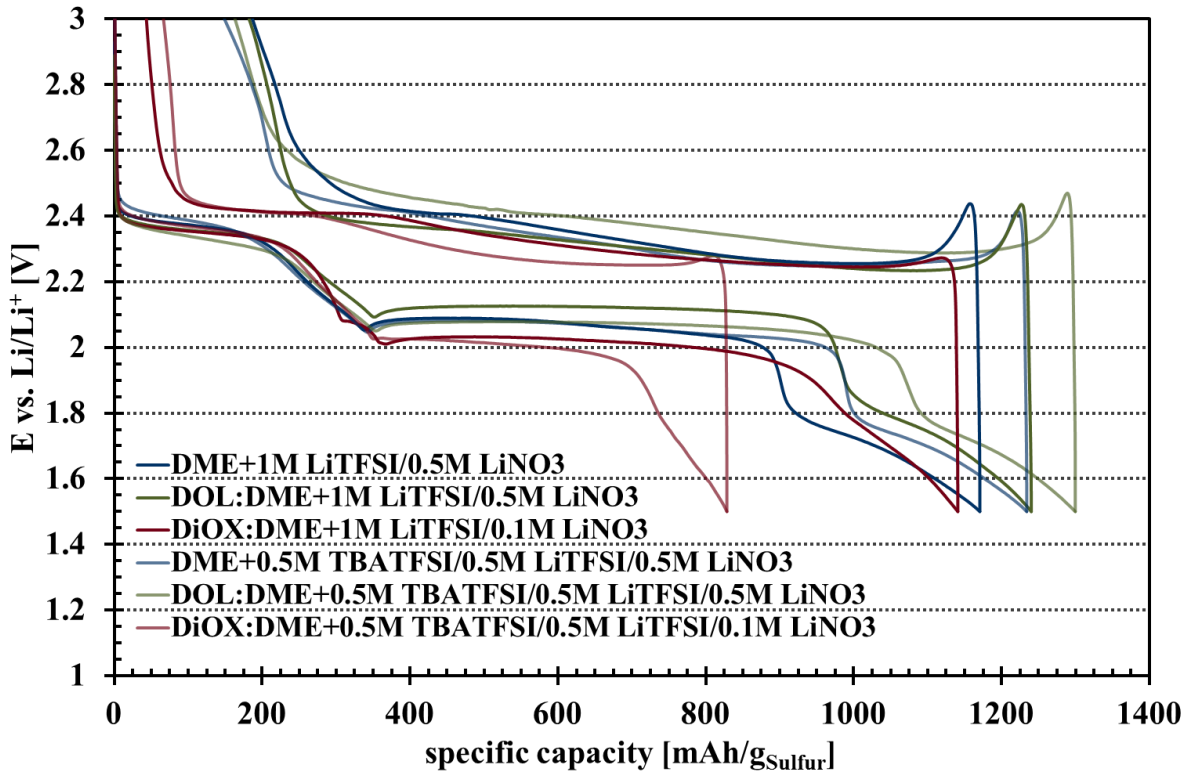

Figure 56: Comparison of the first representative discharge charge cycle of test cells with three different electrolyte solvent compositions with and without TBATFSI salt at C/10. All cells contain 30µL of electrolyte and were cycled between 3V to 1.5V. The used S/C-composite electrodes are based on a Ketjen Black carbon with a weight ratio of 68wt% S to 32wt% C. The average S loadings of the used electrodes range from 0.82 to 0.88 mg_{Sulfur}/cm^2 (more details in Table 13).

second discharge plateau, compared to the one without TBATFSI. The first notable difference was the absence of the little bump at 2.1 $V_{Li/Li+}$. Also, the use of TBATFSI in DiOX:DME resulted in a big loss of over 300 mAh/g_{Sulfur} in the discharge capacity compared to the obtained discharge capacity without the TBA^+-salt.

In Figure 57 the results of the C-rate test with and without TBATFSI is shown. If the solvent DME was used for the electrolyte, TBA^+-cation had a little beneficial effect on the discharge capacity at C-rates till C/2. At high C-rates, it did not matter if TBA^+-cation was used in the electrolyte and both test conditions delivered similar values. When the C-rate went back to C/5, the discharge capacity was recoverable and it seemed that the loss in between the cycles is nearly the same in both cases. For DOL:DME the use of TBA^+-cation had only at slow C-rates an advantageous effect on the discharge capacity. At C-rates over C/2, the value for the average discharge capacity decreased highly and the obtained results with the different test cells scattered very much. But, if the cycling conditions went back to C/5, the full discharge capacity, which was obtained in the first C/5 cycles, could be regained and showed a stable cycling behavior with only small losses of discharge capacity till the end of the test.

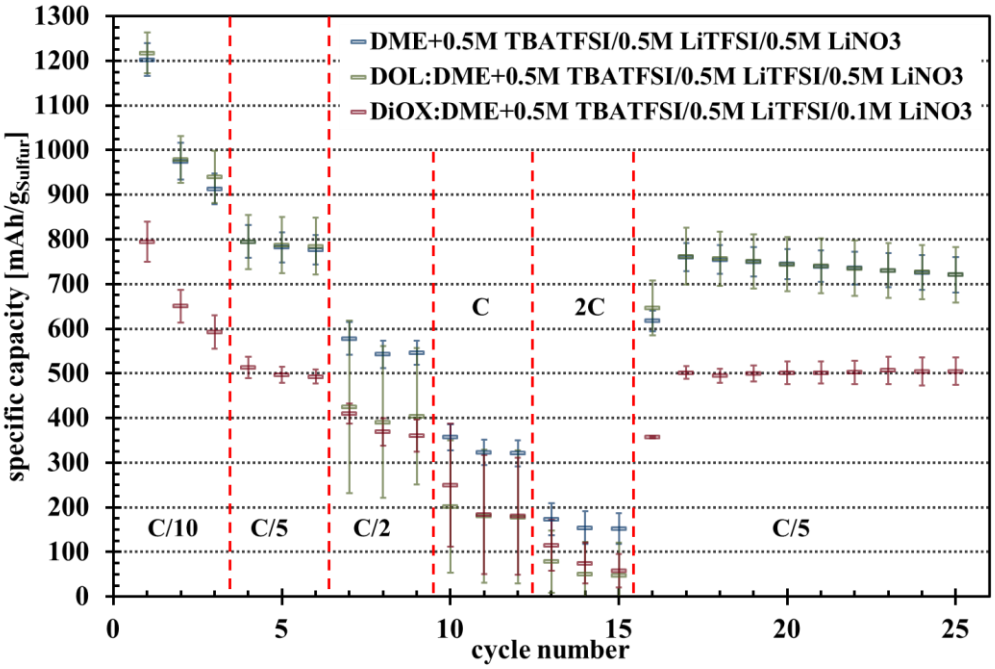

Figure 57: Discharge capacity vs. cycle number for a C-rate test of S/C-cathodes using three different electrolyte solvent compositions and TBATFSI as additional salt beside LiTFSI and $LiNO_3$. The standard deviation value is obtained from 2 to 3 repeated measurements. All cells contain 30µL of electrolyte and were cycled between 3V to 1.5V. The used S/C-composite electrodes are based on a Ketjen Black carbon with a weight ratio of 68wt% S to 32wt% C. The average S loadings of the used electrodes range from 0.82 to 0.88 mg_{Sulfur}/cm^2 (more details in Table 13).

Because in the electrolyte DME with TBATFSI good discharge capacities at higher C-rates could be obtained, there must be some interactions between DOL and the TBA^+-cation, which partially inhibited the discharge process or lower the conductivity of the electrolyte, which also leads to a bad cycling performance. In DiOX:DME the performance at slow C-rates did not benefit from the use of the TBA^+-cation as salt in the electrolyte and the obtained discharge capacities lied significantly below the values, which were reached without TBATFSI. At high C-rates the values for the discharge capacities of both electrolytes converged and showed a similar bad cycling behavior. At the intermediate C-rate C/2, the addition of the TBA^+-cation seemed to be beneficial for the test cells and approximately 100 mAh/g_{Sulfur} of average discharge capacity per cycle could be obtained. Here, the negative influence on the discharge capacity and rate capability of the test cell also were related to some interactions between DiOX and the TBA^+-cation. But in contrast to DOL, the negative interactions influenced the test cell performance at low C-rates and not at higher ones. So, it is imaginable that DiOX forms some complexes with the TBA^+-cation, which maybe also involve polysulfide species and in that case, will lower the discharge capacity. At C/2, the constant of formation is to low and the free TBA^+-cation can evolve its positive effect, which leads to an increase of discharge capacity. At the high C-rates 1 C and 2C, also the

conductivity of the electrolyte played an important role on the obtainable discharge capacity and because of that the values of both cases converged.

In summary, one can say that TBATFSI has a positive or negative effect on the cycling behavior of S/C-composite cathodes depending on the solvents, used in the electrolyte. It seemed that in DME the use of TBATFSI can increase the discharge capacity and rate capability of the S/C-composite cathode. If DOL or DiOX as mixture with DME were used, different side effects lowered the test cell performance. The real issues behind this phenomenon are not yet clarified and only the above described theories are available. So, to solve this riddle, further investigations are needed, like RRDE experiments as well as UV-VIS and IR spectroscopy.

5. Conclusion

In this work, the performance characteristics of S/C-composite powder as cathodes in Li-S cells were examined, synthesised by a bottom-up approach. It was proved that with this S/C-composite synthesis nano-sized S-particles could be precipitated on different carbon black supports and the S/C-composite powder could be successfully processed to S/C-composite cathodes. The electrochemical investigation of the cathodes made of S/C-composite powders from the standard method and an alternative one, showed that the standard route delivered the better results and during the further work all S/C-composite powders were synthesised with the standard route.

Also, the influence of the S loading on the S/C-composite cathode as well as the carbon black support on which the S was precipitated was investigated. It showed that high S loadings and high surface areas on the carbon black support can increase the discharge capacity and the cycling stability. The addition of polysulfides in the standard electrolyte increased the discharge capacity if the S amount from polysulfides in the solution was not included in the calculation of the values. When the S from the solution was taken into account, the calculated discharge capacity was actually lower for polysulfide containing electrolytes. Also, at intermediate and high C-rates the test cells with polysulfides in the electrolyte could not obtain high discharge values and dropped below the discharge capacities, which were achieved with the standard electrolyte solution. Furthermore, at high S loadings on the S/C-composite cathode, the test cell became "oversaturated" and the performance broke down. But it had beneficial effects, too. The capacity loss between the first and second cycle could be lowered and the $Wh/kg_{Battery}$ could be increased with adding only the weight of the polysulfides in the electrolyte, because no other support for the additional S is needed.

At the end, DiOX was introduced as electrolyte solvents, to prove the theory that solvents with a low dielectric constant could stabilize the polysulfide species and so improve the cycling stability and the rate capability of S/C-composite cathodes. Because of the low solubility of the electrolyte salts, DiOX could only be used in mixtures like DiOX:DME in a 1:1- ratio (by volume). But the solvent had no beneficial effect, neither on the cycling stability nor on the rate capability. Last but not least, the salt TBATFSI was incorporated in the electrolyte to stabilize the $S_3^{\cdot-}$ radical with the idea to improve the cycling stability and rate capability. However, only in the pure DME electrolyte better results could be obtained. In the other two electrolytes (DOL:DME and DiOX:DME) the effect of TBATFSI on the cycling

behavior of the S/C-composite cathode were negative rather than positive. The exact reason for the results are not yet clear and further experiments would be needed to understand the underlying mechanism.

6. Acknowledgments

At first I want to thank Mr. Prof. Dr. Gasteiger who gave me the opportunity to acquire my doctoral degree in natural science and supervising me through the past years.

I am deeply in debt to Himendra Jha, who development the bottom-up synthesis route of nano-S particles on a carbon black support. I want to thank him for the discussions, help and cooperation during his time at the chair.

Also, I want to thank all members of the of the LiSSi-project and the following LiMO-project for the valuable discussions, especially Oliver Gröger from VW.

Moreover, I want to thank Manu Patel U.M., Yelena Gorlin and Qi He for the interesting and helpful discussions and the teamwork in the lab during the last period of my work.

Furthermore, I want to thank Hans Beyer for the technical briefing how to use the TGA and the BET instruments and the huge amount of questions I asked him over the time about these devices.

I want to thank Marianne Hanzlik from the Fachbereich Elektronenmikroskopie for the wonderful SEM shots, the EDX analysis and the interesting discussion during the measurement periods.

Special thanks go to Veronika Pichler, who did a great administrative job and was always willing to lend a sympathetic ear when one has something on one´s mind.

I want to thank Rebecca Zeh, Timon Geppert and Thomas Mittermaier for the assistance when I was missing the forest through the trees as well as for the coffee talks, which made every day to a special one.

Furthermore, I want to thank my office mates for the nice and funny working atmosphere, the colleagues I pestered with questions for always have time and the whole group for keeping the lab running.

For the financial support, I want to acknowledge the funding by the Bavarian Ministry of Economic Affairs and Media, Energy and Technology (BMBF) under the auspices of the LiSSi and the following LiMO project.

6. Acknowledgments

Finally, I am grateful for the support of my family who kept me grounded through the whole period of my dissertation. I do not want to miss my friends how were patient with me and did not complain when I had no time. I am deeply indebted to you – thank you very much.

7. List of references

[1] K. Bullis; *Technology Review* **(2009),** *http://www.heise.de/-276451* **(2015)**

[2] R. van Noorden; *Nature* 498 **(2013)** 416

[3] M. Barghamadi, A.S. Best, A.I. Bhatt, A.F. Hollenkamp, M. Musameh, R.J. Rees and T. Rüther; *Engery Environ. Sci.* 7 **(2014)** 3902-3920

[4] A. Rosenman, E. Markevich, G. Salitra, D. Aurbach, A. Garsuch and F.F. Chesneau; *Adv. Energy Mater.*5 **(2015)** 1500212

[5] C.-X. Zu and H. Li; *Energy Environ. Sci.* 4 **(2011)** 2614-2624

[6] K. Dokko, N. Tachikawa, K. Yamauchi, M. Tsuchiya, A. Yamazaki, E. Takashima, J.-W. Park, K. Ueno, S. Seki and N. Serizawa; *J. Electrochem. Soc.* 160 **(2013)** A1304-A1310

[7] S. Zhang, K. Ueno, K. Dokko and M. Watanabe; *Adv. Energy Mater.* 5 **(2015)** 1500117

[8] C. Barchasz, J.-C. Leprêtre, S. Petoux and F. Alloin; *Electrochimica Acta* 89 **(2013)** 737-743

[9] M. Armand and J.-M. Tarascon; *Nature* 451**(2008)** 652-657

[10] N. Angulakshmi and A.M. Stephan; *Front. Energy Res.*3 **(2015)** 17

[11] H. Jha and H. A. Gasteiger; Patent No. DE 10 2013 005 082 A1 **(2014)**

[12] A. Manthiram, Y. Fu, S.-H. Chung, C. Zu and Y.-S. Su; *Chem. Rev.* 114 (**2014)** 11751–11787

[13] M.-K. Song, E.J. Cairns and Y. Zhang; *Nanoscale* 5 **(2013)** 2186-2204

[14] R. van Noorden; *Nature* 507 **(2014)** 26-28

[15] P.G. Bruce, S.A. Freunberger, L.J. Hardwick and J.-M. Tarascon; *Nat. Mater.* 11 (2012) 19–29

[16] C. Barchasz, F. Molton, C. Duboc, J.-C. Leprêtre, S. Petoux and F. Alloin; *Anal. Chem.* 89 **(2012)** 3973–3980

[17] Y. Gorlin, A. Siebel, M. Piana, T. Huthwelker, H. Jha, G. Monsch, F. Kraus, H.A. Gasteiger and M. Tromp; *J. Electrochem. Soc.* 162 **(2015)** A1146-A1155

[18] Y.-C. Lu, Q. He and H.A. Gasteiger; *J. Phys. Chem.* 118 **(2014)** 5733-5741

[19] L. Yuan, X. Qiu, L. Chen and W. Zhu; *J. Power Sources* 189 **(2009)** 127-132

[20] X. Fang and H. Peng; *small* 11 **(2015)** 1488-1511

[21] J. Hassoun and B. Scrosati; *Angew. Chem. Int. Ed.* 49 (**2010)** 2371 – 2374

[22] P. Knauth; *Solid State Ionics* 180 **(2009)** 911–916

[23] T. Zhang, N. Imanishi, S. Hasegawa, A. Hirano, J. Xie, Y. Takeda, O. Yamamoto and N. Sammes; *J. Electrochem. Soc.* 155 **(2008)** A965-A969

[24] N.-S. Choi, Z. Chen, S.A. Freunberger, X. Ji, Y.-K. Sun, K. Amine, G. Yushin, L.F. Nazar, J. Cho and P.G. Bruce; *Angew. Chem. Int. Ed.* 51**(2012)** 9994-100024

[25] R.D. Rauh, K.M. Abraham, G.F. Pearson, J.K. Surprenant and S.B. Brummer; *J. Electrochem. Soc.* 126 **(1979)** 523-527

[26] D.R. Lide; *CRC Handbook of chemistry and physics* 67 **(1986/87)** ISBN 978-0-8493-0467-5.

[27] R. Marom, S.F. Amalraj, N. Leifer, D. Jacob and D. Aurbach; *J. Mater. Chem.* 21 **(2011)** 9938–9954

[28] L.-F. Cui, Y. Yang, C.-M. Hsu and Y. Cui; *Nano Lett.* 9 **(2009)** 3370-3374

[29] R. Yazami; *Nanomaterials for Lithium-Ion Batteries: Fundamentals and Applications*, CRC Press **(2014)** ISBN 978-981-4316-40-8

[30] A. Kawase, S. Shirai, Y. Yamoto, R. Arakawa and T. Takata; *Phys. Chem. Chem. Phys.* 16 **(2014)** 9344-9350

[31] M. Cuisinier, C. Hart, M. Balasubramanian, A. Garsuch and L.F. Nazar; *Adv. Energy Mater.* 5 **(2015)** 1401801

[32] T. Chivers and I. Drummond; *Chem. Soc. Rev.* 2 (**1973)** 233-248

[33] R.D. Rauh, F.S. Shuker, J.M. Marston and S.B. Brummer; *J. Inorg. Nucl. Chem.* 39 **(1977)** 1761-1766

[34] S.S. Zhang; *J. Power Sources* 231 **(2013)** 153–162

[35] J. Nelson, S. Misra, Y. Yang, A. Jackson, Y. Liu, H. Wang, H. Dai, J. C. Andrews, Y. Cui and M. F. Toney; *J. Am. Chem. Soc.* 134 (**2012)** 6337–6343

[36] C. Daniel; *Handbook of Battery Materials*, Wiley-VCH, 2nd completely rev. and enlarged edition, Vol. 1&2 **(2011)** ISBN 978-3-527-32695-2.

[37] J.-M. Tarascon and M. Armand; *Nature* 414 **(2001)** 359-367

[38] 1. M. Dollé, B. Beaudoin, M. Trentin and J.-M. Tarascon; Electrochem. Solid-State Lett. 5 **(2002)** A286-A289

[39] K.J. Harry, D.T. Hallinan, D.Y. Parkinson, A.A. MacDowell and N.P. Balsara; *Nat. Mater.* 13 **(2014)** 69-73

[40] G. Park, N. Gunawardhana, H. Nakamura, Y.-S. Lee and M. Yoshio; *J. Power Sources*199 **(2012)** 293-299

[41] V. Agubra and J. Fergus; *Materials* 6 **(2013)** 1310-1325

[42] G. Derrien, J. Hassoun, S. Panero and B. Scrosati; *Adv. Mater.* 19 **(2007)** 2336 – 2340

[43] Y. Yan, Y. Yin, S. Xin, J. Su, Y. Guo and L. Wan; E*lectrochim. Acta* 91 **(2013)** 58 – 61

[44] C.-M. Park, J.-H. Kim, H. Kim and H.-J. Sohn; *Chem. Soc. Rev.* 39 **(2010)** 3115-3141

[45] C. Pereira-Nabais, J. Swiatowska, A. Chagnes, A. Gohier, S. Zanna, A. Seveux, P. Tran-Van, C.-S. Cojocaru, M. Cassir and P. Marcus; *J. Phys. Chem C* 4 **(2014)** 2919-2928

[46] H. Jha, I. Buchberger, X. Cui, S. Meini and H.A. Gasteiger; *J. Electrochem. Soc.* 162 **(2015)** A1829-A1835

[47] Y. Yang, G. Zheng and Y. Cui; *Chem. Soc. Rev.* 42 **(2013)** 3018-3032

[48] www.sigmaaldrich.com; product nr. 213241

[49] G. He, X. Ji and L. Nazar; *Energy Environ. Sci. 4* **(2011)** 2878-2883

[50] S.-E. Cheon, K. Ko, J. Cho, S. Kim, E. Chin and H. Kim; *J. Electrochem. Soc.*150 **(2003)** A800–A805

[51] H. Chen, C. Wang, W. Dong, W. Lu, Z. Du and L. Chen; *Nano Lett.* 15 **(2015)** 798-802

[52] S. Cheon, K. Ko, J. Cho, S. Kim, E. Chin and H. Kim.; J. Electrochem. Soc.150 (2003) A796–A799

[53] A. Manthiram, Y. Fu and Y.-S. Su; *Acc. Chem. Res 46* (**2013)** 1125–1134

[54] D. Marmorstein, T.H Yu, K.A Striebel, F.R McLarnon, J. Hou and E.J Cairns; *J. Power Sources* 89 **(2000)** 219-226

[55] V.S. Kolosnitsyn, E.V. Karaseva and A.L. Ivanov; *Russian Journal of Electrochemistry* 44 **(2008)** 564–569

[56] B.H. Jeon, J.H. Yeon, K.M. Kim and I.J. Chung; *J. Power Sources* 109 **(2002)** 89-97

[57] G. Zheng, Q. Zhang, J. J. Cha, Y. Yang, W. Li, Z. W. Seh, and Y. Cui; *Nano Lett.* 13 **(2013)** 1265-1270

[58] S.-E. Cheon, S.-S. Choi, J.-S. Han, Y.-S. Choi, B.-H. Jung and H.-S. Lim; *J. Electrochem. Soc.* 151 **(2004)** A2067-A2073

[59] D. Aurbach, E. Pollak, R. Elazari, G. Salitra, C.S. Kelley and J. Affinito; *J. Electrochem. Soc.* 156 **(2009)** A694-A702

[59] W. Li, G. Zheng, Y. Yang, Z.W. Seh, N. Lui and Y. Cui; *PNAS* 110 **(2013)** 7148-7153

[60] D. Aurbach, E. Zinigrad, Y. Cohen and H. Teller; *Solid State Ionics* 148 **(2002)** 405 – 416

[61] Y. Diao, K. Xie, S. Xiong and X. Hong. *J. Electrochem. Soc.*159 **(2012)** A1816–A1821

[62] A. Zhamu, G. Chen, C. Liu, D. Neff, Q. Fang, Z. Yu, W. Xiong, Y. Wang, X. Wang and B.Z. Jang; *Energy Environ. Sci.* 5 **(2009)** 5701-5707

[63] J. Akridge, Y. Mikhaylik and N. White; *Solid State Ionics* 175 **(2004)** 243–245

[64] V.S. Kolosnitsyn and E.V. Karaseva; *Russian Journal of Electrochemistry* 44 **(2008)** 506–509

[65] Y. Mikhaylik and J. Akridge; *J. Electrochem. Soc.* 151 **(2004)** A1969-A1976

[66] J. Shim, K. Striebel and E. Cairns; *J. Electrochem. Soc.* 149 **(2002)** A1321-A1325

[67] J. Song, M.L. Gordin, T. Xu, S. Chen, Z. Yu, H. Sohn, J. Lu, Y. Ren, Y. Duan and D. Wang; *Angew. Chem.* 127 **(2015)** 4399-4403

[68] S. C. Abrahams; *Acta Cryst.* 8 **(1955)** 661-671

[69] D. Moy, A. Manivannan and S.R. Narayanan; *J. Electrochem. Soc.* 162 **(2015)** A1-A7

[70] Y. Mikhaylik and J. Akridge; *J. Electrochem. Soc.* 150 **(2003)** A306-A311

[71] Y. Diao, K. Xie, S. Xiong and X. Hong; *J. Power Sources* 235 **(2013)** 181-186

[72] S. Xiong, K. Yie, Y. Diao and X. Hong; *J. Power Sources* 246 **(2014)** 840-845

[73] Y. M. Lee, N.-S. Choi, J. H. Park and J.-K. Park; *J. Power Sources* 119-121 **(2003)** 964-972

[74] H. Yao, K. Yan, W. Li, G. Zheng, D. Kong, Z. W. Seh, V. K. Narasimhan, Z. Liang and Y. Cui; *Energy Environ. Sci.* 7 **(2014)** 3381-3390

[75] B. Zhang, C. Lai, Z. Zhou and X.P. Gao; *Electrochimica Acta* 54 **(2009)** 3708–3713

[76] Q. Wang, J. Jin, X. Wu, G. Ma, J. Yang and Z. Wen; *Phys. Chem. Chem. Phys.* 16 **(2014)** 21225-21229

[77] X. Ji, K.T. Lee, L.F. Nazar; *Nat. Mater.* 8 **(2009)** 500-506

[78] Y. Zhao, W. Wu, J. Li, Z. Xu and L. Duan; *Adv. Mater.* 26 **(2014)** 5113-5118

[79] J. Zheng, J. Tian, D. Wu, M. Gu, X. Xu, C. Wang, F. Gao, M.H. Engelhard, J. Zhang, J. Liu and J. Xiao; *Nano Lett.* 160 **(2014)** 2345-2352

[80] N. Jayaprakash, J. Shen, S.S. Moganty, A. Corona and L.A. Archer; *Angew. Chem. Int. Ed.* 50 **(2011)** 5904-5908

[81] G. Ma, Z. Wen, J. Jin, Y. Lu, X. Wu, M. Wu and C. Chen; *J. Mater. Chem.* 2 **(2014)** 10350-10354

[82] C. Zhang, H.B. Wu, C. Yuan, Z. Guo and X.W. Lou; *Angew. Chem. Int. Ed.* 51 **(2012)** 9592-9595

[83] L. Sun, M. Li, Y. Jiang, W. Kong, K. Jiang, J. Wang and S. Fan; *Nano Lett.* 14 **(2014)** 4044-4049

[84] S. Zheng, F. Yi, Z. Li, Y. Zhu, Y. Xu, C. Luo, J. Yang and C. Wang; *Adv. Funct. Mater.*24 **(2014)** 4156-4163

[85] C. Barchasz, J.-C. Leprêtre, F. Alloin and S. Petoux; *J. Power Sources* 199 **(2012)** 322-330

[86] Y. S. Choi, S. Kim, S. S. Choi, J. S. Han, J. D. Kim, S. E. Jeon and B. H. Jung; *Electrochimica Acta* 50 **(2004)** 833-835

[87] X. Li, Y. Cao, W. Qi, L.V. Saraf, J. Xiao, Z. Nie, J. Mietek, J. Zhang, B. Schwenzer and J. Liu; *J. Mater. Chem.* 21 **(2011)** 16603-16610

[88] R. Singhal, S.-H. Chung, A. Manthiram, and V. Kalra; *J. Mater. Chem.* 3 **(2015)** 18829-18834

[89] J. Zheng, M. Gu, M.J. Wagner, K.A. Hays, X. Li, P. Zuo, C. Wang, J. Zhang, J. Liu and J. Xiao; *J. Electrochem. Soc.* 160 **(2013)** A1624-A1628

[90] C.O. Ania and T.J. Bandosz; *Langmuir* 21 **(2005)** 7752-7759

[91] S.-H. Chung and A. Manthiram; *Adv. Mater.* 26 **(2014)** 1360-1365

[92] S.-H. Chung and A. Manthiram; *J. Mater. Chem. A 1* **(2013)** 9590-9596

[93] H. Ye, Y.-X. Yin, Y. Xin and Y.-G. Guo; *J. Mater. Chem. A* 1 **(2013)** 6602-6608

[94] B. Zhang, Q. Qin, G.R. Li and X.P. Gao; *Energy Environ. Sci.* 3 **(2010)** 1531-1537

[95] X. Li and X. Sun; *Front. Energy Res.* 2 **(2014)** 49

[96] X. Zhao, D.-S. Kim, H.-J. Ahn, K.-W. Kim, C.-S. Jin and J.-H. Ahn; *J. Korean Electrochem. Soc.* 13 **(2010)** 169-174

[97] X. Zhou, J. Xie, J. Yang, Y. Zou, J. Tang, S. Wang, L. Ma and Q. Liao; *J. Power Sources* 243 **(2013)** 993-1000

[98] H. Chen, W. Dong, J. Ge, C. Wang, X. Wu, W. Lu, and L. Chen; *Sci. Rep.* 3 **(2013)** 1910

[99] F. Wu, J. Chen, R. Chen, S. Wu, L. Li, S. Chen and T. Zhao; *J. Phys. Chem.* 115 **(2011)** 6057-6063

[100] Z.W. Seh, W. Li, J.J. Cha, G. Zheng, Y. Yang, M.T. McDowell, P.C. Hsu and Y. Cui; *Nat. Commun.* 4 **(2013)** 1331-1336

[101] W. Zhou, Y. Yu, H. Chen, F.J. DiSalvo and H.D. Abruna; *J. Am. Chem. Soc.* 135 **(2013)** 16736-16743

[102] S. Lu, Y. Chen, X. Wu, Z. Wang, Y. Li; *Sci. Rep.* 4 **(2014)** 4629

[103] L. Wang, Y. Zhao, M.J. Thomas and H.R. Byon; *Adv. Funct. Mater.* 24 **(2014)** 2248-2252

[104] W. Weng, H. Lin, X. Chen, J. Ren, Z. Zhang, L. Qui, G. Guan and H. Peng; *J. Mater. Chem. A* 2 **(2014)** 9306-9312

[105] S. Huang, L. Li, Z. Yang, L. Zhang, H. Saiyin, T. Chen and H. Peng; *Adv. Mater.* 23**(2011)** 4707 – 4710

[106] H. Lin, W. Weng, J. Ren, L. Qiu, Z. Zhang, P. Chen, X. Chen, J. Deng, Y. Wang and H. Peng; *Adv. Mater.* 26 **(**2**014)** 1217 – 1222

[107] Z. Yang, T. Chen, R. He, G. Guan, H. Li, L. Qiu and H. Peng; *Adv.Mater.* 23**(2011)** 5436 – 5439

[108] R. Elazari, G. Salitra, A. Garsuch, A. Panchenko and D. Aurbach; *Adv. Mater.* 23**(2011)** 5641 – 5644

[109] K. Jin, X. Zhou, L. Zhang, X. Xin, G. Wang and Z. Liu; *J. Phys, Chem. C* 117 **(2013)** 21112 – 21119

[110] Q. Pang, D. Kundu, M. Cuisinier and L. F. Nazar; *Nat. Commun.* 5 **(2014)** 4759

[111] X. Tao, J. Wang, Z. Ying, Q. Cai, G. Zheng, Y. Gan, H. Huang, Y. Xia, C. Liang, W. Zhang and Y. Cui; *Nano Lett.* 14 **(2014)** 5288 – 5294

[112] W. Bao, Z. Zhang, Y. Qu, C. Zhou, X. Wang and J. Li; *J. Alloys Compd.* 582 **(2014)** 334 – 340

[113] Z. Zhao, S. Wang, R. Liang, Z. Li, Z. Shi and G. Chen; *J. Mater. Chem. A* 2 **(2014)** 13509 – 13512

[114] Y. Zhu, S. Murali, W. Cai, X. Li, J.W. Suk, J.R. Potts and R.S. Ruoff *Adv. Mater.* 22 **(2010)** 3906 – 3924

[115] J. Rong, M. Ge, X. Fang and C. Zhou; *Nano Lett.* 14 **(2014)** 473 – 479

[116] Y. Qiu, W. Li, W. Zhao, G. Li, Y. Hou, M. Liu, L. Zhou, F. Ye, H. Li, Z. Wei, S. Yang, W. Duan, Y. Ye, J. Guo and Y. Zhang; *Nano Lett.* 14 **(2014)** 4821 – 4827

[117] H. Wang, Y. Yang, Y. Liang, J. T. Robinson, Y. Li, A. Jackson Y. Cui and H. Dai; *Nano Lett.* 11 **(2011)** 2644 – 2647

[118] M. Zhao, Q. Zhang, J. Huang, G. Tian, J. Nie, H. Peng and F. Wei; *Nat.Commun.* 5 **(2014)** 3410 – 3410

[119] C. Zu and A. Manthiram; *Adv. Energy Mater.* 3 **(2013)** 1008 – 1012

[120] G. Li, Z. Li, B. Zhang and Z. Lin1; *Front. Energy Res.* 3 **(2015)** 5

[121] H.-J.Deiseroth, S.-T. Kong, H. Eckert, J. Vannahme, C. Reiner, T. Zaiß and M.

Schlosser; *Angew. Chem.* 120 **(2008)** 767 –770

[122] D. Golodnitsky and G. Ardel, E. Peled; *Solid State Ionics* 147 **(2002)** 141–155

[123] R. Kanno, T. Hata, Y. Kawamoto and M. Irie; *Solid State Ionics* 130 **(2000)** 97–104

[124] R. Murugan, V. Thangadurai and W. Weppner; *Ionics* 13 **(2007)** 195–203

[125] A.M. Stephan; *EPJ* 42 **(2006)** 21-42

[126] D. Linden and T.B. Reddy; *Handbook of Batteries 3rd edition*, McGraw-Hill Handbooks **(2002)** ISBN 0-07-135978-8

[127] A.L. Dicks; *J. Power Source* 156 **(2006)** 128-141

[128] M. Wissler; *J. Power Source* 156 **(2006)** 142-150

[129] S. Meini, M. Piana, H. Beyer, J. Schwämmlein and H.A. Gasteiger; *J. Electrochem. Soc.* 159 **(2012)** A2135-A2142

[130] G. Salitra, E. Markevich, A. Rosenman, Y. Talyosef, D. Aurbach and A. Garsuch; *Chem. Electro.Chem.* 1 **(2014)** 1492-1496

[131] S.S. Zhang and J.A. Read; *J. Power Sources* 200 **(2012)** 77– 82

[132] S. S. Zhang; *Electrochimica Acta* 70 **(2012)** 344-348

[133] S. Urbonaite and Petr Novak; *J. Power Sources* 249 **(2014)** 497-502

[134 H. Wei, J. Ma, B. Li, Y. Zuo and D. Xia; *ACS Appl. Mater. Interfaces* 6 **(2014)** 20276-20281

[135] S. Thieme, J. Brückner, A. Meier, I. Bauer, K. Gruber, J. Kaspar, A. Helmer, H. Althues, M. Schmuck and S. Kaskel; *J. Mater. Chem. A* 3 **(2015)** 3808-3820

[136] G. He, C. J. Hart, X. Liang, A. Garsuch and L. F. Nazar; *ACS Appl. Mater. Interfaces* 6 **(2014)** 10917-10923

[137] Z. Li, Y. Jiang, L. Yuan, Z. Yi, C. Wu, Y. Liu, P. Strasser and Y. Huang; *ACSNano* 8 **(2014)** 9295-9303

[138] L. Huang, J. Cheng, X. Li, D. Yuan, W. Ni, G. Qu, Q. Guan, Y. Zhang and B. Wang; *J. Mater. Chem. A* 3 **(2015)** 4049-4057

[139] C. D. Liang, N. J. Dudney and J. Y. Howe; *Chem. Mater.* 21 **(2009)** 4724-4730

[140] S. Liu, K. Xie, Y. Li, Z. Chen, X. Hong, L. Zhou, J. Yuan and C. Zheng; *RCS Adv.* 5 **(2015)** 5516-5522

[141] D.-W. Wang, F. Li, M. Lui, G. Q. Lu and H.-M. Cheng; *Angew. Chem. Int. Ed.* 47 **(2008)** 373-376

[142] X.-B. Cheng, J.-Q. Huang, H.-J. Peng, J.-Q. Nie, X.-Y. Liu, Q. Zhang and F. Wei; *J. Power Sources* 253 **(2014)** 263-268

[143] X. Yu and A. Manthiram; *Phys. Chem. Chem. Phys.* 17 **(2015)** 2127-2136

[144] D. Aurbach; *Nonaqueous Electrochemistry*, CRC Press **(1999)** ISBN 0-8247-7334-9

[145] Z. Peng, S.A. Freunberger, Y. Chen and P.G. Burce; *Science* 337 **(2012)** 563-566

[146] W. J. Chung , J. J. Griebel , E. Tae Kim, H. Yoon, A. G. Simmonds , H. Jun Ji , P. T. Dirlam , R. S. Glass , J. Jae Wie, N. A. Nguyen, B. W. Guralnick, J. Park, A. Somogyi, P. Theato, M. E. Mackay, Y.-E. Sung, K. Char and J. Pyun; *Nature Chem.* 5 **(2013)** 518-524

[147] Y. V. Mikhaylik; *Electrolytes for lithium sulfur cells* **(2009)** US Patent 7,553,590

[148] X.Y. Zhao, J.P. Tu, Y. Lu, J.B. Cai, Y.J. Zhang, X.L. Wang and C.D. Gu; *Electrochim. Acta* 113 **(2013)** 256-262

[149] R. Xu, I. Belharouak, J. C. M. Li, X. Zhang, I. Bloom and J. Bareño; *Adv. Energy Mater.* 3 **(2013)** 833-838

8. Abbreviations

general

BET	Brunner-Emmett-Teller analysis
BP	Black Pearls
C	carbon
CC	constant current
DiOX	1,4-Dioxane
DMAC	dimethyl acetamide
DME	1,2-dimethoxyethane
DMSO	dimethyl sulfoxide
DOL	1,3-dioxolane
EDX	energy dispersive X-ray spectroscopy
GARNET	lithium Super-Ionic Conductor
KB	Ketjen Black
Li	Lithium
Li^+-ion	positive charged lithium ion
Li-S battery	lithium Sulfur battery
LiSICON	lithium Super-Ionic Conductor
LTAP	lithium-Titan-Aluminum-Geramanium-Phosphate
NMP	N-methyl pyrolidon
OCV	open circuit voltage
PAN	poly acrylonitrile
PEIS	potential electrochemical impedance spectroscopy
PEO	polyethylen oxide
PS	polysulfide species
PVDF	polyvinylidene fluoride
S	Sulfur
S/C-composite	Sulfur carbon composite
SEI	solid electrolyte interface
SEM	secondary electron microscopy
SC	Super C65
TEGDME	tetraethylene glycol dimethyl ether
TGA	thermal gravemetry analysis
VC	Vulcan XC72
XRD	X-ray diffraction

chemical formulas

gas

Ar	argon
CO_2	carbon dioxide

H_2	hydrogen
H_2S	hydrogen sulfide
N	nitrogen
SO_2	sulfur dioxide

liquid

$H_2C_2O_4$	oxcalic acid
H_2O	water
H_2SO_4	sulfuric acid
HCl	hydrochloric acid
HNO_3	nitric acid
Li_2Sy	polysulfide species
$Na_2C_2O_4$	sodium oxalate

solid

$Li_2SO_2CF_3$	lithium (trifluoromehtyl) sulfonyl
$Li_2NSO_2CF_3$	lithium amino (trifluoromehtyl) sulfonyl
$LiCO_3$	lithium carbonate
Li_2S_2	lithium disulfide
LixCFy	lithium fluoro methan
HCO_2Li	lithium formate
LiOH	lithium hydroxide
Li_xNO_y	lithium nitric oxides
Li_2SO_y	lithium sulfates
Li_2S	lithium sulfide
P_2S_5	phosphorous pentasulfide
PEO	polyethylene oxide
PVDF	polyvinylidene fluoride
S_8	sulfur
TiO_2	titanium oxide

salts

KOH	potassium hydroxide
LiBOB	lithium bis(oxalato)borate
LiBr	lithium bromide
LiF	lithium fluoride
$LiNO_3$	lithium nitrate
$LiNO_3$	lithium nitrate
LiOR	organic lithium base
LiTFSI	lithium bis(trifluoromethane sulfonyl) imide

$Na_2S_2O_3$	sodium thiosulfate
Na_2SO_3	sodium sulfite
NaCl	sodium chloride
$NaNO_3$	sodium nitrate
RCOOLi	organic lithium acid
TBATFSI	tetrabutylammonium bis (trifluoremethanesulfonyl) imide

constant

F	Faraday constant	$9.6485 \cdot 10^4$ C/mol
e-	electron	$1.6023 \cdot 10^{-19}$ C
Li	Lithium	6.9 g/mol
S	Sulfur	32.1 g/mol
Si	silicon	28.1 g/mol
Sn	tin	118.7 g/mol

units

amount of substance	n	mol
Angström	Å	10^{-11} m
charge	Q	C
concentration	c	mol/L
C-Rate	C	1/h
current	I	A
density	ρ	g/cm^3
electrical conductivity	σ	S/cm
electron volt	E	eV
energy density	W	Wh/kg
length	L	km
loading		mg/cm^2
molare mass	M	mol/g
parts per million		ppm
percent	p	%
potential	E	V
pressure	p	bar
resistance	R	Ω
rotation speed	$\vec{\omega}$	rpm
specific capacity		mAh/cm^2

9. List of Tables

10. List of figures